

PROJECT PENGUIN

Robotic Lunar Crater Resource Prospecting



AIAA 2018 Undergraduate Spacecraft Design

Competition Submission

VIRGINIA POLYTECHNIC INSTITUTE & STATE UNIVERSITY

Kevin T. Crofton Department of
Aerospace & Ocean Engineering

TEAM LEAD

Allison Quinn

STUDENT MEMBERS

Ethan LeBoeuf

Brian McLemore

Peter Bradley Smith

Amanda Swanson

Michael Valosin III

Vidya Vishwanathan

FACULTY SUPERVISOR

Dr. Kevin Shinpaugh

AIAA Member Numbers and Signatures

<p>Ethan LeBoeuf Member Number: 918782</p> 	<p>Brian McLemore Member Number: 908372</p> 
<p>Allison Quinn Member Number: 920552</p> 	<p>Peter Bradley Smith Member Number: 530342</p> 
<p>Amanda Swanson Member Number: 920793</p> 	<p>Michael Valosin III Member Number: 908465</p> 
<p>Vidya Vishwanathan Member Number: 608701</p> 	<p>Dr. Kevin Shinpaugh Member Number: 25807</p> 



Table of Contents

List of Figures.....	v
List of Tables.....	vi
List of Symbols.....	vii
I. Team Structure.....	1
II. Introduction.....	2
A. Background & Motivation.....	2
B. Problem Definition.....	4
C. Scope.....	4
D. Requirements.....	5
E. Crater Location.....	6
III. Mission Architecture Decision.....	8
A. Two Rover System ConOps.....	9
B. Pod System Launched from Orbit ConOps.....	10
C. Summary.....	12
IV. Executive Summary.....	12
V. Lunar Surface.....	15
A. Requirements.....	15
B. System Overview.....	16
C. Rover Instrumentation.....	17
D. Rover Structure.....	22
E. Rover Navigation and Guidance.....	25
F. Rover Power.....	28
G. Rover Thermal.....	31
H. Rover Communication.....	33
I. Rover Dust Mitigation System.....	37
J. Rover Avionics.....	37
K. Rover Operations.....	38
L. Mass Budget.....	40
VI. Entry, Descent, & Landing.....	41
A. EDL Trajectory.....	41
B. Requirements.....	43
C. System Overview.....	44
D. Lander Structure.....	45
E. Lander Propulsion.....	47
F. Lander Guidance, Navigation, and Control.....	51
G. Lander Power.....	53
H. Lander Thermal.....	53

I.	Lander Avionics	55
J.	Mass Budget	56
VII.	Earth to Lunar Transfer	58
A.	Requirements	58
B.	Launch Vehicle Selection	58
C.	Transfer Trajectory	60
D.	System Overview	67
E.	Orbiter Structure	68
F.	Orbiter Propulsion	69
G.	Orbiter Power	71
H.	Orbiter Thermal	72
I.	Orbiter Communication	73
J.	Orbiter ADCS	78
K.	Mass Budget	80
VIII.	Systems Analysis	82
A.	Mission Mass Budget	82
B.	Mission Cost Budget	82
C.	Mission Risk Analysis	83
IX.	Conclusion	86
A.	Summary	86
B.	Conclusion	87
X.	References	88

List of Figures

Figure 1: Project Penguin Team Hierarchy.	1
Figure 2: Customer requirements from AIAA.	5
Figure 3: Labeled craters locations for South pole.	7
Figure 4: Labeled craters with LRO LEND data overlaid.	8
Figure 5: ConOps for the Two Rover Mission Design.	10
Figure 6: ConOps of the Pod System Launched from Orbit.	11
Figure 7: Lunar Crater Operations Mapping.	14
Figure 8: Requirements Flowdown for the Rover System.	15
Figure 9: Engineering Views of the Lunar Rover Exterior.	16
Figure 10: Lunar Rover Scientific Instrumentation Components.	17
Figure 11: DAN-PNG and DAN-DE instruments.	19
Figure 12: SansEC sensor used for redundancy in the water concentration measurement.	20
Figure 13: VNIR/SWIR instrument from the Chinese Yutu rover.	20
Figure 14: Percussive Dynamic Cone Penetrometer mounted on the NASA Ames K-10 rover.	21
Figure 15: GPR with similar design to that used for this mission.	21
Figure 16: Lunar Rover Structural Components.	22
Figure 17: Engineering Views of the Rover in Stowed Configuration.	23
Figure 18: Lunar Rover Navigation and Avionics Components.	25
Figure 19: Flowchart of the GN&C Operations.	27
Figure 20: Lunar Rover Power Components.	28
Figure 21: Lunar rover thermal components.	31
Figure 22: Rover Thermal Control System.	32
Figure 23: Lunar Rover Communications Components.	33
Figure 24: ConOps of the Communication Link Architecture.	34
Figure 25: Image of STK Model of Communication Link.	34
Figure 26: Graph of access times between the Orbiter and the rover for two passes.	35
Figure 27: Three-Phase AC Source powering Nodes for Electrodynamic Particle Movement.	37
Figure 28: Rover Operations Schedule.	39
Figure 29: Image of STK model of overall EDL trajectory.	42
Figure 30: Image of STK model of final portion of EDL trajectory.	42
Figure 31: Timeline for the EDL Trajectory.	43
Figure 32: Lander Requirements Flowdown.	44
Figure 33: Lander System Overview of Exterior.	44
Figure 34: Ramp in stowed and extended configurations is highlighted.	45
Figure 35: Lander Configuration with Rover Deployment.	45
Figure 36: Housing for the lander is highlighted.	46
Figure 37: Landing legs are highlighted.	46
Figure 38: Lander labeled with dimensions.	47
Figure 39: Lander Propulsion System.	48
Figure 40: Lander Overview with Lander GN&C Components in Blue.	51
Figure 41: Lander Isometric View with Radiator in Blue.	53
Figure 42: Lander Front and Back Isometric View with Avionics in Blue.	55
Figure 43: ConOps of Lander Avionics during EDL maneuver.	56
Figure 44: Orbiter Requirements Flowdown.	58
Figure 45: Falcon 9 FT PLF assembly containing the lunar orbiter and two landers.	60
Figure 46: Diagram Theoretical Earth-to-Moon Transfers.	62
Figure 47: Model of the Hohmann transfer in STK.	64
Figure 48: Model of the bi-elliptic transfer in STK.	64
Figure 49: Model of the elliptic-bi-parabolic transfer in STK.	64
Figure 50: Theoretical GTO transfer to the Moon.	65
Figure 51: GTO transfer to the Moon.	66
Figure 52: Engineering Views of Lunar Orbiter Exterior.	67
Figure 53: Orbiter Configuration Dimensions.	68
Figure 54: Overall Configuration of the Orbiter with the Propulsion System in Blue.	69

Figure 55: Isometric View of the Orbiter with the Communication System in Blue.73
 Figure 56: Graph of access times between Orbiter and rover.74
 Figure 57: Picture of the full communication link shown in STK.74
 Figure 58: Contour plot of beamwidth, carrier frequency, and antenna diameter.75
 Figure 59: Contour plot of power required, beamwidth and carrier to noise density ratio.76
 Figure 60: Top and Isometric View of Orbiter with ADCS in Blue.78
 Figure 61: Graph of momentum versus time of the Orbiter.80

List of Tables

Table 1: Summary of NASA SKGs.3
 Table 2: The trade study used to determine which lunar craters this mission would investigate.8
 Table 3: Trade study for the overall mission architecture.9
 Table 4: Mission Segment Breakdown.13
 Table 5: Trade Study to Determine Primary Scientific Instrumentation.18
 Table 6: Rover Traverse and Stow Configuration Dimensions.23
 Table 7: Super elastic mesh wheel versus conventional aluminum-milled wheel mechanical properties.24
 Table 8: Trade Study of Different Rover Navigation Systems.26
 Table 9: Rover Instrument Power Draw.29
 Table 10: Rover Operating Mode Power Requirements.30
 Table 11: Rover Thermal Analysis.32
 Table 12: Link Budget Between the Orbiter and the Rovers.36
 Table 13: Rover Operation Phase Time Table.38
 Table 14: Rover Operations Table with Time and Power Requirements.39
 Table 15: Mass budget for lunar rover.40
 Table 16: Lander Dimensions Table.47
 Table 17: Trade Study of Different Landing Methods.49
 Table 18: Propellant Freezing and Boiling Temperatures.50
 Table 19: Masses and Diameters of Engines Representative of different Thrust Echelons.50
 Table 20: Masses and Volumes of Propellant for the Landing Maneuver.51
 Table 21: Trade study performed on the lander attitude control systems.52
 Table 22: Power Requirement Breakdown for the Lander.53
 Table 23: Lander Thermal Analysis Summary.54
 Table 24: Mass Budget for Lander.57
 Table 25: Trade study to determine mission launch vehicle.59
 Table 26: Summary of STK model results for LEO Transfers.65
 Table 27: Maximum fuel that can be carried by the Falcon 9.66
 Table 28: STK model results for the LEO and GTO trajectories.67
 Table 29: Overall Orbiter Dimensions Table.68
 Table 30: Trade Study of Different Orbiter Engines.70
 Table 31: Masses and Volumes of Propellant for the Landing Maneuver.70
 Table 32: Orbiter Power Draw Summary.71
 Table 33: Link budget between the Orbiter and the DSN.77
 Table 34: Results of a trade study for the Orbiter ADCS.79
 Table 35: Mass Budget for Lunar Orbiter.81
 Table 36: The Overall Mission Mass Budget.82
 Table 37: Overall Mission Cost Budget.83
 Table 38: Risk Consequence Definition.83
 Table 39: Risk Assessment Matrix.84
 Table 40: Risk Events, Status, and Mitigation Strategies.85

List of Symbols

A_c	Solar Panel Area
ADCS	Attitude Determination & Control System
AHP	Analytical Hierarchy Process
AIAA	American Institute of Aeronautics and Astronautics
CMG	Control Mounted Gyros
ConOps	Concept of Operations
DAN	Dynamic Albedo of Neutrons
DC	Direct Current
DSN	Deep Space Network
E	Energy
EDL	Entry, Descent, and Landing
EOY	End of Year
ESA	European Space Agency
FT	Full Thrust
g_0	Gravity
GN&C	Guidance, Navigation and Control
GPHS	General Purpose Heat Source
GPHU	General Purpose Heat Units
GTO	Geosynchronous Transfer Orbit
IMU	Inertial Measurement Unit
IR	Infrared
Isp	Specific Impulse
ISRO	Indian Space Research Organization
JPL	Jet Propulsion Lab
LAMP	Lyman-Alpha Mapping Project
LCROSS	Lunar Crater Observing and Sensing Satellite
LEND	Lunar Exploration Neutron Detector
LEO	Low Earth Orbit
Li	Lithium Ion
LIBAS	Laser-Induced Breakdown Spectroscopy
LiDAR	Light Imaging, Detection, and Ranging
LMDE	Lunar Module Descent Engine
LOS	Line of Sight

LPO	Lunar Polar Orbit
LRO	Lunar Reconnaissance Orbiter
LROC	Lunar Reconnaissance Orbiter Camera
M ³	Moon Mineralogy Mapper
m _d	Dry Mass
MER	Mars Exploration Rover
m _f	Mass of the Fuel
MIP	Moon Impact Probe
MMH	Momethylhydrazine
MSL	Mars Science Laboratory
NASA	National Aeronautics and Space Administration
NASEM	National Academies of Sciences, Engineering, and Medicine
NiTi	Nickel Titanium
NTO	Dinitrogen Tetroxide
PDCP	Percussive Dynamic Cone Penetrometer
PSR	Permanently Shadowed Region
PLF	Payload Fairing
P _{max}	Maximum Power
PNG	Pulsing Neutron Generator
RFP	Request for Proposal
RTG	Radioisotope Thermoelectric Generator
RWA	Reaction Wheel Assembly
SAM	Sample Analysis at Mars
SKG	Strategic Knowledge Gaps
SLS	Space Launch Vehicle
STEM-RTG	Segmented Thermoelectric Modular Radioisotope Thermoelectric Generator
STK	Satellite Tool Kit
TOF	Time of Flight
USD	United States Dollar
VHF	Very High Frequency
WEB	Warm Electronics Box
ΔV	Change in Velocity
η _{max}	Maximum Efficiency

I. Team Structure

The overarching mission design was broken up into three main phases: problem definition/research, preliminary mission design, and final mission design. During the fall semester, the problem definition and historical research portions were completed, and the preliminary mission design begun. During the spring semester, the preliminary and final mission design were concluded. This report outlines the final design and the overarching design decisions.

To ensure the technical and organizational success of this team, the mission was broken up into six technical subsystems and a managerial team lead. This ensures cohesiveness within the mission design decision making process and efficiency in allocated work. The responsibility of the team lead is to direct the overall systems engineering of the design process and facilitate subsystem cooperation. This role is in place to provide a point of contact for the overall mission design and ensure key deadlines and requirements are met. Each technical subsystem had one lead, receiving support from other team members when needed. The team hierarchy is depicted in Figure 1.

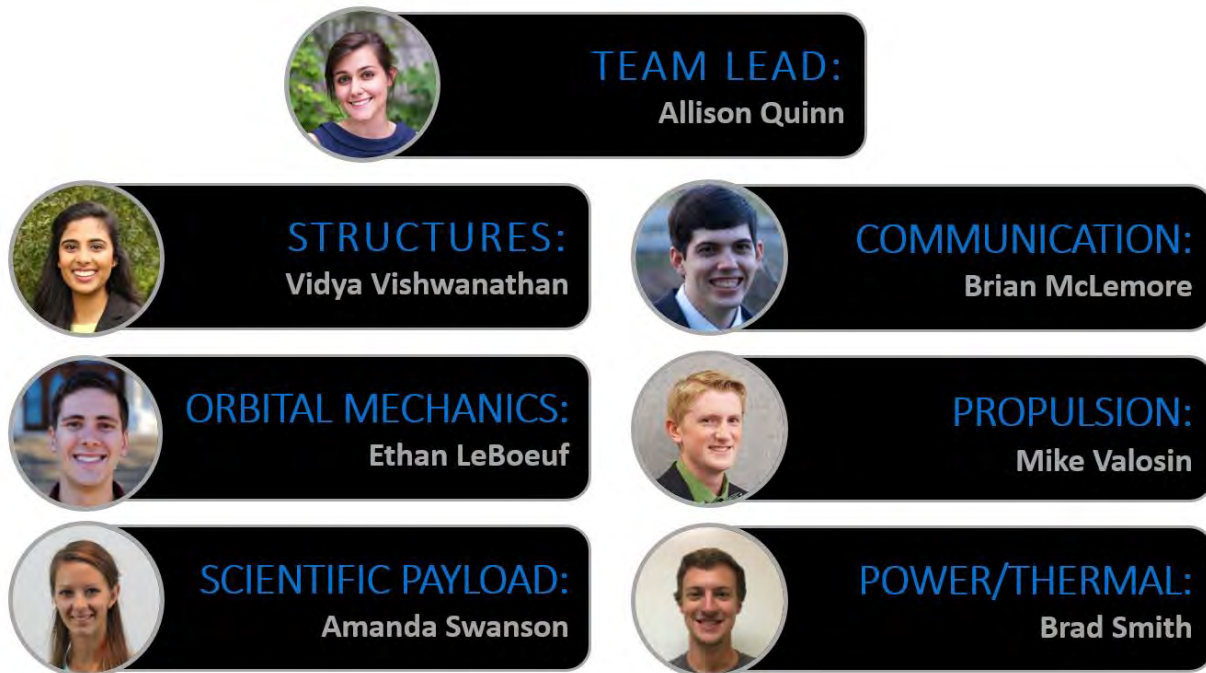


Figure 1: Project Penguin Team Hierarchy. This chart outlines each member of the design team as well as the subsystem they lead.

II. Introduction

A. Background & Motivation

American Institute for Aeronautics and Astronautics (AIAA) recently released a Request for Proposal (RFP) for a National Aeronautics and Space Administration (NASA) sponsored robotic mission to the Moon. The objective of this mission is to obtain water-to-regolith concentrations from two separate lunar craters. On December 11th, 2017, President Trump signed a new policy to facilitate government and industry efforts to put humans back on the Moon. “It marks a first step in returning American astronauts to the Moon for the first time since 1972, for long-term exploration and use. This time, we will not only plant our flag and leave our footprints -- we will establish a foundation for an eventual mission to Mars, and perhaps someday, to many worlds beyond” [1]. As NASA prepares for manned missions beyond Low Earth Orbit (LEO), water becomes an increasingly vital payload consideration to help sustain life in space for long periods of time. Water is necessary not only for sustaining human physiology, but also for growing food, maintaining suitable environmental living conditions, and in-space manufacturing of propellant. Utilizing planetary objects with high concentrations of water allows for less water, food, and propellant to be carried during the initial launch for long-range missions. NASA has proposed setting up incremental ports on the Moon, near-Earth asteroids, Martian Moons, and eventually the Martian surface to gradually advance human settlement. The initial mission proposed will determine concrete concentrations of water within lunar craters to confirm the findings of previous Orbiters and help ascertain future lunar gateway locations. If possible, the proposed mission will also provide additional scientific data to assist in future manned missions to the Moon and the fundamental understanding of the formation of the Moon.

Investigating the lunar polar environments is a priority according to the Committee on the Scientific Context for Exploration of the Moon from the National Academies of Sciences, Engineering, and Medicine (NASEM) [2]. Using robotic missions to investigate the possibility of volatiles at the bottom of polar, lunar craters is a precursor to the primary goal of beginning human lunar exploration. The committee ranks investigation of polar composition within the top five prioritized science goals; this information could provide fundamental understanding about history and formation of the Moon due to the presence of some of the oldest impact craters in the lunar poles. Additionally, NASA has a list of Strategic Knowledge Gaps (SKGs) regarding the moon. The ones addressed by this mission are

summarized in Table 1. The proposed mission aims to meet as many of the goals set by these organizations as possible, prioritizing the water deposit samples.

Table 1: Summary of NASA SKGs. NASA has proposed mission goals to explore the lunar surface to better understand the resource potential and formation of the moon [3].

NASA ID	Objective	Description
I-D Polar resources 3	Geotechnical characteristics of cold traps	Landed missions are required to understand regolith densities with depth, cohesiveness, grain sizes, slopes, blockiness, association and effects of entrained volatiles.
I-D Polar resources 4	Physiology and accessibility of cold traps	Needs landed missions to understand slopes, elevations, block fields, cohesiveness of soils, trafficability
I-D Polar resources 6	Composition, Form, and Distribution of Polar Volatiles	Water and possibly other exotic volatile species are present in lunar polar regions; must determine the form, concentration (including mineralogical, elemental, molecular, isotopic make-up of volatiles), and distribution of these species and how they vary from depths 0-3 m over distances of 10-100m scales. Required “ground truth” in-situ measurement within permanently shadowed lunar craters or other sites identified using LRO data.
I-E	Composition/Volume /Distribution/form of pyroclastic/dark mantle deposits	Need to understand the volatile contents of regional dark mantle deposits, as well as their depth and distribution in order to fully assay resource potential and develop useful processing technologies.

Previous lunar Orbiters, such as the Indian Space Research Organization (ISRO) Chandrayaan I and NASA’s LRO, have already found evidence of water and hydrogen in lunar craters. Chandrayaan I was a lunar remote sensing Orbiter that was designed to orbit the Moon over a two-year period. Chandrayaan’s primary objectives were to generate a 3D atlas of the Moon’s geography, perform high spatial resolution chemical and mineralogical mapping of the lunar surface, and detect regions of high concentrations of water [4]. To find lunar water, Chandrayaan was equipped with the Moon Minerology Mapper (M³) and Moon Impact Probe (MIP) [5]. The M³ was an imaging spectrometer designed by research teams at Brown University and NASA JPL to characterize and map the lunar surface composition [6]. The most significant discovery M³ made was of the existence of water molecules at both the lunar poles. The MIP, designed by ISRO, was released from the Orbiter and performed an impact landing in the Shackleton Crater [7]. The probe impacted into the regolith and released soil that was then analyzed by the orbiting Chandrayaan I, confirming the existence of water [7]. The LRO used the Lyman-Alpha Mapping Project (LAMP)

sensor to find ice in the craters on the lunar south pole. The LAMP data discovered ice deep in the craters using ultraviolet light from the stars and hydrogen atoms spread throughout the solar system [8]. The LRO mission also took detailed images of the Moon and created topographical maps using a laser altimeter. The data from the LRO and Chandrayaan I has provided future Moon missions vital information regarding landing sites and locations of higher water concentrations. The crater locations for the proposed mission are based off the findings from these spacecraft. The topographical maps from LRO provide resources to determine landing locations inside craters that are permanently shadowed. Both Chandrayaan and LRO measured data using visual sensors from an Orbiter. The proposed mission will help quantify the exact ratios of water-to-regolith from the surface of lunar craters.

B. Problem Definition

The proposed mission is in response to an RFP from AIAA concerning a NASA sponsored robotic lunar prospecting mission to obtain information on water deposits in lunar craters. Specifically, the objective of the mission is to obtain water-to-regolith ratios from two separate lunar craters while maximizing the output of scientific data. Specific data regarding the concentration of water within lunar craters is a precursor to in-space gateways to decrease the water, food, and fuel payloads necessary for long-term manned missions. This section outlines the scope and constraints involved in this mission.

C. Scope

Several deliverables are required to fully meet the objectives of the mission set by AIAA and NASA in the RFP and the self-imposed constraints of the mission. The detailed design and operation of the following elements are within the scope of the mission: the overall spacecraft/rover structure, the communication system, the instrumentation system, the propulsion system, the power system, and the thermal system. In addition, the overall mission operation, including orbital mechanics and data transfer schedules, must be outlined. These elements are to be designed to optimally meet the goals and objectives of the mission while fitting into the constraints specified by the RFP. Priority is placed on the explicit instrumentation and scientific measurements to be obtained in the duration of the proposed mission. To comply with these requirements, there will be an emphasis on methods of determining scientific information, including data acquisition schedules, geological studies, and environmental impacts. The motivation behind all design decisions must be articulated, along with technical analysis to support the decision.

As previously mentioned, this mission design is broken up into three phases to complete the mission within the scope outlined: problem definition/research, preliminary mission design, and final mission design. This report outlines the overarching design decisions and final mission design.

D. Requirements

The primary objectives for this mission are constrained by the customer requirements outlined in the AIAA RFP and Figure 2. The purpose of the mission is to determine water-to-regolith ratios at two separate lunar craters with a budget of \$500 million by December 31st, 2024. In addition to obtaining the ratio, the mission must maximize the scientific return with the given budget. The decision was made to design the mission to utilize the full \$500 million and obtain as much scientific data as possible.

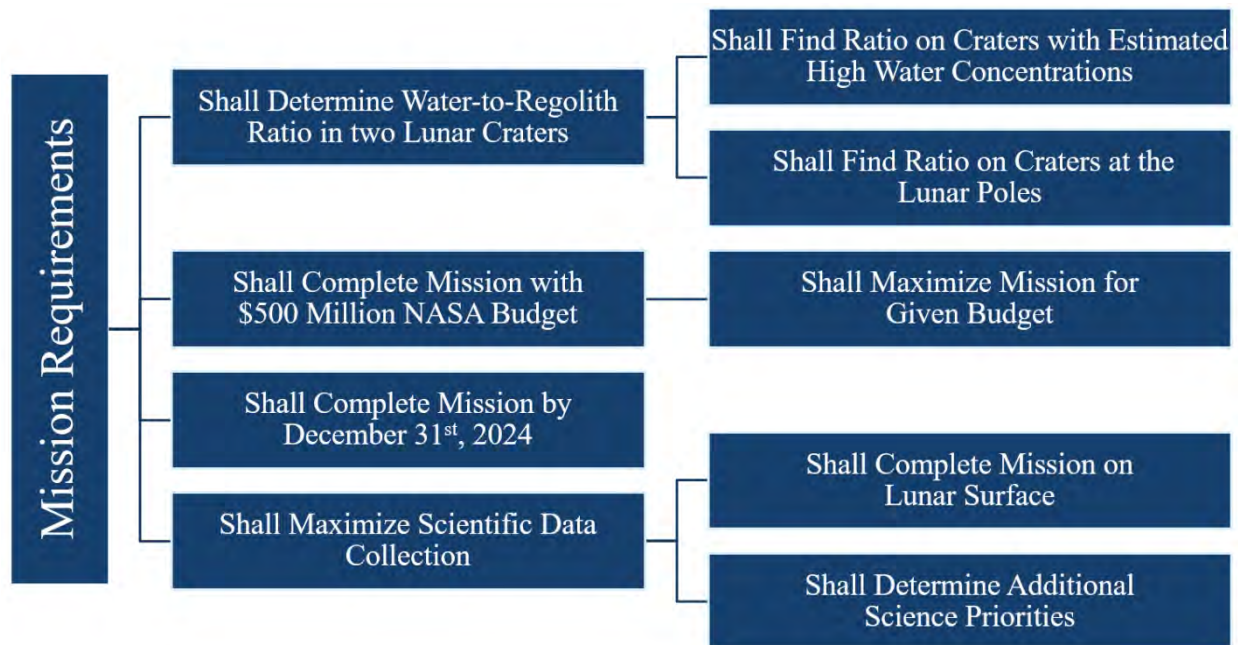


Figure 2: Customer requirements from AIAA. The figure displays the customer requirements given for the project from AIAA and some of the overall derived requirements for the mission.

Given the scientific need of the mission, primary consideration was given to the crater location and selection. The regional location of these craters and their proximity relative to one another affects the design of the robotic vehicle transport. Additionally, this alterable affects the selection of the scientific payload and associated apparatus as consideration must be given to water deposit depth within the crater, and exposure to sunlight. Lunar craters that are older and deeper are more likely to contain greater concentrations of water due partially to the extreme shadow

coverage [9]. According to the National Academies of Sciences, Engineering, and Medicine, these craters exist primarily in the lunar south pole [9]. Thus, to ensure maximum scientific output, the crater selection was limited to polar craters.

As previously stated in Section II.A, there have been several missions to the Moon to obtain similar data (water concentration, composition, topography) to this mission. These missions all used Orbiters to optically obtain scientific data, while sometimes using impact probes to confirm images obtained from orbit. Due to this plethora of orbital data, this mission was constrained to obtaining scientific data on the surface of the Moon, rather than sending additional Orbiters. Constraining the mission to the lunar surface allows for the mission to confirm findings of orbital missions with alternative measurement techniques while obtaining data that cannot be measured from orbit, such as the geotechnical properties of the regolith and the stratigraphy to understand the formation of the Moon.

E. Crater Location

The first step in planning a mission to prospect concrete locations of water on the moon was to determine the craters to investigate. The location, topographical characteristics, and history of each crater greatly impact the proposed mission timeline, architecture, and orbital trajectory. The proximity of the two chosen craters to one another dictates whether the mission can be done with a single system traversing to each crater.

The Moon has a small, low density atmosphere, which coupled with the extreme temperature fluctuations makes the presence of liquid water impossible. The presence of water in the form of ice has mainly been detected in the Moon's Permanently Shadowed Regions (PSR) where the temperature is constantly cold and the ice cannot thaw. PSRs are located in deep craters predominantly in the south pole and around the equator. LRO's Lyman-Alpha Mapping Project (LAMP) instrument searched the surface of PSRs for ice illuminated by interplanetary hydrogen emission, known as Lyman-Alpha line. The Lunar Exploration Neutron Detector (LEND) instrument created a map of the water equivalent hydrogen distribution. Lunar Crater Observing and Sensing Satellite (LCROSS), which accompanied the LRO, was also equipped with water detection sensors for its journey through the plume of gases related by the impact of the Centaur upper stage into the Cabeus crater [10].

Using data from LRO, the list of potential craters to visit on this mission was narrowed to South Pole PSRs, specifically Haworth, Cabeus, Shoemaker, and Shackleton. Next, other parameters were considered including

proximity to other craters, diameter of the crater, and slope of the crater. The proximity of these craters to others is vital if the mission were to use one system to complete the mission and it fails to traverse from one crater to the next. Transit time between craters limits the distance the systems can travel before the mission requirement to find the water concentration at two lunar crater by end of year (EOY) 2024. Transit time is also driven by the diameter of the crater. To maximize scientific data return and map each crater for specific water deposit locations, the system will have to take measurements throughout the entire crater no matter the size. Lastly, the gradient of terrain will drive the system design as the system may have to traverse through steep and rough terrain.

Using the information gathered from previous lunar missions, possible locations were investigated. Figure 3 shows the craters at the South pole that were initially selected from the investigation into LRO's LEND data, shown in Figure 4 [11]. A trade study was performed using an Analytical Hierarchy Process (AHP) with the parameters previously outlined: concentration of water, diameter, proximity to other craters, and relative slope. Haworth and Shoemaker craters were selected for the mission due to their high concentration of water, as shown in Table 2. Cabeus, while also high in water concentration, was not chosen partially due to the previous LCROSS investigation. In order to maximize the scientific data return from this mission, craters that had not previous been visited were chosen.

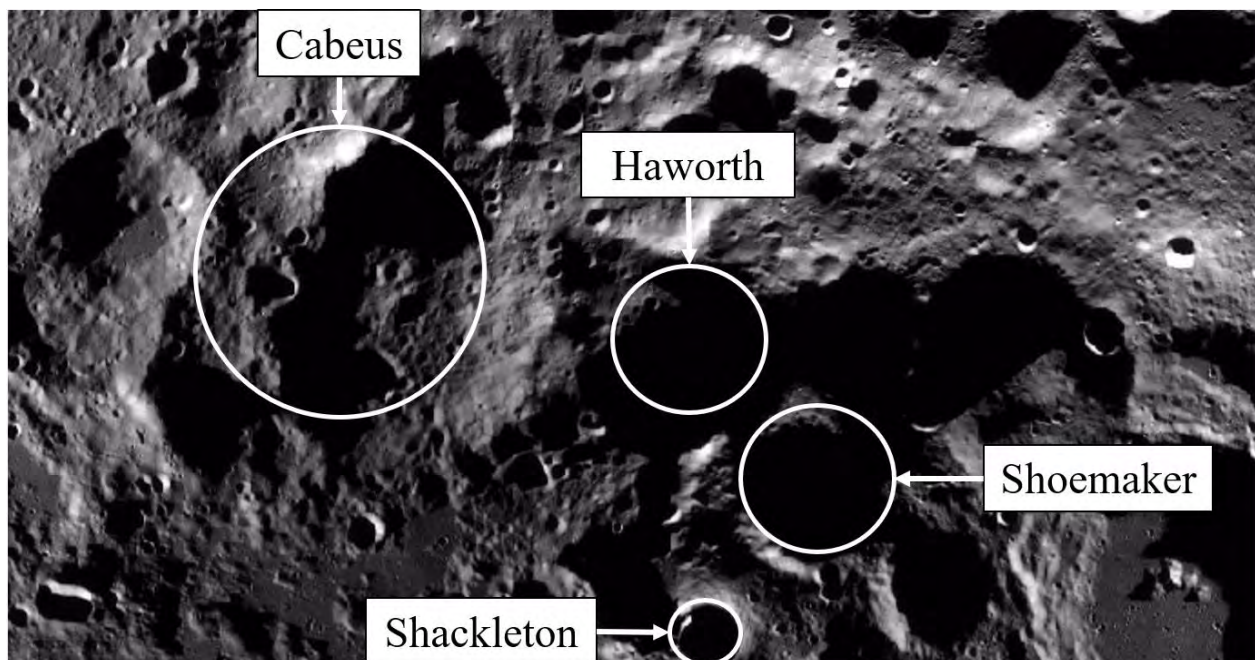


Figure 3: Labeled craters locations for South pole. The LROC imaged the Moon using two narrow angled cameras and a wide angle camera to obtain high resolution photographs for lunar mapping. This image depicts the South pole of the Moon, with Cabeus, Haworth, Shoemaker, and Shackleton craters labeled [11].

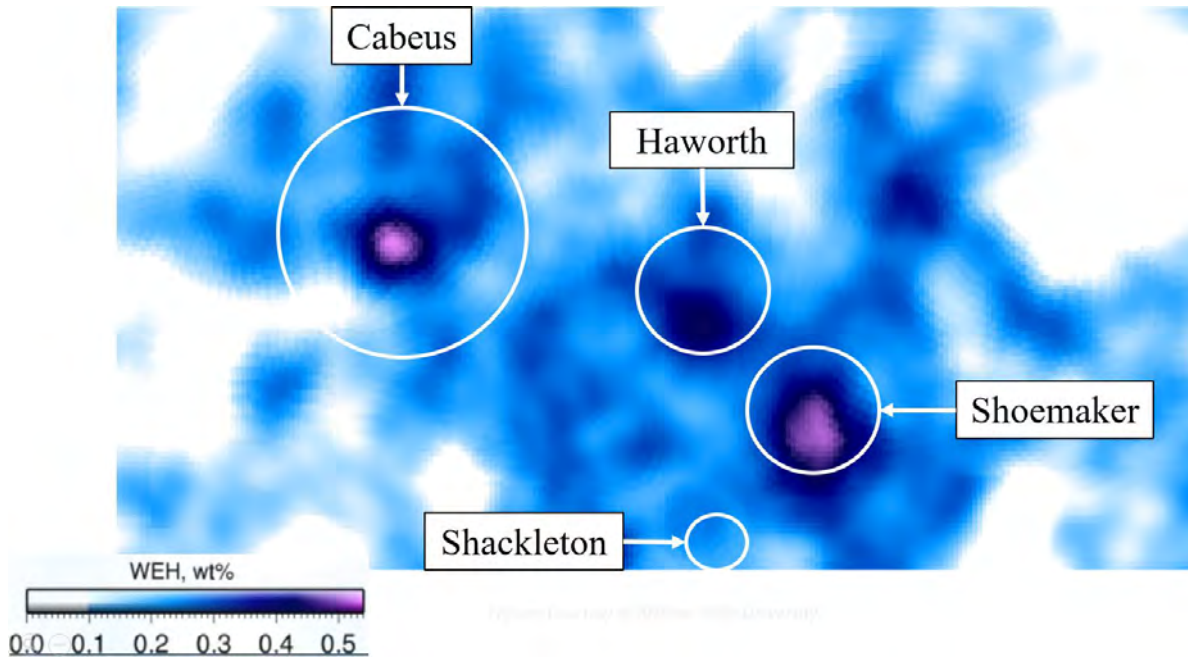


Figure 4: Labeled craters with LRO LEND data overlaid. The LEND instrument onboard the LRO mapped the water equivalent hydrogen distribution around the South pole of the Moon. This data is superimposed on Figure 3 to show the probable locations of water in correlation to the craters [11].

Table 2: The trade study used to determine which lunar craters this mission would investigate. The parameters chosen to determine these craters reflected the importance of obtaining valuable scientific data, while maintaining mission feasibility in mapping each crater and reducing mission risk. Haworth and Shoemaker craters were chosen for this mission.

Parameters	Slope	Proximity to Other Craters (avg km)	Diameter (km)	Amount of Water (WEH, % wt)
Weight	0.193	0.233	0.252	0.321
Shackleton	0.20	99.57	21	20
Cabeus	0.04	132.13	98	90
Shoemaker	0.10	94.70	50.9	90
Haworth	0.14	84.60	35	70

Total	
Shackleton	5.204
Cabeus	7.194
Shoemaker	7.663
Haworth	7.292

III. Mission Architecture Decision

To complete the robotic portion of the mission and successfully find the water-to-regolith ratio in two craters, various mission architectures were considered. By adding the self-imposed constraint of limiting the crater location to lunar poles and self-imposed goal of transporting between two separate craters within two years, it allowed for mission architectures to be designed. Each of the mission architectures considered include an Orbiter to relay data to and from

the lunar-surface vehicle and Earth. This was chosen to maximize the communication opportunity with the lunar-surface vehicle to maximize data transfer and control of the vehicle. Many feasible ideas were generated and evaluated based on the guiding parameters outlined in Section II.D using an AHP. The results from the trade study (seen in Table 3) indicated two top solutions for the mission: landing two rovers in two different craters to collect data and launching several pods from the Orbiter with small instrumentation into the desired craters. The top two solutions are looked at more in depth below.

Table 3: Trade study for the overall mission architecture. The Table below shows the determination of the best overall method of obtaining water-to-regolith samples at two separate lunar craters. Clearly, the two rover system won the quantitative decision-making process.

Parameter	Time (days)	Cost (\$ mill)	Power (W)	Mass (kg)	Risk	# of Samples
Weight	0.33	0.18	0.04	0.12	0.29	0.04
One Rover	30	25	20	50	3	50
Two Rover	0	50	40	100	1	100
Propelled Rover	1	70	800	300	5	70
Mechanical Bouncing Rover	13000	0.003	30	10	9	3
Orbitally Launched Pods	0	0.036	12	10	7	20

Total	
One Rover	5.89
Two Rover	9.28
Propelled Rover	7.09
Mechanical Bouncing Rover	3.83
Orbitally Launched Pods	7.54

A. Two Rover System ConOps

The Concept of Operations (ConOps) of the two rover mission architecture can be seen in Figure 5. A spacecraft consisting of an Orbiter and two lander/rover systems will initially be launched into an Earth parking orbit (Stage 1). The spacecraft will then use in-space propulsion to transfer into a 30 km lunar parking orbit (Stage 2-3), where the Orbiter will deploy the two landers to land in the two previously chosen polar craters where they will deploy their rovers (Stage 4). Simultaneously, each rover will traverse their respective crater and collect water-to-regolith ratios throughout the crater (Stage 5). Finally, the rovers will transmit their data up to the Orbiter, which will transmit this data back to Earth (Stage 6).

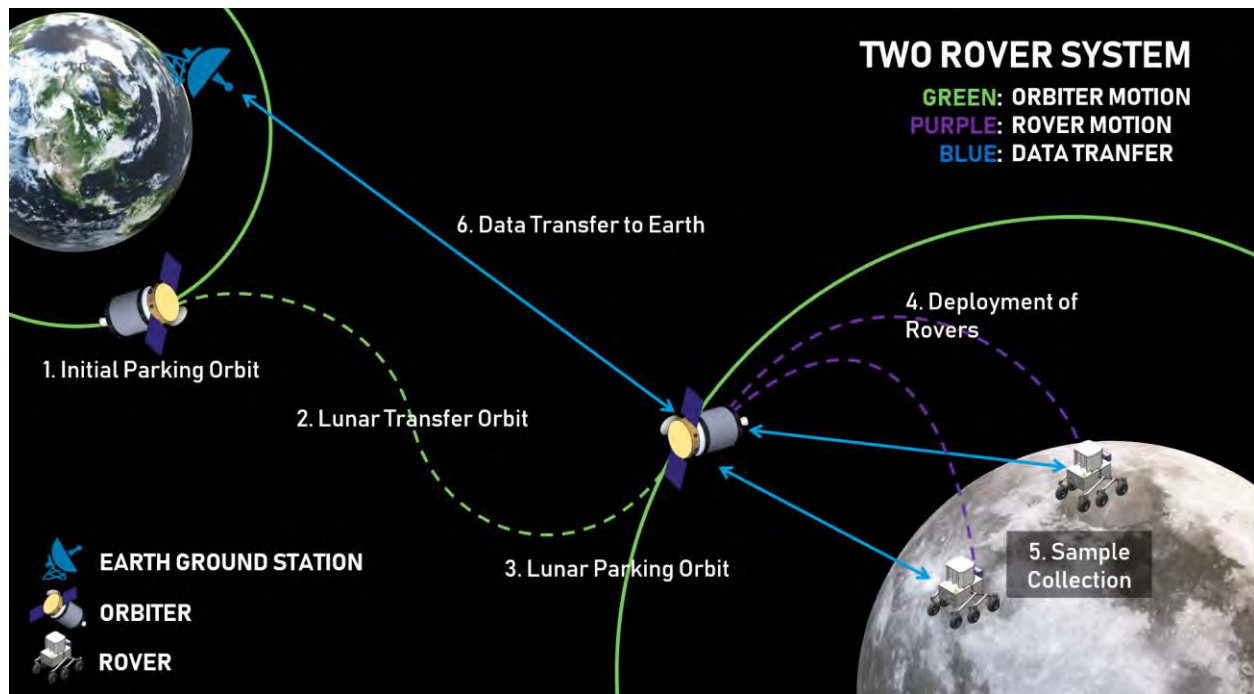


Figure 5: ConOps for the Two Rover Mission Design. This figure depicts the overall mission design concept using two rovers to simultaneously collect samples from two different craters. The scientific data collected from these two rovers will be relayed to the Orbiter, then from the Orbiter to the Earth ground stations.

This mission architecture performed exceptionally well in the trade study due to the lack of travel time between craters, the ability to continually take data for the duration of the rover’s lifetime, and the reduced risk of failing to complete the mission. Since an objective is to maximize the science data returned, using rovers which can be equipped with extra instrumentation would maximize that performance parameter. Due to the steepness of the crater walls, the rovers must be equipped with an advanced wheel or climbing system to allow for measurements to be taken outside of the two chosen craters. Since the mission objective only requires that water-to-regolith ratios from two craters, the steepness of the craters did not greatly impact the decision making process.

B. Pod System Launched from Orbit ConOps

The second design chosen, depicted in Figure 6, consisted of small pods descending to the lunar surface to collect samples. Consistent with the two rover design, the pods and distribution structure would be carried to lunar orbit by the Orbiter through cislunar space (Stages 1-3). Once in a lunar parking orbit, the Orbiter will release the distribution structure to begin descending towards the lunar surface using decaying orbits (Stage 4). Once at an altitude close to the lunar surface the distribution structure will fire retrorockets to slow its descent. This will allow for the pods to be

ejected from the structure and impact the lunar surface at a much lower velocity than if they were dropped from orbit (Stage 5). The pods will individually sample data and relay the data back to the Orbiter (Stage 6). The Orbiter will then transfer the information back to Earth (Stage 7).

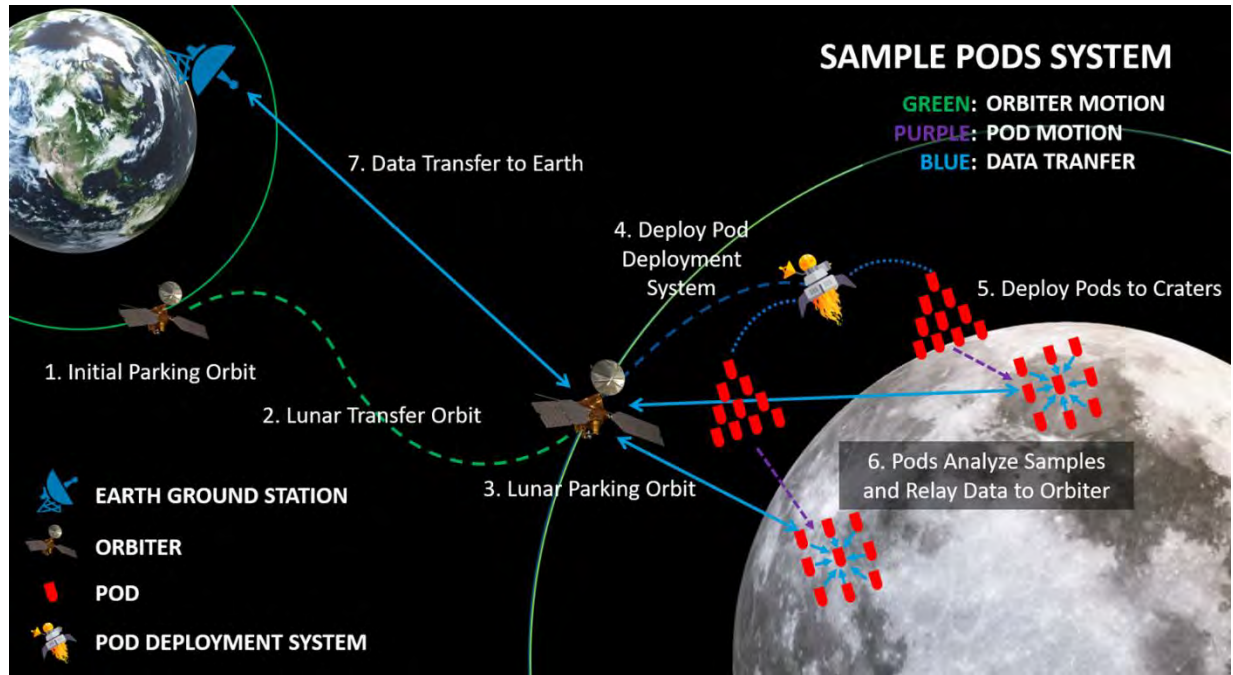


Figure 6: ConOps of the Pod System Launched from Orbit. The figure depicts the spacecraft and Orbiter moving from an Earth parking orbit to a lunar parking orbit, then launches a deployment system. The deployment system deploys the pods into specific craters. Each pod will collect samples and then transfer the data back to Earth.

The mission architecture calls for twenty total pods - ten for both of the crater destinations. These pods will be designed to withstand the hard landing and burrow throughout the crater to provide water-to-regolith measurements from various locations. This allows for the pods to collect samples below the lunar surface where ice may be more prevalent. Two types of pods will be sent to the surface: sample collection pod and data transfer pod. For each crater, one data transfer pod will be sent to the center of the crater and the nine sample collection pods will be located around the center. The sample collection pods will contain a drill, sample measurement device, antenna, and a computer to analyze the data. The antenna on the sample collection pod will be less powerful to reduce costs; therefore, all data will be sent to the data transfer pod for communication to the Orbiter. The data transfer pod will consist of a larger antenna, receiver, and a computer to command the sending of data to the Orbiter. The data transfer pod will use its larger antenna to send the data from the nine sample collection pods to the Orbiter during its passes.

This design was ranked second in the AHP due to its innovation, ability to robustly take samples simultaneously, and redundancy in measurements. However, unlike the rover options, there is a finite amount of data able to be taken using these pods since they are unable to move around the lunar surface.

C. Summary

While both design options allow for scientific data collection and fit within the parameters of the proposal, the two rover design allows for the largest amount of flexibility within the instrumentation design and minimal risk in meeting the overall mission objectives. In addition, the two rover architecture gives more opportunity for sample collections throughout the crater to give a mapping of the water-to-regolith ratio. The two rovers also considerably lower the risk associated with the mission. Rover missions have been very successful over multiple missions and the pod technology would be a new way to explore the lunar surface. While novel, the risk of the pods does not correspond to increased return over the two rover design, therefore the two rover mission architecture was chosen as the final design

IV. Executive Summary

As NASA looks forward to expanding humanity beyond Earth's gravity, steps must be taken to better understand the solar system and ease humanities transition into settlement on another planetary object. When planning human settlement, the most important payload consideration is life support to sustain humans in the unforgiving void of space and propellant to push humanity millions of miles from Earth. Water is the common thread between nutrition, thermal systems, and propulsion. If humans could acquire water from incremental planetary gateways, the initial payload cost would dramatically decrease. Therefore, NASA is contracting a mission to concretely determine locations on the Moon, the first interplanetary gateway, with water rich regolith. The mission requires completion by the end of 2024 with a budget of \$500 million. This paper outlines a mission to fulfil and exceed these requirements called Project Penguin.

As previously stated, the mission is constrained to lunar, polar craters for the purpose understanding more about the polar environment on the lunar surface. The lunar south pole is currently considered one of the coldest regions in the solar system, as the deepest parts of shadowed craters can reach down to 20 K. Project Penguin was chosen as the mission name because penguins are indigenous to Earth's south pole, living in some of the coldest environments on the planet. To stay warm, penguins are equipped with an insulating layer of feathers and huddle together to reduce

heat loss. The spacecraft proposed will be residing in the coldest region of the Moon, having a sophisticated thermal system, like the penguin, to stay operational.

On January 7th, 2023, a SpaceX Falcon 9 will launch from Earth carrying a 4654 kg spacecraft to GTO. The spacecraft, or the Orbiter, will house two landers each containing one rover and connected to the spacecraft by pyrotechnic rings. The spacecraft will use a monomethylhydrazine (MMH) and Dinitrogen Tetroxide (NTO) bipropellant propulsion system to place itself into a highly elliptical orbit with three burns, eventually burning into a lunar polar orbit. The burn times are outlined in Table 4 below. Once in a lunar polar orbit, the Orbiter will communicate to Earth via the DSN to determine when to begin the Entry, Descent, & Landing (EDL) maneuver with each lander. When the Orbiter receives the sign from Earth, the EDL of Lander 1 will begin the deployment of the lander via pyrotechnic rings. The first lander will then fire a MMH and NTO propulsion system and begin 3 burns to the lunar surface, described in Table 4. The lander, equipped with a Light Imaging, Detection, and Reduction (LiDAR) imaging sensor to determine a flat landing location within Haworth crater, will cease burning its engines 1 meter above the lunar surface, freefalling with an initial velocity of 2.5 meters per second. Aluminum honeycomb legs will absorb the impact of the fall, keeping the rover inside intact. Once on the lunar surface, the lander will deploy a ramp for the rover to drive down. Rover 1, landing in the stowed position, will transfer to the traverse position and drive down the ramp and onto the lunar surface.

Table 4: Mission Segment Breakdown. The table details the Time of Flight (TOF) and ΔV for the various mission segments for the Orbiter and Landers.

Mission Segment Orbiter	TOF (hours)	ΔV (m/s)	Mission Segment Lander	TOF (hours)	ΔV (m/s)
Initial GTO Orbit	10.6	N/A	Burn 1	0.02	44
Burn 1	0.6	240	Phasing	2.5	N/A
Elliptic Transfer Orbit 1	17.9	N/A	Burn 2	0.1	204
Burn 2	0.55	240	Flight to 30 km	0.65	N/A
Elliptic Transfer Orbit 2	41.5	N/A	Final Burn	0.041	1781
Burn 3	0.51	240			
Transfer to Moon	72.5	N/A			
Burn into Polar Orbit	1.50	871			
Polar Orbit	Indefinite	N/A			

Each rover is equipped with a Radioisotope Thermoelectric Generator (RTG) to provide power and thermal support in PSRs, instruments to determine scientific data, a camera and a LiDAR system to provide guidance and navigation, avionics to process data, and a communications system to relay information back to the Orbiter. Using the instruments on board, each rover will be able to obtain the water-to-regolith ratio, determine the full chemical composition of the surface, the geotechnical properties of the regolith, and the stratigraphy of the lunar crust, exceeding the requirements of the mission and maximizing the scientific data collected over the course of the mission. Initially, Rover 1 will plan a path using the on-board navigation system and traverse out of the contamination area from the Lander 1 engines. Rover 1 will then begin scientific data collection. Using the NASA standard of taking samples in groups of five, 10 meters apart, Rover 1 will traverse the crater similar to the path depicted in Figure 7. Rover 1 will communicate with Earth via the Orbiter to guide the overall trajectory of the rover every day to ensure full coverage of the Haworth crater. Data, initially stored on the rover computer, will be sent back to Earth when the Orbiter is in sight overhead.

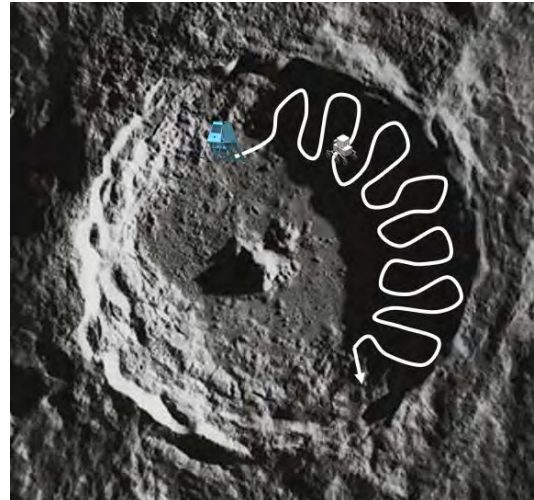


Figure 7: Lunar Crater Operations Mapping. *The image depicts the general mapping pattern of the rover in the PSRs.*

Once the normal operations of Rover 1 have begun, the Orbiter will receive the signal from Earth to launch Lander 2 in the same method as Lander 1, only headed to Shoemaker crater. Rover 2 will begin operations in the same fashion as Rover 1 on Shoemaker crater.

Similar to Opportunity and Spirit, both Rover 1 and Rover 2 will continue mapping their respective craters until a full map of each crater is created, which is estimated as 345 days, or until the end of 2024. If at the end of this time Rover 1 and Rover 2 are still operational, a request will be submitted to NASA to continue the lunar surface operations, possibly attempting to drive the rovers out of their craters. If no funding extension is accepted, Rover 1 and Rover 2 will transition to stowed mode and turn off all idle functions while the Orbiter will impact into Shoemaker crater.

V. Lunar Surface

The design of Project Penguin was completed in three distinct phases, beginning with the operations on the lunar surface. As outlined in previous sections, the mission requirements will be completed by landing a rover into both Haworth and Shoemaker crater.

A. Requirements

To complete the objectives outlined in Figure 2, a requirements flowdown was generated for the rover, as depicted in Figure 8. The driving factors for the rover design were the instrumentation to acquire scientific data. These instruments would dictate the size, weight, power supply, and environmental conditions of the rover while fulfilling the requirements to determine the water-to-regolith ratio and maximizing scientific data return. Additionally, the rover was required to traverse within PSRs of the lunar surface. This required the system to function without sunlight in extremely cold environments, while withstanding regolith dust.

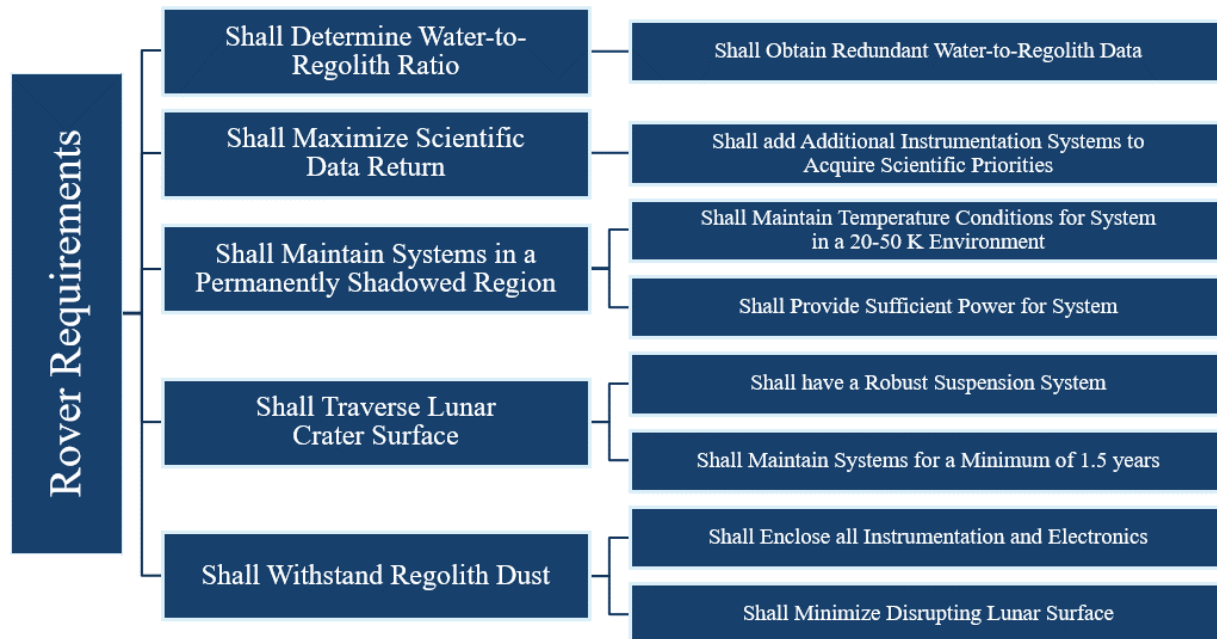


Figure 8: Requirements Flowdown for the Rover System. The figure depicts the main requirements that dictated the design of the rover system.

As the Moon lacks a significant atmosphere, the top layer of lunar regolith is often exposed to micrometeorites, that causes the soil to break down into sharp fragmented particles, and solar wind irradiation, that inflicts a static charge causing the particles to attach to surfaces [12]. The existence of lunar dust was an issue on the Apollo missions

as the jagged particles often scratched equipment and in other cases causing them to retreat [13]. Lunar dust plumes that are generated from Lander impact and Rover traversing poses as a risk as the dust could jam equipment, thus negatively impacting on board instrumentation and mechanical parts. Thus, it is a mission requirement to develop a rover design that implements a dust mitigation procedure to maximize mission performance.

B. System Overview

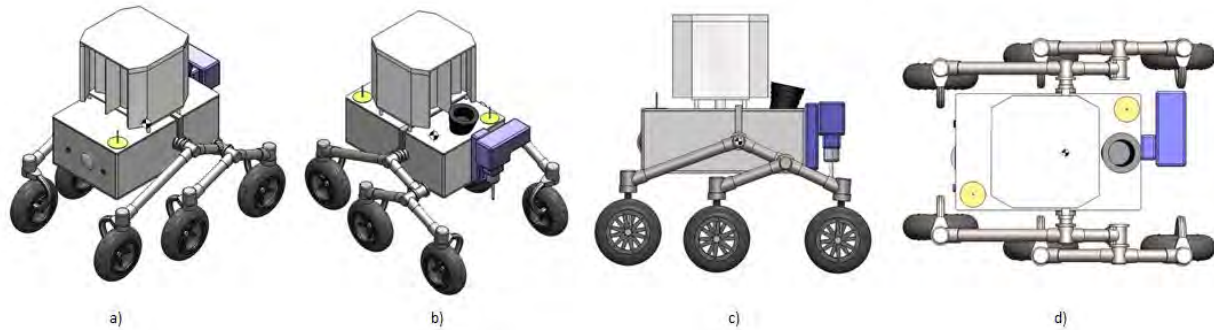


Figure 9: Engineering Views of the Lunar Rover Exterior. Engineering perspectives of the exterior of the lunar rover are shown; a) front isometric view, b) back isometric view, c) left view, d) top view. Note the center of mass is shown in the figures and is in line with the main pivot of the rocker-bogie system.

As mentioned in the Section II.E to complete the mission requirements, Project Penguin will send a rover to both Haworth and Shoemaker crater. The rover designs themselves are identical to one another to allow ease of manufacturing and lander design. Figure 9 depicts the mission's rover concept design. Given the existence of very dense lunar regolith on the surface as well as extremely cold temperatures due to the lack of sunlight within the crater depths, the main considerations and constraints for the Rover design were environmental, as evident in Figure 8. The rover needed to be designed to allow for optimal heat distribution as well as ensure the capability to traverse across a dense terrain. The following sections of this report will further elaborate on each of the Rover's components by subsystem.

C. Rover Instrumentation

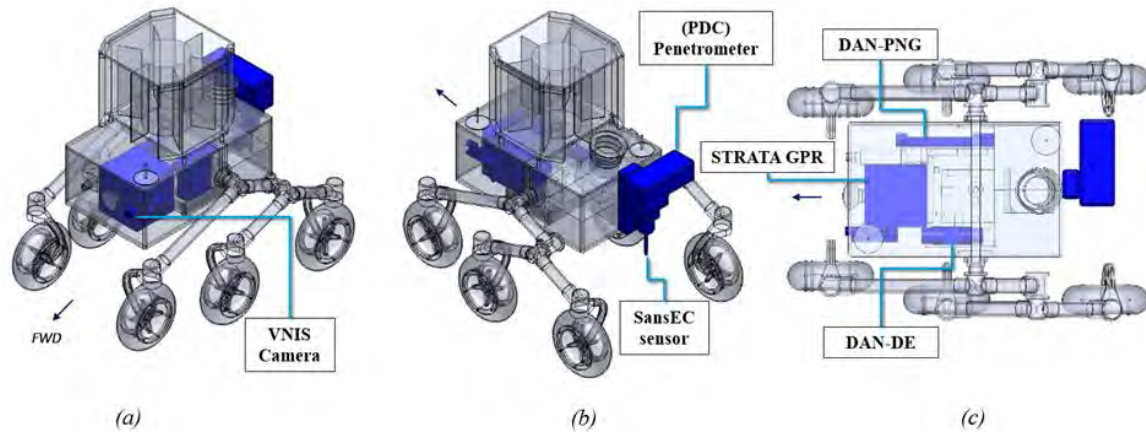


Figure 10: Lunar Rover Scientific Instrumentation Components. These engineering views, (a) isometric front, (b) isometric back, (c) top views, are shown with the rover's instrumentation components highlighted.

The primary instrumentation for the rover, depicted in Figure 10, was selected by reviewing historical approaches to finding water on extraterrestrial bodies, such as the Mars Science Laboratory (MSL), Curiosity. These instruments included the Sample Analysis at Mars (SAM), an instrument suite consisting of a Gas Chromatograph, a Quadrupole Mass Spectrometer, and a Tunable Laser Spectrometer capable of analyzing atmospheric and powdered rock samples to characterize organic and inorganic molecules [14]. Another is the ChemCam, which utilizes Laser-Induced Breakdown Spectroscopy (LIBS) to analyze samples for their full chemical composition from a distance [15]. Lastly is the Dynamic Albedo of Neutrons (DAN), which used a Pulsing Neutron Generator (PNG) to find subsurface ice deposits [16, 17]. In addition, three unique concepts were also explored: an oven-weighing system, an Arduino moisture sensor, and a SanSEC sensor [18].

In addition, three unique concepts were also explored: an oven-weighing system, an Arduino moisture sensor, and a SanSEC sensor [18]. The oven-weighing system would collect a physical sample and weigh it. Then the sample would be heated to evaporate all water present in the sample, before weighing it again to calculate the concentration of water. The Arduino sensor would be a low cost solution that could take off-the-shelf components to measure the water concentrations. This option was most viable with the pod mission architecture when many instruments would be required. And lastly the SansEC sensor is a NASA developed open-circuit, dielectric, spectroscopic sensor that uses electric and magnetic fields to determine the physical properties of a sample [18].

By performing a trade study using an AHP in Table 5, each of these ideas were investigated and ranked against one another on metrics such as mass, size, power requirement, complexity, and scientific data obtained. An important consideration when selecting the primary instrument was considering the dust’s corrosiveness and the impact it would have on the instruments. Choosing a remote sensing system that didn’t require a physical sample collection became a driving factor to reduce complexity of the system. Also, to maximize the scientific data obtained from these measurements, systems that produced results throughout a depth, instead of only surface investigations were ranked more favorably.

Table 5: Trade Study to Determine Primary Scientific Instrument. This trade study, completed using an AHP, was utilized to determine that the DAN instrument was the best option for the primary instrument for this mission due to the size, complexity, and ability to determine water to regolith ratios without disrupting the lunar surface and kicking up regolith dust.

Parameters	Mass (kg)	Size (cc)	Power Required (W)	Complexity	Scientific Return
Weight	0.10	0.05	0.20	0.45	0.20
SAM	40	41300	50	2	7
ChemCam	5.6	8900	3.9	5	7
DAN	4.7	4500	17.5	9	6
Oven/Weighing System	20	30000	41.7	4	2
Arduino System	1	10	4	2	3
SansEC on Penetrometer	0.1	1	0.2	7	6



Total	
SAM	3.06
ChemCam	6.49
DAN	8.14
Oven/Weighing System	3.540
Arduino System	4.93
SansEC on Penetrometer	7.640

Based on the evaluation shown in Table 5, the DAN was selected as the primary instrument for determining the water to regolith ratio. The DAN consists of two components, the PNG and the Detectors and Electronics (DE), shown in Figure 11. This instrument works by focusing a beam of neutrons into the surface using the PNG. Since hydrogen slows down neutrons, the reflected neutrons will be slower if they encounter water-logged minerals. The DAN-DE unit measures the die-away time after each neutron pulse to develop a hydrogen distribution profile throughout a one to three-meter depth. DAN is capable of finding subsurface ice deposits as low as 0.1% [16].

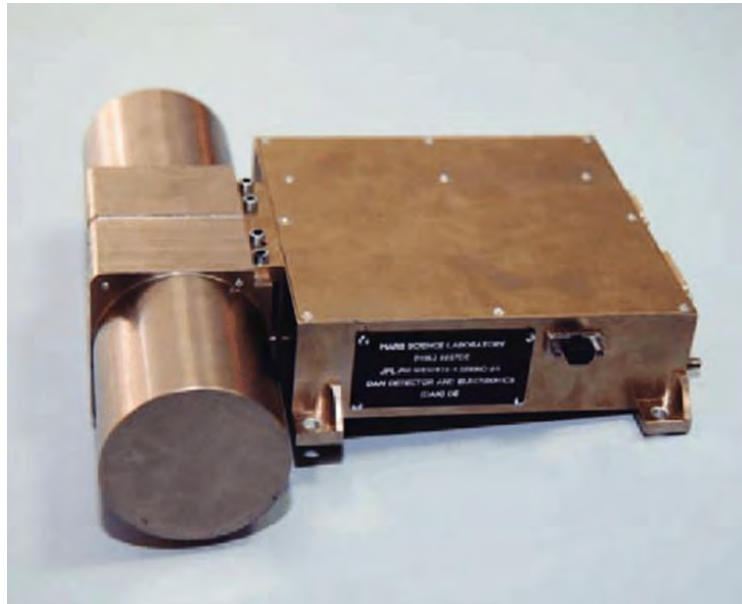


Figure 11: DAN-PNG and DAN-DE instruments. This instrument will serve as the primary method for detecting water concentrations within the craters [16].

For redundancy, two secondary instruments were selected to determine the water-to-regolith ratio. The SansEC sensor, seen in Figure 12, also rated highly using the AHP, and thus was selected to be attached to a penetrometer so that it can take measurements as the penetrometer moves 0.7 m through the surface. The SansEC sensor is a thin film, open circuit made of electrically conductive material. During sample collection, the sensor transmits a harmonic to induce an electromotive force in the sensor. A time history of the sensor's magnetic field response is recorded for the harmonic nearest the resonant frequency to determine the measured physical property [18]. Additionally, a near infrared camera similar to the VNIR/SWIR from the China's Yutu rover on the Chang'e-3 mission will be used to determine the full chemical composition of the surface [19]. The Infrared (IR) camera, shown in Figure 13, will also be used to address a NASA SKG regarding the physiography and accessibility of the craters by understanding the slopes, elevations, and trafficability [3].

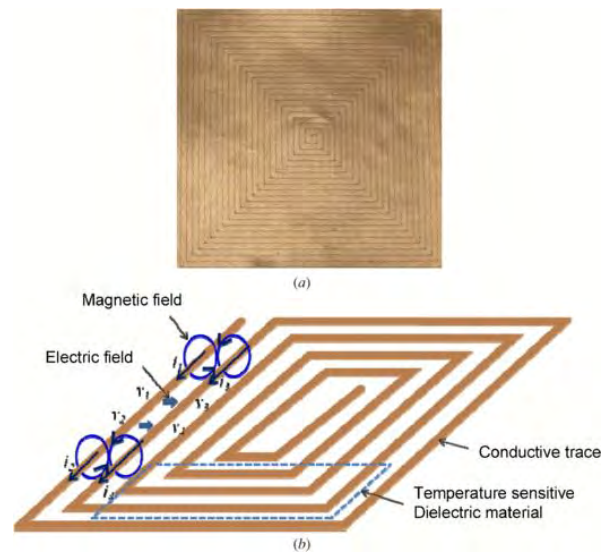


Figure 12: SansEC sensor used for redundancy in the water concentration measurement. This is a NASA developed sensor that uses electric and magnetic fields to measure the physical properties of the substance in contact with the sensor. It will be mounted on the tip of the penetrometer [18].

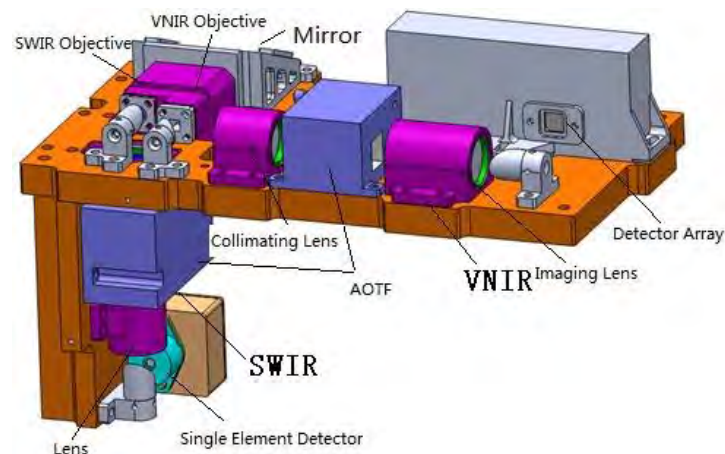


Figure 13: VNIR/SWIR instrument from the Chinese Yutu rover. This instrument will be used to determine the full chemical composition of the surface, including the water concentrations by using a spectrometer [19].

To comply with the mission objective to maximize the scientific data obtained during this mission, additional tertiary instruments were also included on the rover. Two additional instruments were chosen after researching the NASEM priorities and NASA's SKGs. The Percussive Dynamic Cone Penetrometer (PDCP) tested on the NASA Ames K-10 rover, shown in Figure 14, will be used to measure the geotechnical characteristics of the cold traps. The percussive variant of this instrument was chosen to reduce the force and power required to penetrate the surface, while maximizing the penetration speed [20]. The STRATA GPR will be similar in design to the instrument in Figure 15. It will be used to determine the subsurface stratigraphy to depths of 10-15 meters [21]. It

will also provide information on the depth of regional dark mantle deposits to further understand the volcanic nature of the moon's formation [3].

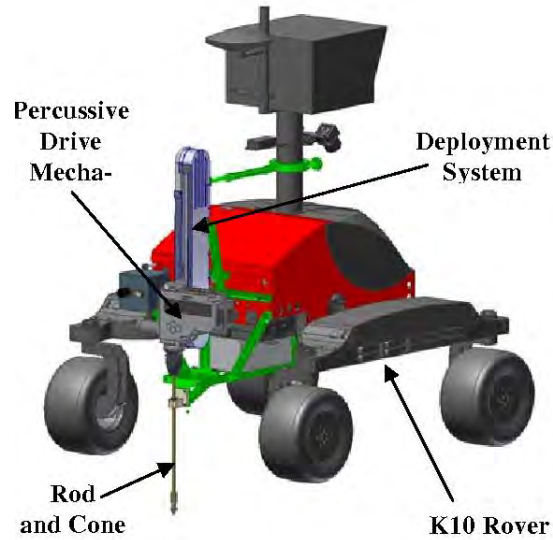


Figure 14: Percussive Dynamic Cone Penetrometer mounted on the NASA Ames K-10 rover. This instrument will determine the geotechnical properties of the regolith such as density and particle cohesiveness [20].

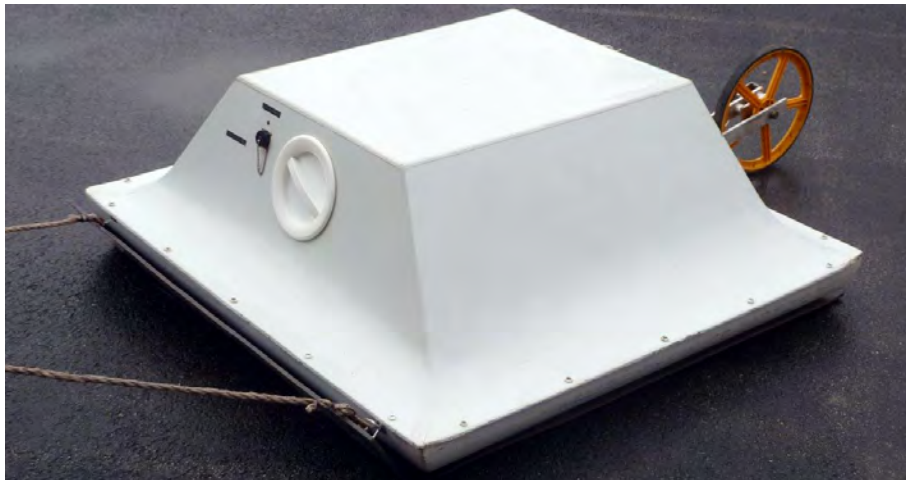


Figure 15: GPR with similar design to that used for this mission. It will use radar to determine the subsurface stratigraphy through a depth of 10-15 meters [21].

D. Rover Structure

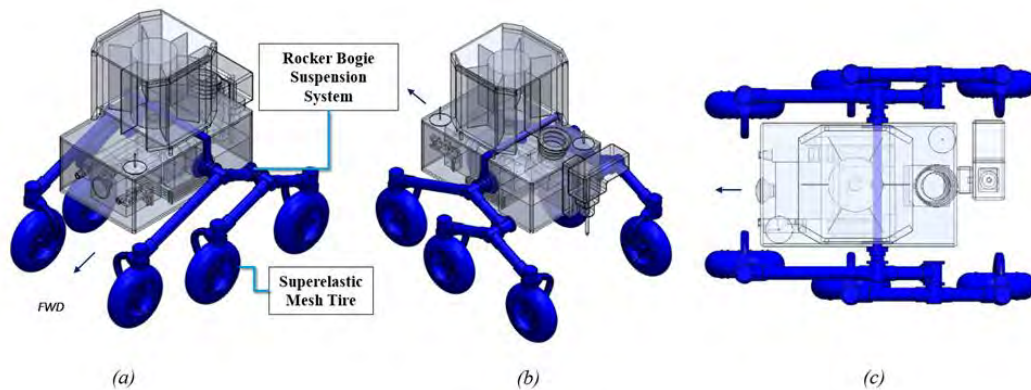


Figure 16: Lunar Rover Structural Components. These engineering views, (a) isometric front, (b) isometric back, (c) top views, are shown with the rover's structural components highlighted.

The rocker-bogie system is NASA's preferred type of traverse mechanism and has been implemented in several of NASA's previous and future Mars rover concepts. The design of the suspension and traverse system for both the lunar prospecting mission rovers will be a derivation of previous NASA Mars missions such as Pathfinder, Mars Exploration Rover (MER), and Curiosity [22]. As the name of the system implies, this mechanism includes a rocker, containing one wheel, connected to a bogie, containing two drive wheels. The rocker on either side of the Rover is connected via a differential bar that is pivoted at the center of the Rover's top WEB. The differential allows for the right and left rocker bogie systems to traverse at different angles, thus increasing the capability to move across a wide range of terrain, while maintaining a constant weight on each of the Rover's wheels [23].

Figure 16 shows configuration of Rover 1 and Rover 2 structural components, the rocker is at the front of the vehicle while the bogie is connected aft. The beams connecting the rocker to the bogie are at 135° relative to each other. The beams connecting the middle and aft wheel of the bogie system are also at the same orientation of 135° relative to each other. This tilt angle was chosen as it allowed for the greatest simultaneous mobility for the rocker and bogie. This highest angle of tilt allows the rover to traverse across terrain as high as 28 cm. Anything above this height, the rover's on-board navigation camera will indicate to traverse around this obstacle.

The rocker-bogie systems on Rover 1 and Rover 2 are designed to collapse in a stowaway position, as shown in Figure 17, and will then extend into the traverse mode as shown in Figure 16. This highest angle of tilt allows the rover to traverse across terrain as high as 28 cm. Anything above this height, the rover's on-board navigation camera

will indicate to traverse around this obstacle. The stow configuration was designed to allow compact stowage during transit inside the lander as the center of gravity is moved closer to the ground, thus increasing the stability during transit. The overall rover dimensions in both the stow and traverse configurations are given in Table 6. As the table indicates, the overall height of the Rover decreases while the length increases with the collapsed rocker-bogie system.

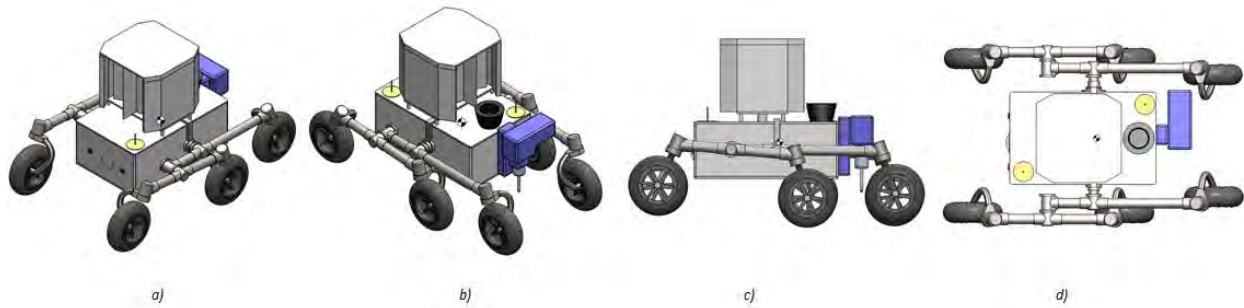


Figure 17: Engineering Views of the Rover in Stowed Configuration. The Rover will be placed in the lander in this configuration during all transit phases. a) Front isometric view, b) back isometric view, c) left view, d) top view.

In the past, NASA has utilized tread wheels milled from solid aluminum for rovers [24]. However, given the damage observed on the Curiosity’s wheels, NASA Glenn Research Center and Goodyear developed an alternative super elastic mesh tire, similar to the mesh-concept utilized on the Apollo lunar rover. This new wheel design is composed of a nickel titanium (NiTi) shape memory alloy [25]. When a stress is applied to conventional materials, such as the previously used aluminum, the bonds between the atomic structures

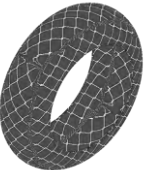
are stretched. However, the NiTi material has a unique characteristic that allows for atomic rearrangement when the stress is applied. This allows for greater durability of the material, and approximately thirty times more stress than can be applied without plastic deformation occurring [25]. The volumes for the wheels were approximated using the washer method of calculating the volume of a revolution. The wheel diameters were sized so the base of the rover warm electronics box extended at least 30 cm above the ground when the rocker-bogie system was traversing across the highest threshold of terrain. As Table 7 below indicates, the overall volume requirement for the shape memory alloy mesh wheel design offsets the relatively higher density of NiTi, thus making it a lighter wheel than the conventional aluminum wheel. As thermal considerations were key for the rover design, operating temperatures of

Table 6: Rover Traverse and Stow Configuration Dimensions. This table shows the dimensions of the Rover WEB and overall dimensions in both the traverse and stow configurations. The overall dimensions include the extension of the rocker-bogie system and the other protruding instruments (i.e. penetrometer, and STEM-RTG).

Rover Dimensions (m ³)	
Warm Electronics Box	0.465 x 0.72 x 0.3
Traverse Overall	0.9 x 1.24 x 1.15
Stow Overall	0.92 x 1.5 x 0.95

NiTi alloys were verified. According to the Granta Design CES Edupack software, the minimum service temperature, that is a material’s lowest operating temperature before becoming too brittle, for austenitic nickel titanium alloy is 0 K, which is still lower than the lowest expected temperature within the crater. In addition, the thermal systems equipped on the rover, which will be discussed in the next section will also maintain the entire rocker-bogie system and the wheels at thermal equilibrium temperatures.

Table 7: Super elastic mesh wheel versus conventional aluminum-milled wheel mechanical properties. This table shows the mass calculation for two wheel designs. As the table indicates, due to the low volume of a mesh design, the nickel-titanium wheel had less mass due despite the high density.

Material	Shape	Density [kg/m ³]	Volume [m ³]	Mass of One Wheel [kg]
Aluminum 6061-T6		2.98x10 ³	7.42x10 ⁻⁴	2.21
Nickel-Titanium		6.41x10 ³	2.22x10 ⁻⁴	1.44

A majority of the rover’s instruments are enclosed within the warm electronics box (WEB), which essentially serves as the rover’s chassis. This enclosure serves as thermal protection from the cold temperatures as well as a barrier for dust mitigation. The WEB is composed of a 3 mm layer of aluminum 6061-T6 for structural support as well as 6 mm aerogel silica for added thermal insulation. As shown in Figure 9, the WEB is designed to be a rectangular prism. Several other WEB shapes were considered such as trapezoid and T-shape prism. However, a rectangular prism was ultimately chosen to minimize the overall rover volume and stress concentrations.

To allow for optimal heat distribution, the RTG was placed at the top center of the rover’s WEB, which can be observed in both Figure 9 and Figure 17. Due to the RTG’s high mass, this component greatly impacted the location of the center of mass, thus dictating the placement of the instruments on the WEB’s interior. The center of mass was

also an important metric for the placement of the main hinge of the rocker-bogie system. Figure 9b shows the placement of the rocker-bogie's main pivot in line with the Rover's center of mass.

E. Rover Navigation and Guidance

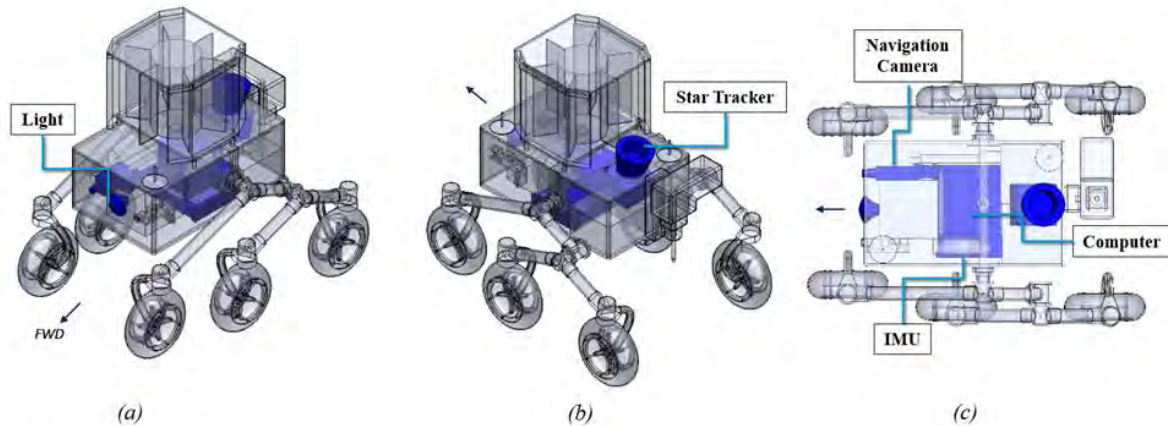


Figure 18: Lunar Rover Navigation and Avionics Components. These engineering views, (a) isometric front, (b) isometric back, (c) top views, are shown with the rover's navigation and avionics components highlighted.

For the Guidance Navigation and Control system the requirements are to determine the location of the rover and be able to traverse the crater in 10 m segments. To determine the location and orientation of the rover multiple methods will be used. The first is a star tracker that will be able to determine the rover's direction at any given time. A sun sensor could not be used for this mission due to the majority of the mission being inside a crater that is almost always in eclipse. The star tracker has a 20° field of view and an error of up to 8 arcseconds. This system should be sufficient to determine the rover's pointing direction. Additionally, as a redundant system an Inertial Measurement Unit (IMU) will be used to determine the pointing direction of the rover. Also, methods like magnetic compasses and gyro-compassing cannot be used due to the Moon not having a magnetic field and the slow rotation of the Moon respectively [26]. Figure 18 shows all the instruments used for navigation highlighted in blue.

Due to there being no GPS-like system on the Moon determining the location of the rover is difficult, so two redundant methods will be used. The first method will use radio signals from the Orbiter for ranging. By knowing the location and velocity of the Orbiter as well as the time the signal was sent from the rover, the distance to the rover can be determined. With at least three measurements at different times, the location of the rover can be determined [27]. The second position determining method will be using odometers on the motors of the wheels. In addition, the

odometers will be used to determine when the 10 m has been traversed. The position data in combination with the pointing direction will create a version of dead-reckoning which will allow the position in the crater to be determined. The largest problem with this method is that the position error increases constantly with time. To aid in overcoming this, the radio ranging will be done when the Orbiter passes over each crater. By doing the ranging during each pass the position error will not grow to large values. Using all these systems allows for the requirement to know the location of the rover in each crater is met.

The other requirement for the Guidance, Navigation and Control system is to enable the rover to traverse across the lunar surface in 10 m increments. This requires that the rover has the ability to identify obstacles and determine a course. For the majority of their operations the rovers will be autonomous. One of the exceptions to this is when the desired direction of the rovers is sent from Earth.

Determining an optimal course while avoiding obstacles is difficult in a crater with very limited times in sunlight. A few options were considered for navigation systems. These included LiDAR, camera and visible light, and a walking stick similar to a cane that is used by a blind person to identify obstacles. Judgement of these systems was done using the following criteria: Cost, Mass, Resolution, Power, Size, and Risk. A trade study was performed, and the results can be seen in Table 8. For the trade study the both category that included both the LiDAR and the light and camera systems. The results showed that the both category with both the LiDAR and light and camera systems won. Using two systems allows for redundancy in the case that one fails or if one of the systems cannot identify an obstacle that the other can.

Table 8: Trade Study of Different Rover Navigation Systems. Four different options were analyzed in six different categories. The resolution and risk categories are normalized values because both were difficult to quantify for some systems. The table on the right shows the results with the both option winning.

Parameters	Cost (\$)	Mass (g)	Resolution	Power (W)	Size (cc)	Risk
Weight	0.032	0.137	0.151	0.173	0.056	0.451
LiDAR	10000	210	6	12	500	5
Light and Camera	6000	750	5	45	200	6
Both	16000	960	8	57	1000	9
Stick	3000	200	4	1	200	4



Total	
LiDAR	5.549
Light and Camera	5.490
Both	6.638
Stick	5.257

Operations of the navigation system can be seen in Figure 19. Each day the desired location will be sent to the rovers telling them where they should go. The rover will then use its current location, determined from the position determination system, to determine a desired route. After the desired route has been found the LiDAR system will activate and attempt to identify any obstacles within 10 meters of the desired direction. Additionally, a light will turn on and a picture will be taken. Both sets of data will be sent to the computer which will identify any obstacles in the desired path. If no obstacles are found, the rover will begin to traverse the route. In the case that an obstacle is found, the rover will attempt to plot a course around the obstacle. If at any point the rover cannot determine an alternate route or if it gets stuck, the rover will stop moving and power down into idle mode. Once in idle mode, the rover will wait for commands to be sent from Earth after the pictures and data can be analyzed. This process will be repeated in 10 m increments until the desired location is reached. Utilizing these systems satisfy the requirement of the Guidance Navigation & Control (GN&C) system to allow the rover to traverse the crater.

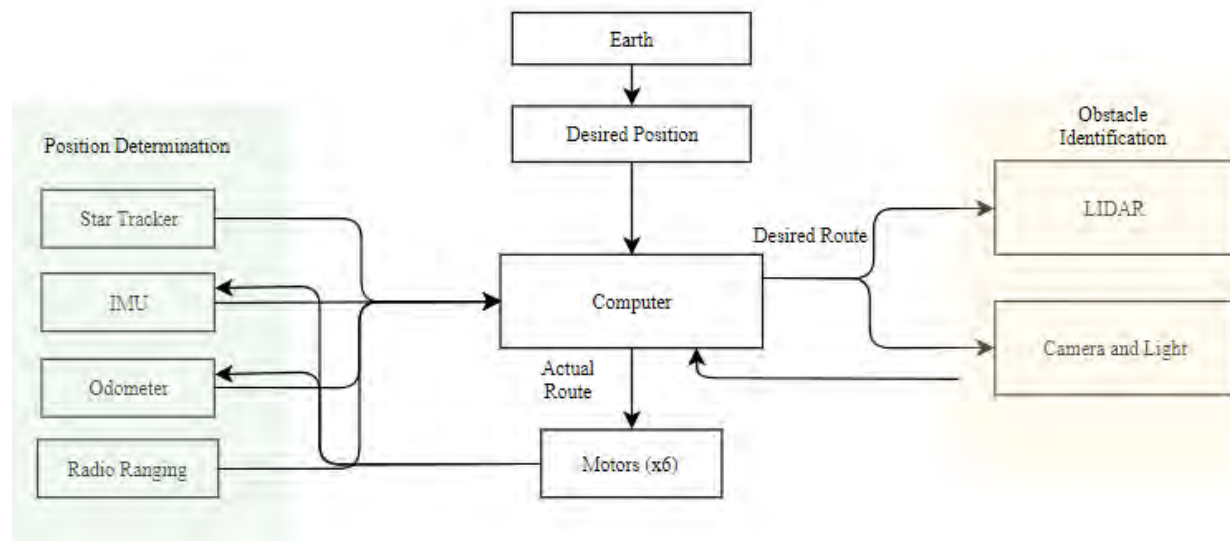


Figure 19: Flowchart of the GN&C Operations. This flowchart shows how the GN&C system will function including the Position Determination system in green on the left and the Obstacle Identification system in orange on the right.

F. Rover Power

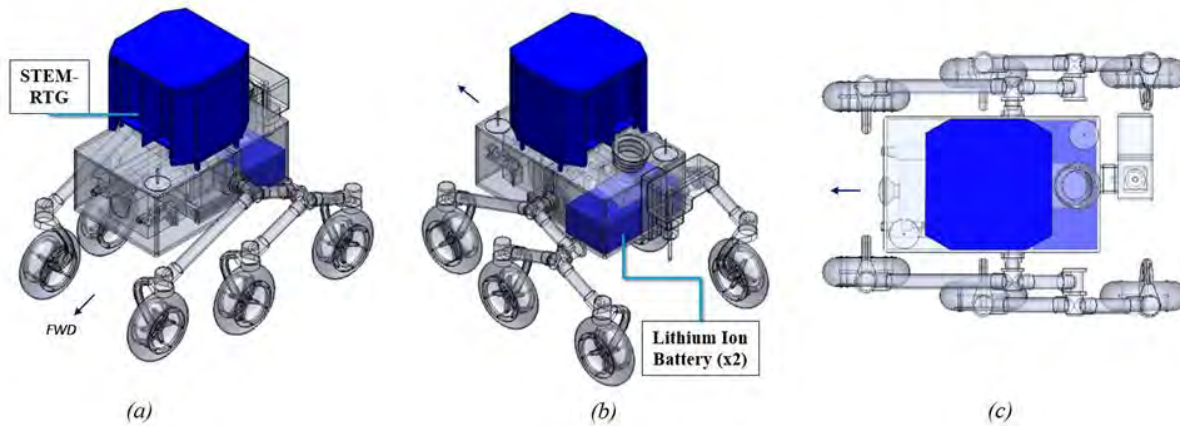


Figure 20: Lunar Rover Power Components. These engineering views, (a) isometric front, (b) isometric back, (c) top views, are shown with the rover's power components highlighted.

Figure 20 depicts each power components in the rover. Each rover will utilize an RTG as the primary power source since lunar surface operations will take place in PSRs [28]. The decision was made to use RTGs due to the length of the rover mission - relying only on batteries as a source of power for an estimated year and a half would have been impractical. An RTG works by containing the radioactive decay of Pu-238 and converting the heat created during this process into usable electrical energy at an efficiency of about 10% [29]. RTGs have been utilized in various deep space missions like Voyager, and NASA's Curiosity, a Martian rover launched in 2011 [29].

The Segmented Thermoelectric Modular Radioisotope Thermoelectric Generator (STEM-RTG) was chosen for the rovers since the STEM-RTG can be scaled to meet the power requirements of this particular mission [30]. The STEM-RTG is modular because the number of General Purpose Heat Units (GPHU) is variable depending on the desired power output. The number of GPHUs to be used with this RTG was selected so that the rover could charge its on-board Lithium (Li) -Ion batteries while in an idle power phase. The number of Li-Ion batteries was selected such that the rover could perform full phases of lunar surface operations without having to stop to recharge batteries, and without the batteries running under 50% charge. Maintaining batteries above 50% charge is necessary to help extend the lifetime of the batteries and maintain full functionality of the rovers.

Table 9 shows the power requirement breakdown of each rover component and the respective idle and active power requirements. The rover total propulsion (or wheel motor) requirement was estimated from that of former

interplanetary rovers, by creating a relationship between rover mass and power requirement and fitting a linear regression [31]. All instruments operate nominally at 28V except for the LiDAR and Transceiver, which each require 12V. If all systems were active, the required current from batteries would be about 7.5A; this was a consideration in choosing which Li-Ion batteries would be used.

Table 9: Rover Instrument Power Draw. This table shows the idle and active power draw from all instruments, sensors, and other electronics on board each rover.

Instrument	Idle Power Draw (W)	Active Power Draw (W)
Propulsion (Wheels)	2	25
Transceiver (Antenna)	1	10
DAN-PNG	1.5	14
DAN-DE	3.5	4
STRATA GPR	1.5	7
Instrument Camera	2	20
SanSEC	0	0.5
Penetrometer	1	5
Computer/VME Data Bus	18	18
Navigation Camera	2	3
Navigation Light	2	50
LiDAR	1	8
Star Tracker	5	12
Temperature Sensors	-	1
IMU	-	1
Heat Pipes System (Pump)	1	4
TOTAL	43	183

There would be instruments on-board the rover which would not be able run at idle, such as the IMU and temperature sensors; this is accounted for in Table 9 by having idle and active power draw equivalent for these instruments. Additionally, there would never be a time when the rover would require every instrument to run at the same time. Therefore, the rover's discrete operations were defined in Table 10, which shows the breakdown of the power requirements and required time for each phase completion. The rover traverse time was estimated given that the rover top speed is 4 cm/s and that each rover will only travel 10 m at a time between sample collection locations. This speed was estimated based on past interplanetary rovers [31]. The final, more realistic idle power requirement, accounting instruments that cannot be turned to idle mode, is 48 W. This idle power requirement prompted the decision

to select a three General Purpose Heat Source (GPHS) unit STEM-RTG, which would provide 80 W of power at the beginning of its life, decaying by less an 5% over the course of the mission [30]. The efficiency was assumed to be 10%, with an estimated cost of \$19M each, weighing 20.5 kg, not including housing structure [30].

Table 10: Rover Operating Mode Power Requirements. This table shows the energy required for each rover to complete various tasks during its lunar surface operations.

Operating Mode	Time Required for Operating Mode (min)	Time Required for Operating Mode (hr)	Energy Required for Operating Mode (Wh)
Traverse	4.17	0.07	6.27
Routing	10	0.17	21.27
Communications	30	0.5	37.05
DAN (short)	2	0.03	2.66
DAN (long)	30	0.5	39.86
Penetrometer	5	0.08	5.85
IR	0.1	0.08	7.58
STRATA	1	0.02	1.12

Given that the RTG has an output of 80 W of power, the RTG would be charging the Li-ion batteries at 30 W during the rover's idle. This 30 W charge allows the power source input to be in substantial excess of the rover's idle power requirement, which means the batteries would be able to charge during normal rover operations if necessary. Two Saft 28V Space Grade Li-Ion batteries were chosen, both capable of storing 84 Wh and discharging at a continuous rate of 30 A [32]. These batteries satisfy the requirements for the rover to get through each operating mode without having to recharge batteries and would do so without running under 50% charge. With the 80 W STEM-RTG and two Saft Li-Ion batteries, the rover will complete its requirement to provide power throughout the entire duration of its lunar surface operations.

G. Rover Thermal

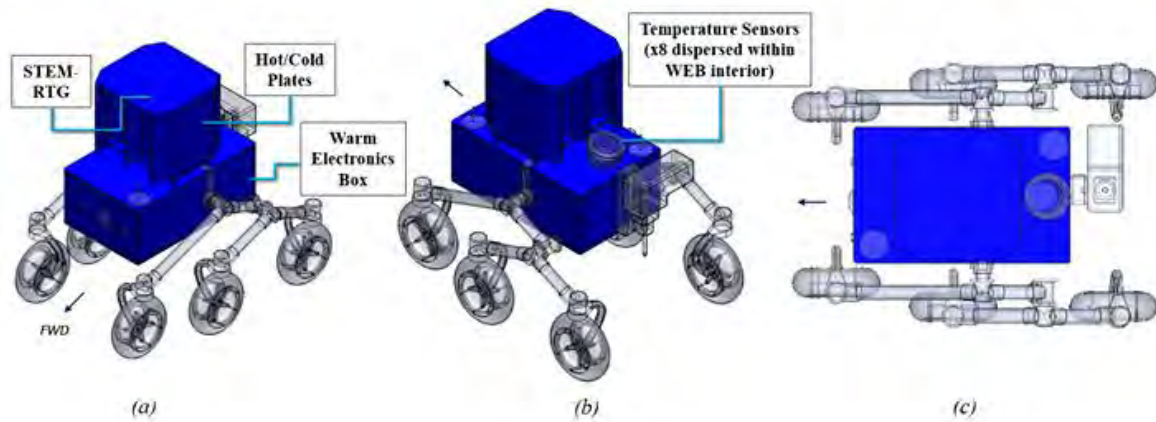


Figure 21: Lunar rover thermal components. These engineering views, (a) isometric front, (b) isometric back, (c) top views (a) isometric front, (b) isometric back, (c) top views, are shown with the rover's thermal components highlighted.

The expected operating temperature range for the rovers within the Haworth and Shoemaker craters is between 0 and 50 K [33]. The ideal operating temperature for the rover was estimated to be 283 K to allow for safe instrument and electronics conditions. To accomplish this, 283 K requirements, the rovers will route excess RTG heat to the WEB using a heat loop pipe, powered by a 4 W pump. The heat pipe system was inspired by the Curiosity system for thermal control [34]. Figure 22 depicts the layout of the heat loop pipe system. The RTG was enclosed in a housing constructed of inner panels called “hot plates” and outer panels called “cold plates”. A honeycomb composite will be used between the two plates to provide sufficient insulation (as used on Curiosity) and prevent heat from leaking through from the hot plates to the cold plates. The exposed surface of each plate will be embedded with pipes that make up the heat pipe loop [34]. About 75% of the heat from the RTG will radiate into the hot plates and enter the heat pipe loop. The heat is pumped into a mixing valve, where new heat into the system and circulating heat come together and run through the pump. The pump pushes the combination into a splitter, which sends the necessary heat into the WEB, while rejecting the excess to the cold plates, where this heat radiates away from the rover.

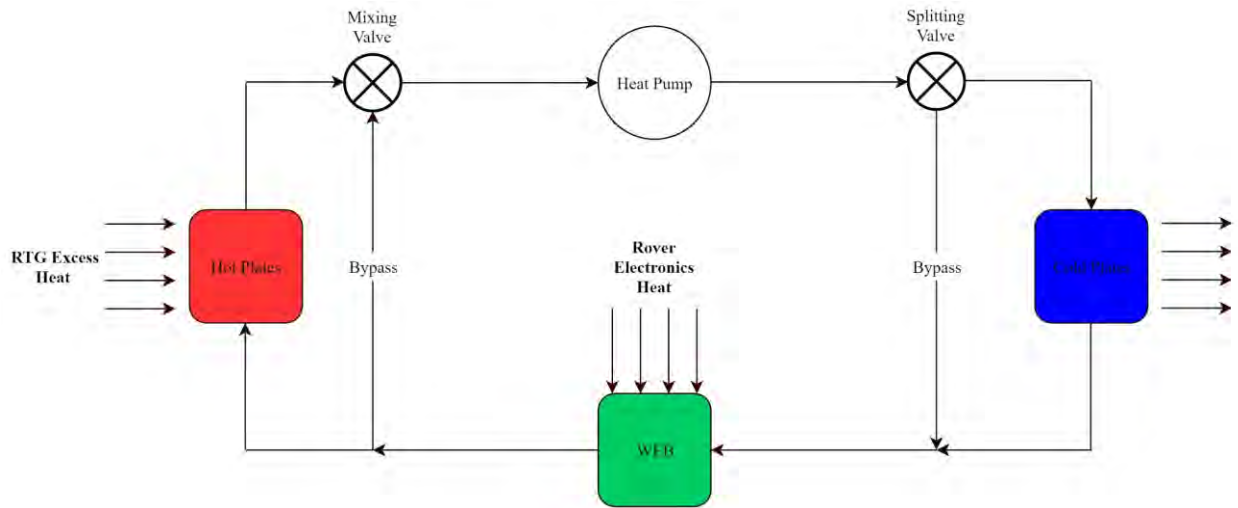


Figure 22: Rover Thermal Control System. This schematic shows how the heat is transferred into and out of the rover during lunar surface operations. A majority of the heat entering the system originates from the rovers' RTG.

Equilibrium analysis was used to determine how much heat would be lost through the rover walls when held at 10 degrees Celsius, thus determining how much heat would need to be inputted into the system to maintain this temperature at equilibrium. The results from this analysis are shown in Table 11. Using the assumption that the rover will be a grey body with an emissivity of 0.85, radiation heat transfer analysis found that the rover would need to radiate 146 W to maintain thermal equilibrium. The Rover WEB heat output was computed assuming that Direct Current (DC)-DC converters are 90% efficient, with the remaining 10% being lost in the form of heat [36]. The amount of heat that the loop needs to move around was used to estimate the power requirement for the heat pumps used in the system, knowing that of Curiosity and scaling accordingly [34]. This analysis validates that the rover satisfies the requirement that the rovers will maintain thermal equilibrium during lunar surface operations.

Table 11: Rover Thermal Analysis. This table summarizes the thermal analysis completed on the rover, to ensure that each rover would maintain thermal equilibrium during its mission by validating the equivalence of heat in and out of the system.

RTG Excess Heat, assuming 75% heat captured by hot plates (W)	540
Rover WEB Heat Output, peak (W)	12
Total Heat into Rover (W)	552
Heat Loss through Rover Walls at 10°C (W)	406
Heat to Pump Out of Radiators (W)	146
Total Heat out of Rover (W)	552
Heat Pump Power Req. with 1.5 FS (W)	4

H. Rover Communication

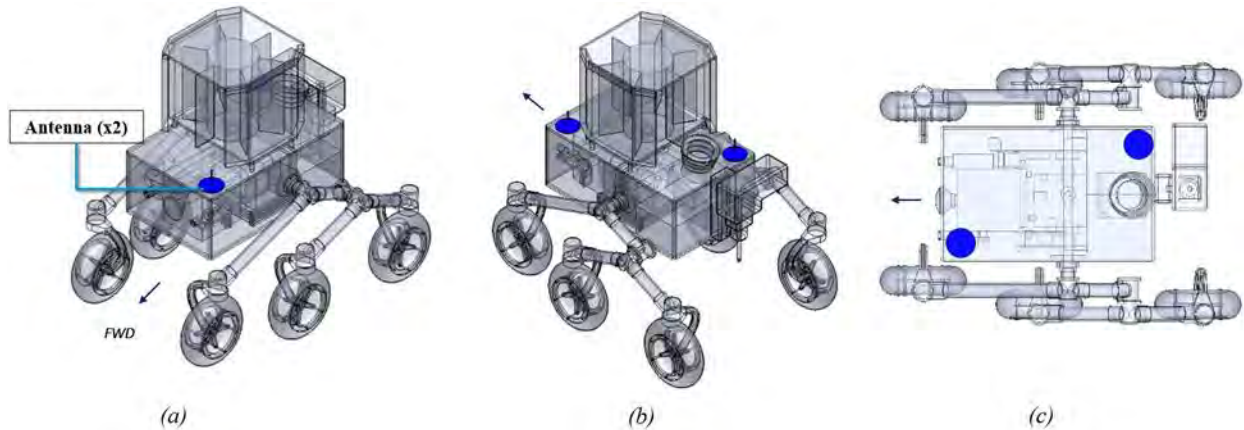


Figure 23: Lunar Rover Communications Components. These engineering views, (a) isometric front, (b) isometric back, (c) top views, are shown with the rover's communications components highlighted.

The communication system was designed to allow for the downlink of telemetry and commands to both rover systems and the uplink of scientific data from the rovers back to ground stations on Earth. Historically, communication with Earth during lunar missions has been done directly. The communication process involved using a targeted antenna with a high gain to communicate with a ground station on Earth. For example, the Apollo missions used S-band antennas to communicate with Earth and Very High Frequency (VHF)-band antennas for communication between astronauts [37]. Radio waves take approximately 2.5 s to travel the distance between Earth and the Moon. This means that for direct communication the delay can be neglected. For this mission, there will be significantly more delay due to the location of the rovers. Figure 18 shows the components of the communication system highlighted in blue.

Figure 24 shows a picture of the current link architecture for the mission. The picture shows that communication with Earth will be accomplished using one of the three Deep Space Network (DSN) stations spread out across the Earth. The DSN is a proven system that has been used for a multitude of deep space missions. Antennas at the DSN stations use S-band or X-band signals [38].

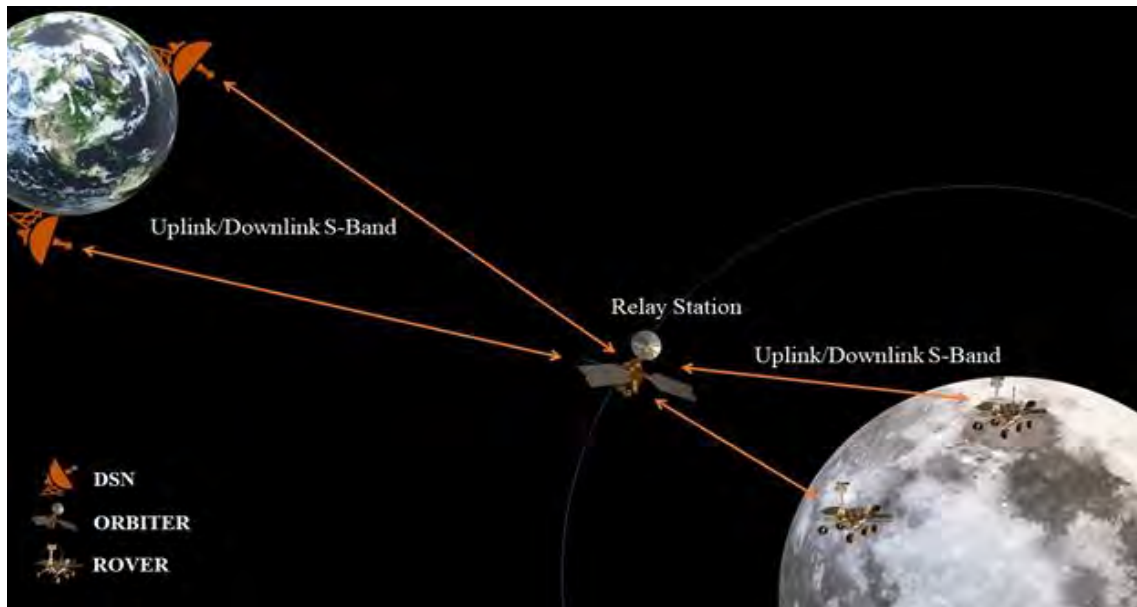


Figure 24: ConOps of the Communication Link Architecture. A relay station is needed between Earth and the rovers because the depth of the craters makes direct communication nearly impossible. The link between Earth and the Orbiter will use an S-band carrier frequency, and the link between the Orbiter and the rover will most likely use UHF.

Since the rovers will be on the South Pole of the Moon and in deep craters, there is little direct access between them and Earth ground stations. This requires there to be a relay between the rovers and Earth to limit the amount of data storage required on the rover. The use of the Orbiter as a relay can be seen in Figure 24. Using the current orbit of the Orbiter and an azimuth elevation mask to simulate the depth of the crater, the average access time per pass between the rover and the Orbiter was found to be 35 minutes per pass followed by a gap of about 2.5 hours. This calculation was done using Satellite Tool Kit (STK). Figure 25 shows a picture of the Orbiter during a pass over Shackleton Crater. Passes occurred seven to eight times per day at regular intervals. Therefore, the data storage requirements of the rover will be minimal. An issue with the irregular communication times with each rover is that commands will only be able to be sent during a pass over the crater which occurs

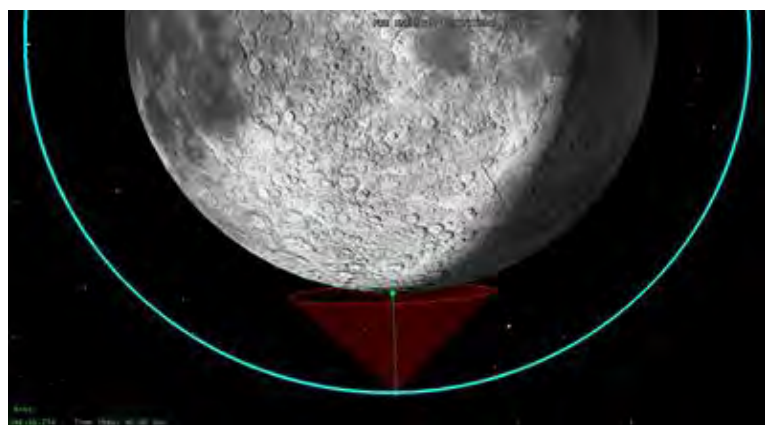


Figure 25: Image of STK Model of Communication Link. The image shows the communication link between the Orbiter and the rover in Shackleton Crater. To simulate conditions in the crater, an azimuth-elevation mask was created. The crater was modeled to be the bottom half of the sphere with a constant slope. While this is not the most accurate method, detailed terrain maps of the Moon are difficult to find.

roughly every two hours. A graph of the access between the Orbiter and the rover during two passes can be seen in Figure 26. This amount of time without communication to the rovers will require some autonomy in the rovers' control system.

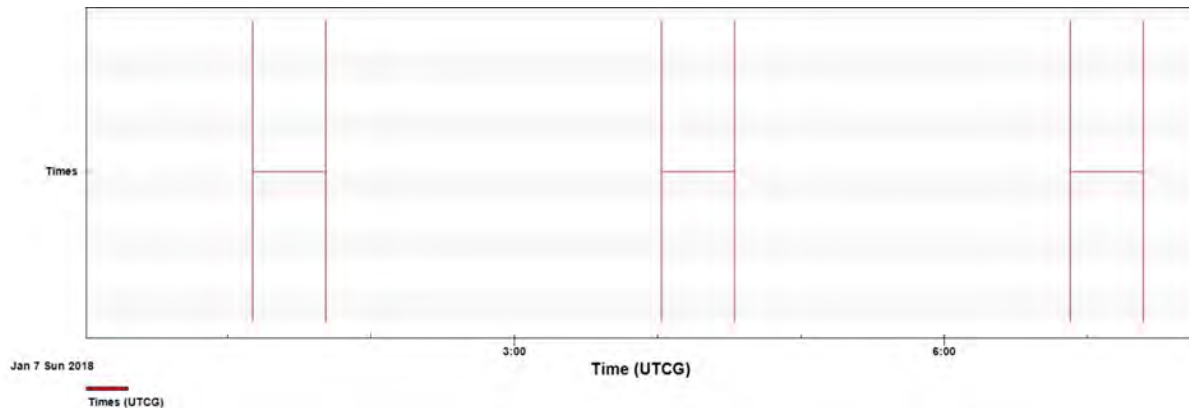


Figure 26: Graph of access times between the Orbiter and the rover for two passes. Each pass is about 35 minutes with passes occurring every two and a half hours. This cycle repeats every time the orbit passes over Shackleton crater.

The rovers will use two quadrifilar helix antennas on opposite corners of the rover. These antennas are right-hand polarized which is the same polarization as the antennas on the Orbiter. Also, the antenna pattern shows that power is radiated only above 20° elevation. This was chosen so that no actuation was needed to point the antennas in the correct direction lowering cost, mass, and power requirements. Additionally, almost no power is being transmitted into the walls of the crater which form a natural elevation mask of around 20°. Communications will be on the S-band with a large bandwidth to allow for uplink and downlink. Uplink and downlink will be on slightly different frequencies both with a 40 MHz bandwidth. Uplink will be from 2.65-2.69 GHz and downlink will be from 2.5- 2.54 GHz. The data rate for the system will be 5 Mbps. At this rate, 10.5 Gb of data can be transferred every time the Orbiter passes overhead. With data from all the instruments it is estimated that with each measurement cycle 2 Gb of data will be generated. Using the current data rate, 5 cycles of measurements can be transmitted in one access interval. A complete link budget can be seen in Table 12 below.

Table 12: Link Budget Between the Orbiter and the Rovers. This table shows all the link budget parameters for the link between the antenna on the rover and the antenna on the Orbiter.

Frequency	<i>GHz</i>	2.67	Propagation and Polarization Loss	<i>dB</i>	0
Transmitter Power	<i>Watts</i>	1.1	Receive Antenna Diameter	<i>m</i>	0.05
Transmitter Power	<i>dBW</i>	0.41	Peak Receive Antenna Gain	<i>dB</i>	1.36
Transmitter Line Loss	<i>dB</i>	-1	Receive Antenna Beamwidth	<i>deg</i>	5.78
Transmit Antenna Beamwidth	<i>deg</i>	150	Receive Antenna Pointing Error	<i>deg</i>	0.2
Peak Transmit Antenna Gain	<i>dB</i>	0.78	Receive Antenna Pointing Loss	<i>dB</i>	-0.01
Transmit Antenna Diameter	<i>m</i>	0.05	Receive Antenna Gain	<i>dB</i>	1.35
Transmit Antenna Pointing Offset	<i>deg</i>	0.2	System Noise Temperature	<i>K</i>	135
Transmit Antenna Pointing Loss	<i>dB</i>	0	Data Rate	<i>Mps</i>	5
Transmit Antenna Gain	<i>dB</i>	0.78	Eb/No	<i>dB</i>	97.02
Equiv. Isotropic Radiated Power	<i>dBW</i>	0.19	Carrier-to-Noise Density Ratio	<i>dB-Hz</i>	147
Propagation Path Length	<i>km</i>	110	Bit Error Rate		1.00E-06
Space Loss	<i>dB</i>	-82	Required Eb/No	<i>dB</i>	11

Also included in each rover will be a transponder and an S-band power amplifier that produces and interprets the signals being sent and received. A small data storage of 20 GB will be included with the computer that will allow for data taken in between accesses with the Orbiter to be stored. All discussed systems combined satisfy the requirement for the rover to send the scientific data back to Earth.

I. Rover Dust Mitigation System

Lunar dust is a unique substance in that when it is exposed to mechanical parts, it begins to corrode and jam the moving features. To mitigate lunar dust, an active electrodynamic system is employed to guide the dust off of the surfaces of the rover [39]. A multi-phase alternating current signal is broadcast to nodes with a 0.5 mm spacing to effectively create a traveling charged wave, as seen in Figure 27. Though lunar dust consists of charged particles, this system is effective for both charged and uncharged particles.

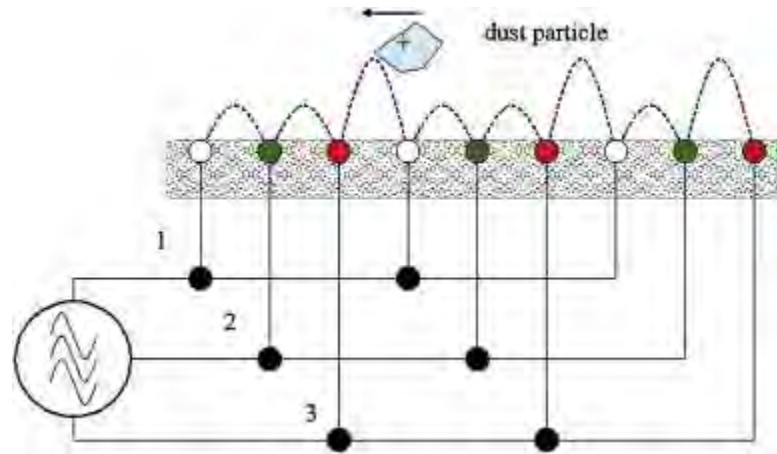


Figure 27: Three-Phase AC Source powering Nodes for Electrodynamic Particle Movement. This diagram shows the electrical network between the nodes and the AC source and how the signal moves the dust particle. The AC source sends a voltage of 400 V at 10 Hz to the nodes in an alternating pattern as shown. The dust reacts to the electrical field as if it was a wave moving the dust particle.

Dust particles interact with the electrostatic and dielectrophoretic forces to move laterally to the surface of the rover in a restorative or preventative manner. As

long as the frequency of the signal is appropriate to the frequency the dust moves at, then the science will come to fruition. The experimental methods that validated this phenomenon suggested a 400 V voltage and a 10 Hz frequency for the signal [40]. Dielectric material, measuring 5 mils thick, is placed between the structure of the rover and the gold paint coating the surface. A smaller thickness in the dielectric material is advantageous for thermal qualities.

J. Rover Avionics

The avionics on the rovers that was not discussed in the Guidance and Navigation or power sections are fairly straightforward. The rovers will both have a computer to analyze the information from the GN&C systems which will then provide input to the motors of the wheels. The computer will also take in data from the instrumentation on-board the rover, package the data, and send the data to the Orbiter to then be relayed to Earth. These two main functions of the computer, packaging and sending data, and analyzing GN&C data, are vital to the mission.

In addition to the computer, the avionics on board will include temperature sensors. The temperature sensors are on board to ensure that the instruments are all operating at their proper temperatures. The on-board computer is able to analyze the sensor data and send commands to the instruments to turn them off in case of an emergency.

K. Rover Operations

As mentioned in Section V.F, the rovers will have six phases for general lunar surface operations. The time and power required for each phase is outlined in Tables 13 and 14. When no operations are being performed or the rover is waiting for communication from Earth, the rover will be in Idle Phase. During the Routing phase, the rover will plot a path for the estimated 10 m, and then will traverse the plotted path in the Traverse Phase. When the rover has traversed 10 m, the Sample Collection Phase will begin. Due to the nature of the DAN instrument, there are two separate Sample Collections Phases - Short and Long. The Sample Collection Long Phase takes a higher resolution sample but is 30 minutes instead of the 2 minutes in the Short Phase. To allow for higher resolution data while not drastically increasing overall mission time, the rover will default to the Sample Collection Short Phase, but switch to Sample Collection Long Phase every 5 sample collections. Assuring sufficient power availability, the rover will begin the Data Transmission Phase during the two hour period when the Orbiter is in the Rover’s Line of Sight (LOS). This operation schedule can be seen in Figure 28.

Table 13: Rover Operation Phase Time Table. The table depicts the phases in which the rover operates and the breakdown of how much time each instrument takes to run. This was utilized to estimate total mission time.

Instrument	Routing Phase	Traverse Phase	Sample Collection Short	Sample Collection Long	Data Transmission
Transceiver	-	-	-	-	120 min
DAN-PNG	-	-	1 min	15 min	-
DAN-DE	-	-	1 min	15 min	-
STRATA GPR	-	-	1 min	1 min	-
Instrument Camera	-	-	0.5 min	0.5 min	-
SanSEC	-	-	0.5 min	0.5 min	-
Penetrometer	-	-	4 min	4 min	-
Computer and VME Data Bus	4 min	-	-	-	-
Navigation Camera	0.5 min	-	-	-	-
Navigation Light	0.5 min	-	-	-	-
LIDAR	5 min	-	-	-	-
Wheel Motors	-	10 min	-	-	-
Total Time	10 min	10 min	13 min	41 min	120 min

Table 14: Rover Operations Table with Time and Power Requirements. Depicted below are the phases the rovers will operate in, calling out which specific instruments are active and how much average power and time the phase consumes.

Instrument	Idle Phase	Routing Phase	Traverse Phase	Sample Collection Short	Sample Collection Long	Data Transmission
Transceiver	IDLE	IDLE	IDLE	IDLE	IDLE	ACTIVE
DAN-PNG	IDLE	IDLE	IDLE	ACTIVE	ACTIVE	IDLE
DAN-DE	IDLE	IDLE	IDLE	ACTIVE	ACTIVE	IDLE
STRATA GPR	IDLE	IDLE	IDLE	ACTIVE	ACTIVE	IDLE
Instrument Camera	IDLE	IDLE	IDLE	ACTIVE	ACTIVE	IDLE
SanSEC	IDLE	IDLE	IDLE	ACTIVE	ACTIVE	IDLE
Penetrometer	IDLE	IDLE	IDLE	ACTIVE	ACTIVE	IDLE
Computer and VME Data Bus	ACTIVE	ACTIVE	ACTIVE	ACTIVE	ACTIVE	ACTIVE
Navigation Camera	IDLE	ACTIVE	IDLE	IDLE	IDLE	IDLE
Navigation Light	IDLE	ACTIVE	IDLE	IDLE	IDLE	IDLE
LIDAR	IDLE	ACTIVE	IDLE	IDLE	IDLE	IDLE
Star Tracker	ACTIVE	ACTIVE	ACTIVE	ACTIVE	ACTIVE	ACTIVE
Temperature Sensors	ACTIVE	ACTIVE	ACTIVE	ACTIVE	ACTIVE	ACTIVE
IMU	ACTIVE	ACTIVE	ACTIVE	ACTIVE	ACTIVE	ACTIVE
Wheel Motors	IDLE	IDLE	ACTIVE	IDLE	IDLE	IDLE
Phase Time	-	10 min	10 min	13 min	41 min	120 min
Phase Average Power	48 W	199 W	82 W	68 W	68 W	65 W

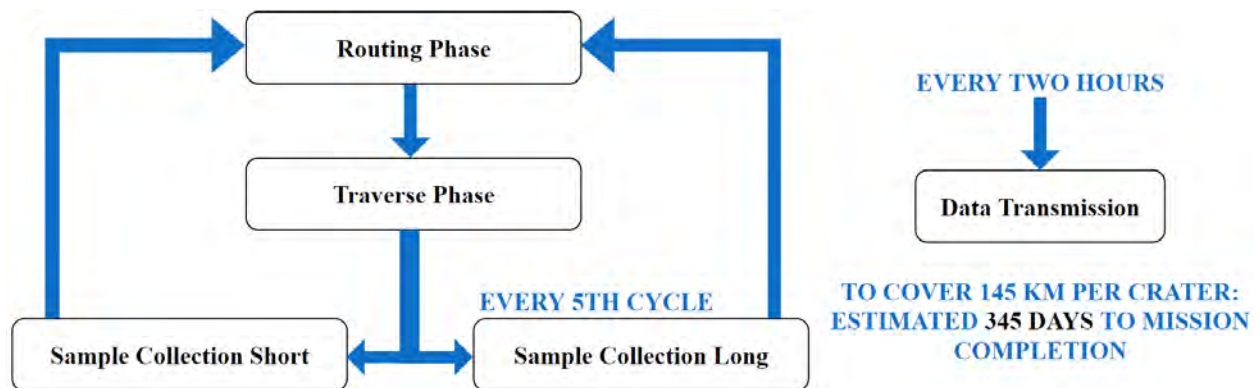


Figure 28: Rover Operations Schedule. The figure shows the cycle of phases the rover completes when on the lunar surface. From Tables 12 and 13, the full mapping of each crater was estimated to be 345 days.

The total mission time for the rover traverse and data collection pattern was estimated based on crater diameter. Assuming no instrument failure, each rover was estimated to map the entire crater within 345 days. The RFP outlines that the mission needs to obtain water-to-regolith ratios from two separate lunar craters. This mission requirement will be fulfilled after one sample from each rover. Any operations after the initial measurement are intended to increase the resolution of the measurement by mapping the entire crater for water concentrations and maximize the scientific data by utilizing the secondary and tertiary instruments. This plan also addresses a NASA SKG of gathering data at 10 m intervals to develop an accurate understanding of the polar volatile distributions throughout the polar craters.

L. Mass Budget

Table 15 below indicates the breakdown of the mass budget for each of the lunar rovers by subsystem. Each rover in its current configuration is estimated to have a mass of 119 kg each, totaling 238 kg allocated for the total rover mass. The base mass for each rover is below the threshold of the 125 kg mass limit. As the table indicates, a majority of the Rover mass derives from structural and power components, the STEM-RTG being the heaviest part. Due to the high mass of the STEM-RTG, the configuration of the Rover WEB interior was highly dependent on the placement of this integral power component to allow for an optimal center of mass location.

Table 15: Mass budget for lunar rover. This table indicates the mass allocation and limits for each of the lunar rovers by subsystem at a component level.

Subsystem	Part	Basic Mass (kg)	MGA (%)	Predicted Mass (kg)	Mass Limit (kg)
Avionics	Computer	6.5	1%	6.6	7
	IMU	0.2	1%	0.2	0.5
	VME Data Bus	2.5	1%	2.5	2
Communications	Antenna	0.5	1%	0.5	0.5
	Transceiver	0.1	1%	0.1	0.5
Instrumentation	Camera	5.4	2%	5.5	6
	DAN-DE	2.8	2%	2.9	3
	DAN-PNG	1.9	2%	1.9	2.5
	Dielectric Sensor (SanSEC)	0.1	2%	0.1	0.5
	Penetrometer	13	2%	13.3	15
	STRATA GPR	3	2%	3.1	4
Navigation	Camera	0.3	1%	0.3	0.5
	LiDAR	0.2	1%	0.2	0.5
	Light	0.5	1%	0.5	1
	Star Tracker	2	1%	2	1
Power	Lithium Ion Batteries (28V)	6.9	5%	7.2	7
	STEM-RTG	27	5%	28.4	25
	Wire Harness	2	5%	2.1	3
Structure	Rocker Bogie Suspension	14.6	7%	15.6	15
	WEB	17	7%	18.2	17
	Wheels	11.4	7%	12.2	10
Thermal	Temperature Sensors	1.8	1%	1.8	3
TOTALS:	-	119	-	125	125

VI. Entry, Descent, & Landing

This section outlines the second phase of Project Penguins design process - the Entry, Descent, and Landing. Because there is no atmosphere on the Moon, this design only includes descent and landing phases.

A. EDL Trajectory

To fulfil the requirement of having a robotic mission to the surface of the Moon an Entry, Descent, and Landing trajectory needed to be designed. This task was completed using STK, specifically the Astrogrator feature. The trajectory required that the lander start at the polar orbit and end in the craters. It was assumed that the lander would stop its burn 1 meter above the ground and would then drop the rest of the way before landing on struts.

To accomplish the landing in the crater, the lander first separates from the Orbiter before making the first of three main burns. This first burn adjusts the inclination of the lander's orbit to make it line up with the target site. After this first burn, the lander begins the phasing portion of its landing. During this, the Orbiter maintains the same altitude above the Moon's surface but continues in its orbit to prepare for the descent towards the surface. Once in position for the descent, the lander performs a burn to send the lander towards the surface. This burn sends the lander on a trajectory towards the target site. Once on this trajectory, the lander moves towards the surface rapidly and transitions from an altitude of 600 km to 34 km. The last burn begins at 34 km and continues until 2 m above the surface. The STK model uses the engine selected for the mission and the mass determined by the structures team. This allows for accurate fuel use calculations to be computed by STK. The main fuel use is during the final long burn towards the 2 m stopping point. Once this burn has finished, the lander drops the final meter and hits the Moon at 2.5 m/s. The landing struts are used to absorb the force of the lander as it hits the ground.

The trajectory to the surface can be seen in Figures 29 and 30. The blue portion of trajectory corresponds to the phasing portion of the trajectory described above. The second burn occurs between the blue and green portions of the trajectory. The green portion of the trajectory is the lander travelling to 30 km above the surface before initiating the final burn of the trajectory which is shown in red.

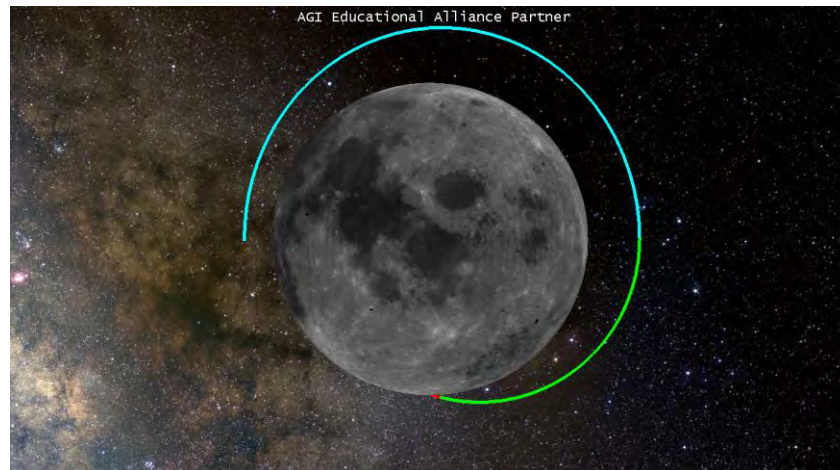


Figure 29: Image of STK model of overall EDL trajectory. The overall trajectory of the EDL maneuver is shown in this image. The phasing, descent to 30 km above the surface and the very beginning of the final burn are shown here.

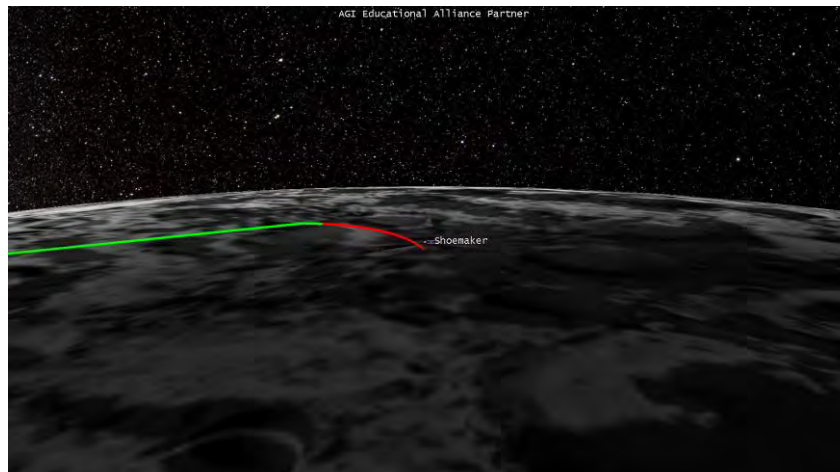


Figure 30: Image of STK model of final portion of EDL trajectory. The image shows the final portion of the trajectory including the entire last burn which is shown in red. The image appears to show the lander missing the target location, but it is meeting it at a point below the surface of the Moon but actually on the ground in the crater.

After releasing from the Orbiter and performing the first burn, the lander phases in its orbit for 2.5 hours. The descent to an altitude of 30 km takes 39 minutes, while the final burn to 1 meter takes just over 2 minutes. This gives a total trajectory time of 3 hours and 11 minutes. The overall timeline for the EDL trajectory can be seen below in Figure 31. The total ΔV needed for this trajectory is 2028.5 m/s and the total fuel needed is 468 kg while carrying a total of 515 kg for a 10% margin fuel reserve.

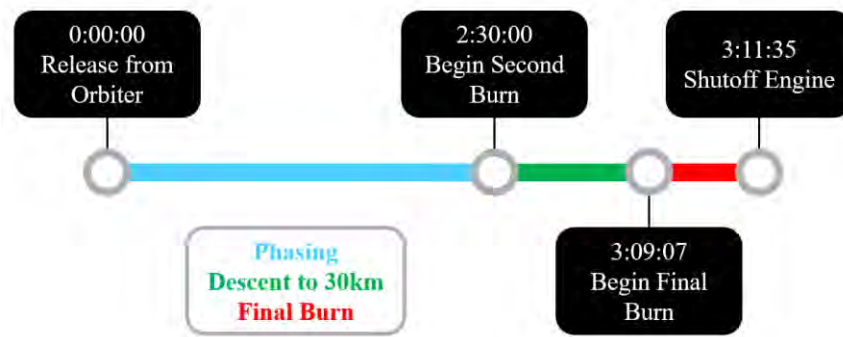


Figure 31: Timeline for the EDL Trajectory. The timeline displays the main events of the trajectory as it releases from the Orbiter and descends to the surface. The colors on the timeline match those in the STK model and the times are shown in hours:minutes:seconds with 0:00:00 being the release from the Orbiter.

B. Requirements

The lander has three main requirements: to descend the rover to the lunar surface, to absorb the impact force of landing, and to maintain necessary environmental conditions of the rover while in transit from GTO to lunar polar orbit. The full requirements flowdown is depicted in Figure 32. The most complicated design aspect was descending to the lunar surface. The lander was equipped with several pieces of navigation and imaging equipment to allow the lander to stably descend into either Haworth or Shoemaker crater and land on a flat surface. Additionally, the lander needed to be responsible for dissipating excess heat from the rover RTG during transit to the Moon. While the heat generated from the RTG is necessary to maintain the rover systems in the Moon's PSRs, that heat would melt the rover while attached to the orbiter if not regulated.

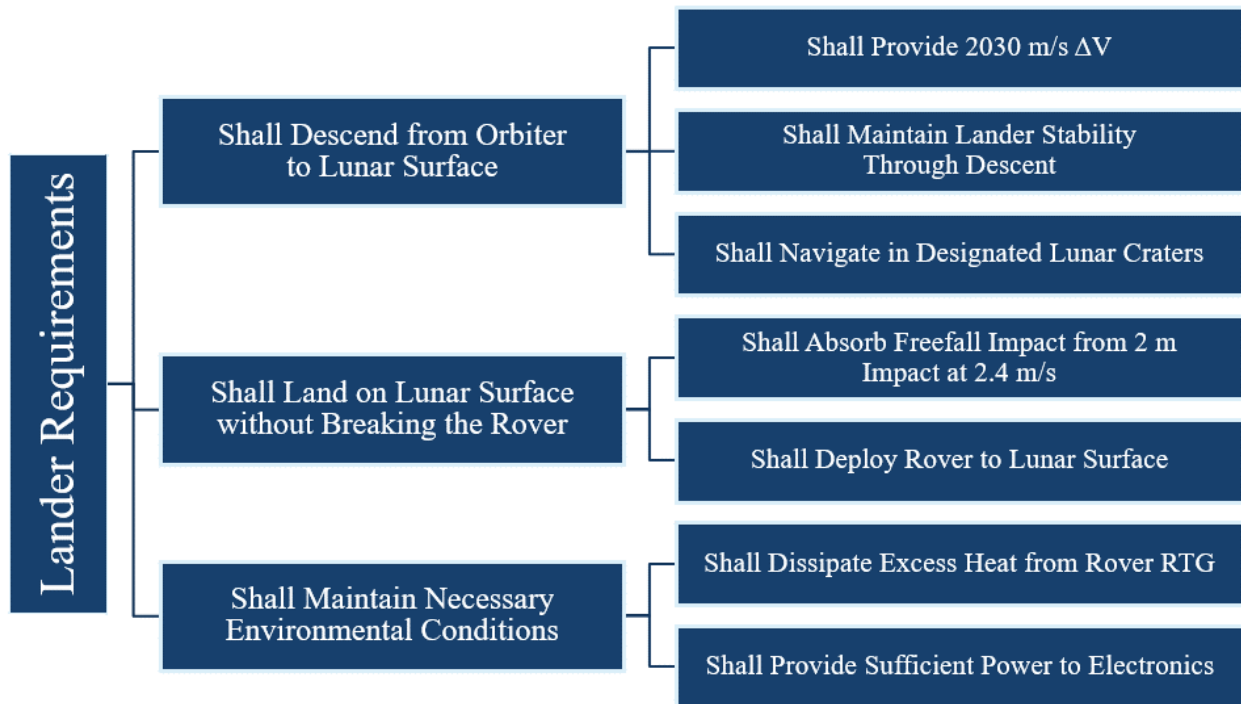


Figure 32: Lander Requirements Flowdown. This image displays the upper level system requirements for the lander, including the main responsibilities and some derived requirements.

C. System Overview

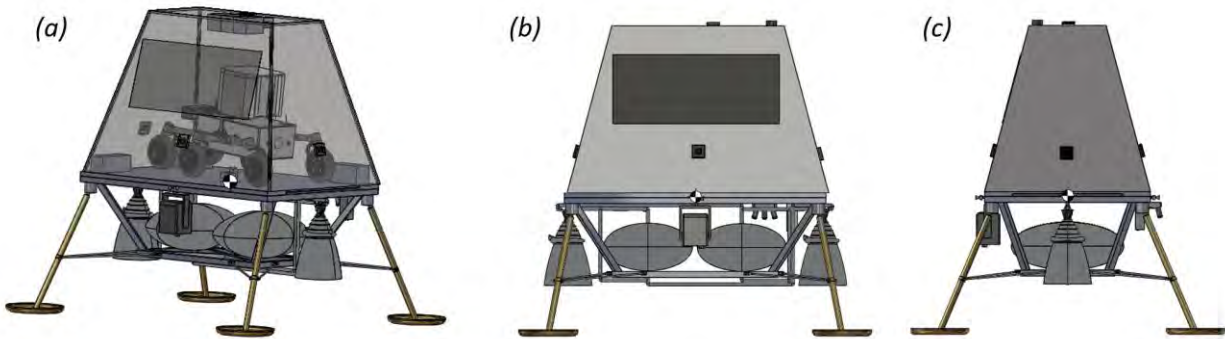


Figure 33: Lander System Overview of Exterior. Engineering perspectives of the exterior of the lunar lander are shown; a) front isometric vie, b) side view, c) side view. Note that (a) shows the rover in the stowed position on the interior of the lander. The center of mass is shown with 10% remaining fuel.

As seen in Figure 33, each rover is housed within a lander that will descend into the respective lunar crater. To ensure the selection of a safe landing site, the landers are equipped with a high precision guidance, navigation and control system for obstacle avoidance to ensure a safe landing. The lander descent will be controlled via retro-rockets and honeycomb landing legs to absorb the impact upon landing from the residual velocity.

D. Lander Structure

Each rover will sit on the lander base which is made of 3 cm aluminum honeycomb sandwiched between two 2mm aluminum plates. The base will be attached to the thrust structure made of 5cm x 5cm box beam aluminum with a wall thickness of 5mm. The engines and attitude control thrusters will be mounted to the thrust structure to support the loads during descent. A ramp for the rover's descent is nested within the lander base, which can be seen in Figures 34 and 35. A spring actuated system will be used to deploy the ramp, which will rotate down to a maximum angle of 37° to rest on the surface when fully extended. While the rover should be more than capable of handling the 37° angle for descent, the top surface of the ramp will be textured to induce additional friction. This will improve the rover's traction to ensure a safe descent to the surface.

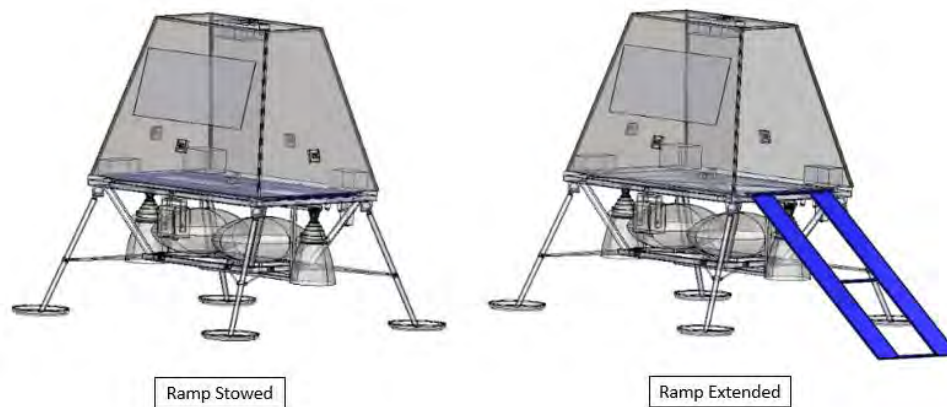


Figure 34: Ramp in stowed and extended configurations is highlighted. The ramp is stowed within the lander base and extends and rotates down for the rover deployment.

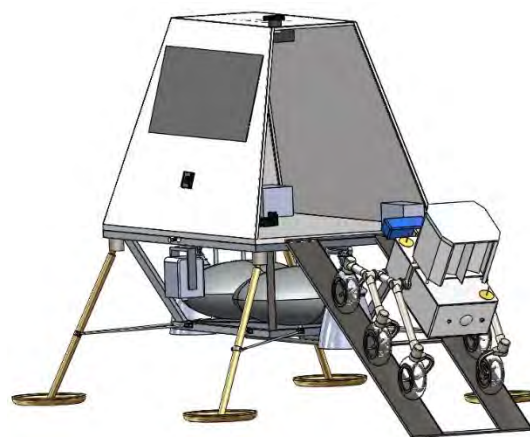


Figure 35: Lander Configuration with Rover Deployment. The figure depicts the rover traversing on the ramps out of the lander once on the lunar surface.

A housing, shown in Figure 36, for the rover was also included to prevent dust contamination during landing. The housing will consist of a frame made of 2cm x 2cm box beam aluminum with a wall thickness of 2 mm. The walls and top will be made of thin 2 mm aluminum sheet metal to keep the dust out of the enclosure. The housing was designed to not need to support any significant loads during landing, allowing it to be a very lightweight, protective structure.

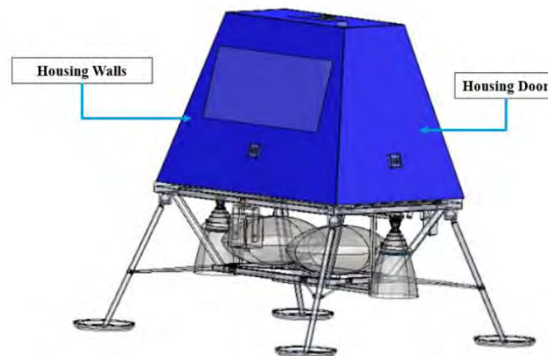


Figure 36: Housing for the lander is highlighted. Lightweight housing is used to prevent dust contamination from plumes formed during descent.

The lander legs, shown in Figure 37, will be made of aluminum honeycomb to absorb the impact of landing. The honeycomb should crumple, lowering the overall height of the lander and therefore reducing the angle of the ramp for rover deployment. However, the outer casing of the legs will ensure the legs will not fail completely. The legs also have a landing pad of 0.5 m diameter to ensure stability upon landing. The legs will be supported with secondary struts attached to the thrust structure for additional stability and strength.

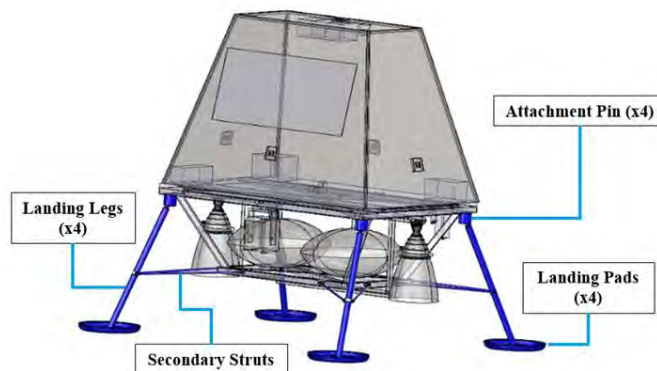


Figure 37: Landing legs are highlighted. The lander will impact the surface on aluminum honeycomb legs supported by secondary struts.

The instruments required for guidance, navigation, and control for landing will be placed according to their respective function. The altimeter, Lunar Imaging Sensor, Doppler LiDAR optics, and FLASH LiDAR optics will be mounted on the thrust structure and lander base to allow full visibility during descent for precision landing. The electronics for these components, the computer, IMU, and batteries will be located within the lander housing to ensure they are maintained within their operating temperature range. A radiator will be located on one wall of the lander housing to ensure the interior of the housing does not exceed any instrument’s operation survival temperature. The dimensions for the lander components can be seen in Table 16, with the overall dimensions labeled in Figure 38.

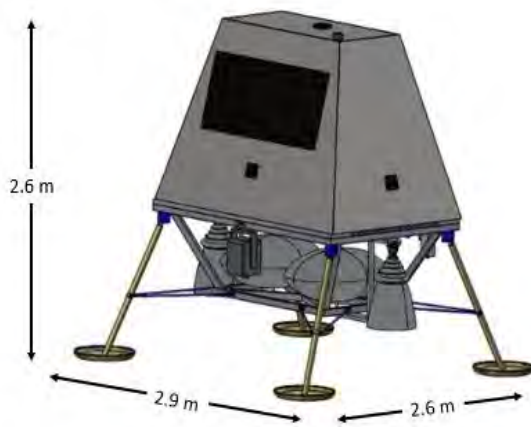


Table 16: Lander Dimensions Table.

Lander Dimensions (m ³)	
Housing	2.2 x 1.4 x 1.4
Legs	2.9 x 2.6 x 0.9
Total	2.9 x 2.6 x 2.6

Figure 38: Lander labeled with dimensions. The lander will have a height of 2.6m and a footprint of 2.9m by 2.6m.

E. Lander Propulsion

The propulsion system for the lander is required to be capable of decelerating from the lunar polar orbit speed of 1.6km/s, providing 8kN of thrust to lower the lander from orbit into the basin of the crater, and safely descending the lander to 2m above the lunar surface. The major features of the propulsion system are a hypergolic fuel and oxidizer combination as the bipropellant and two Aerojet R-40b engines. The propulsion system is mounted under the lander in a truss structure to keep the propulsion system away from the rover. A turbopump drives the fuel and oxidizer through the pipe system from the tank to the engine and multilayer insulation covering the system ensures that the fuel and oxidizer are kept within the acceptable temperature ranges for maintaining a liquid state. The propulsion system is shown in Figure 39.

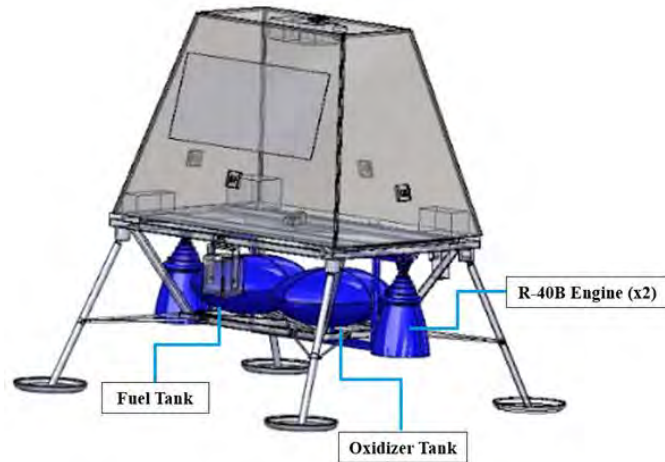
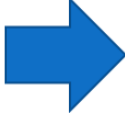


Figure 39: Lander Propulsion System. The lander propulsion system consists of two R-40b engines at either side with a fuel tank and an oxidizer tank in the middle. Pipes circulate propellant from both tanks to each engine. The pipes also move propellant back into the tank to maintain ullage pressure.

From past missions, three methods of landing were determined as potential candidates for to get the payload from the lunar orbit to the crater surface. The more unconventional Pathfinder airbag landing and Curiosity sky crane landing methods were investigated in addition to the Apollo strut impact landing [41,42,43,44]. The factors considered in the trade study between the options were cost, complexity, holistic system-level risk, proximity to a designated landing location, and surface contamination level from hydrazine [45,46,47]. The complexity factor was defined as the number of working parts in the system. Since the scientific objective is to determine the amount of water in the soil and hydrazine is known to add traces of water to the surface when burned, it was necessary to factor in the contamination in addition to more relevant criteria. Completing the landing by impacting on struts was objectively the best design as shown in Table 17 because it was the most accurate and had the lowest risk associated with the maneuver. Consequentially, the scientific mission architecture was then forced to adapt to the high contamination levels associated with this method by starting the data collection process farther away from the landing site.

Table 17: Trade Study of Different Landing Methods. Three options were analyzed in five categories. The risk and contamination categories are normalized values because both were holistically quantified. The table on the right shows the results with landing on struts being the preferred landing method.

Parameters	Cost (\$ millions)	Complexity (parts)	Risk (Norm)	Proximity Accuracy (km ²)	Contamination (Norm)
Weight	0.291	0.072	0.328	0.294	0.015
Impact on Struts	50	50	8	75	5
Sky Crane	500	100	7	120	4
Airbags	4	24	6	3000	7



Total	
Impact on Struts	7.304
Sky Crane	4.627
Airbags	5.567

Due to the ΔV and thrust requirements, electric and solid options for propulsion were disqualified. Electric options do not provide enough thrust while solid motors have neither the ability to restart nor the variability in thrust range to accommodate the maneuver. Monopropellant options were disqualified as well because bipropellants exhibit the highest Isp of liquid propellants, meaning they have the lowest propellant mass.

The first decision made when selecting an appropriate fuel for this stage of the mission was whether to use cryogenic bipropellant or hypergolic bipropellant [48]. Given emphasis on scientific exploration, hypergolic fuels were chosen because they did not require as much thermal attention as cryogenic fuels, leading to more usable mass for scientific payloads. Another driving factor for choosing hypergolic fuel over cryogenic fuel is ease of the performing engine restarts for adjustments during descent and landing. An additional reason for selecting hypergolic fuels is that industry engines, which cater to the thrust requirements for this craft, use hypergolic fuels. A final deciding factor was the mission length because cryogenic fuels boil-off in space, meaning mass is wasted and the range of usable propellant is limited. Table 18 shows a comparison of hypergolic and cryogenic propellants in terms of liquid temperature ranges.

Table 18: Propellant Freezing and Boiling Temperatures. The first three chemicals are cryogenic propellants and the last three chemicals are hypergolic propellants. Cryogenic propellants require much lower temperatures to maintain them at a liquid state, which in turn requires more energy.

Chemical Formula	Density kg/m ³	Freezing Point C	Boiling Point C
O₂	1140	-218.8	-183
H₂	71	-259.3	-252.9
CH₄	423	-182.5	-161.6
N₂O₄	1450	-9.3	21.15
N₂H₄	1004	1.4	113.5
CH₃NHNH₂	866	-52.4	87.5

The approach to selecting a hypergolic fuel and oxidizer pair was coupled with the selection of an engine. Since these two aspects of the overall propulsion system share common design constraints, coupling the limitations for each was the best way to focus on realistic design options. The thrust requirement for the engine eliminated the high thrust engine echelon (>50kN), which included the Merlin engine and the Lunar Module Descent Engine (LMDE) as well as the low-thrust engine echelon (<1kN), which included HiPAT and other Aerojet engines [49]. From this thrust requirement, the R-40b was deduced to be the best commercial option with a thrust capability of 4kN [50]. This engine operates using MMH as the fuel and NTO as the oxidizer in an O/F ratio of 1.65. The engine has a low risk of failure due to a proven flight history. The masses and diameters for each engine are shown in Table 19.

Table 19: Masses and Diameters of Engines Representative of different Thrust Echelons. Three engines representing different thrust capabilities are compared. The mass of the engines with lower thrust are much closer to each other than to the mass of the high thrust engine, suggesting that the highest thrust per kilogram is near the lower echelons.

Engine	Thrust (kN)	Mass (kg)	Diameter (m)
HiPAT (Aerojet)	0.445	5.2	0.325
R-40b (Aerojet)	4	7.23	0.4
Merlin (SpaceX)	914	470	1.25

The mass of fuel needed can be calculated needed using Equation 1, having selected an engine and knowing the dry mass of the lander and the ΔV of the EDL phase. The Tsiolkovsky rocket equation is the underlying theory for determining the limitations of payload mass for a certain engine's performance; and derivations allow it to be versatile enough for this situation. Given a 345.3 kg lander, an engine Isp of 293 seconds, and a ΔV of 2.25 km/s, 469 kg of

propellant is needed: 292 kg of oxidizer and 177 kg of fuel given an oxidizer to fuel ratio of 1.65 for the engine. The fuel and oxidizer tanks were sized using ellipsoid tanks appropriate to the size of the thrust structure on the lander. Both tanks were sized to the fuel tank volume so that there is static stability when the burn concludes and the center of mass of the lander changes. A 10% margin for both fuel and oxidizer was used as emergency propellant and because the pumps are less effective at lower tank volumes. Therefore, the total mass of propellant is 515 kg.

$$m_f = m_d \left(e^{\frac{\Delta V}{g_0 I_{sp}}} - 1 \right) \quad (1)$$

Table 20: Masses and Volumes of Propellant for the Landing Maneuver. The masses of propellant are found using theory in addition to STK simulations. The tolerance was added to leave emergency fuel in the tanks. The volume of propellant in each tank was used to determine the tank size.

Propellant	Mass Required (kg)	Mass with Tolerance (kg)	Tank Volume (m ³)
NTO	292	321.2	0.222
MMH	177	194.7	0.225

F. Lander Guidance, Navigation, and Control

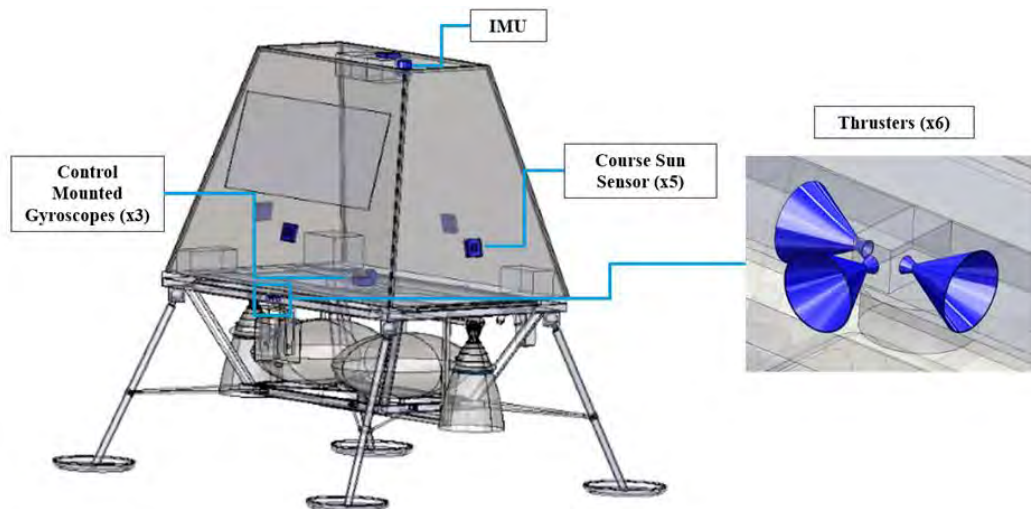


Figure 40: Lander Overview with Lander GN&C Components in Blue. The sun sensors, Control Mounted Gyros (CMG), thrusters, and IMU are called out. A closer view of the thrusters is shown on the right.

As outlined in Section VI.B, the lander must be able to safely land in its designated crater without tumbling and damaging the rover inside of it. To meet this requirement, the lander has an attitude determination and control system. To determine the relative attitude of the lander two independent instruments are used. One is a system of coarse sun sensors. Each side of the lander will have one for a total of six. The sun sensors have an accuracy of about one and a

half degrees. These will be used to ensure that the lander is pointed in the correct direction. The second instrument is an IMU which will be used to measure rotation rates and translational accelerations of the body. The IMU will be used to ensure that the lander is not spinning out of control and remains in the correct orientation for the entire landing process. These components are called out in Figure 40.

Once the attitude has been determined, a system is needed to control the lander to rotate it until it is in the correct orientation. Three different systems were analyzed to determine the best Attitude Determination & Control System (ADCS). Table 21 shows the results of the trade study performed. The three systems were RWA, CMG, and thrusters which were compared with their cost, mass, effectiveness, complexity and lifetime. A catastrophic risk of the mission is lander failure, so the decision was made to include two of the systems: thrusters and control mounted gyro. There will be a total of six thrusters, three on each side. This will allow for translational motion and rotation about one axis to be controlled. The thrusters will use about two kilograms of hydrazine gas for a total of no more than 5 m/s ΔV . The thruster configuration was chosen for its simplicity as well as its efficiency [51]. CMG are a small system of three gyros which will be used to control rotation about all three axes of the lander. Adding the CMG was for redundancy and also because the height of the lander made it difficult to control some of the axes spin rates due to their moments of inertia. The spinning CMG also have inertia to help maintain the correct orientation of the lander.

Table 21: Trade study performed on the lander attitude control systems. Thrusters ended up winning due to their low weight and complexity. Adding a RWA was too complicated and required too much room, so CMG were selected as a redundant system.

Parameters	Mass (kg)	Effectiveness	Cost (\$)	Complexity	Lifetime (yrs)
Weight	0.296	0.104	0.055	0.438	0.107
RWA	12	9	20000	7	10
Control Mounted Gyro	1	8	5000	5	5
Thrusters	28	8	15000	9	<1



Total	
RWA	7.046
Control Mounted Gyros	6.768
Thrusters	7.148

While the lander is descending, a lunar imaging sensor will be used to identify any hazards on the lunar surface. When a safe landing site has been identified, the attitude control thrusters will fire to help guide the lander to the desired location. The lunar imaging sensor will have a resolution of greater than 0.25 m at an altitude of 300 m and will be able to identify a safe landing zone of 5x5 m [52]. These systems allow the lander to meet the requirement for the GN&C system.

G. Lander Power

The decision was made that each lander would carry enough Saft Li-Ion batteries to complete its mission, with no power source on board. The power budget also included the potential need for an emergency orbit, as shown in Table 22. This was necessary to mitigate the risk of not having an on-board power supply. With three 84 Wh Li-Ion, for a total of 252 Wh, the landers will satisfy its power requirements with an additional factor of safety close to two.

Table 22: Power Requirement Breakdown for the Lander. This table shows the three primary descent phases for the lander, along with their energy requirements. The total of 130 Wh includes the potential need for an emergency orbit. This would take place if the lander was not in the correct orientation for an unforeseen reason and the need for a second orbit was necessary.

Operating Mode	Duration (min)	Energy (Wh)
Release from Orbit	1:00:00	24.5
Descent to 70 km	0:39:59	18.8
Burn to 1 m	2:28	11
Emergency Orbit	2:48:00	85.3
Total	~	139.6

H. Lander Thermal

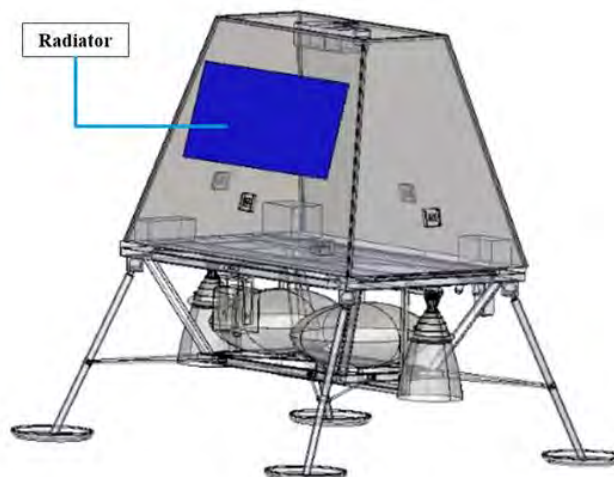


Figure 41: Lander Isometric View with Radiator in Blue.

The greatest challenge with the lander thermal system was managing the RTG heat. Contained within the lander, all 720 W of excess RTG heat will dissipate directly into the system. To account for this, an extension of the rover thermal loop was developed, based on the Curiosity thermal control system [29]. The heat from the RTG cold plate and the remainder of heat from the RTG is collected by the landers heat pipe system, within its shell, and then transferred to

a radiator on the exterior of the lander. Table 23 shows a summary of the thermal analysis used on the lander. The lander loss was computed knowing the lander surface area and designing for a one square meter radiator to be installed on one of the sides of the lander. Heat loss was computed using the Stefan-Boltzmann Law. The design variable for this analysis was the thermal coating used on the rover. Having a large surface area, the lander needs lower relative emissivity to maintain an internal temperature of 10°C. Through this, the best option regarding thermal coating for the landers was Beryllium Lap Finish, which has an emissivity of 0.12 [53]. Given this analysis, the lander will satisfy the requirement to maintain thermal equilibrium during descent to the lunar surface.

Table 23: Lander Thermal Analysis Summary. This table summarizes the analysis used on the rover. The lander electronics/instruments heat output was computed in the same manner as that of the rover. The rover is idle during the descent. The peak case for the lander was used for this analysis as a worst case scenario test case.

Operating Mode	Value
RTG Excess Heat, assuming 100% heat retained within Lander (W)	720
Rover WEB Heat Output, idle(W)	5
Lander Electronics/Instruments Heat Output (W)	22
Total Heat into the Lander (W)	747
Heat Loss through Lander Walls at 10°C (W)	537
Heat to Pump Out of Radiator (W)	210
Total Heat out of Rover (W)	747
Cold Plate Radiating Temperature (C)	-16
Heat Pump Power Req. with 1.5 FS (W)	4

I. Lander Avionics

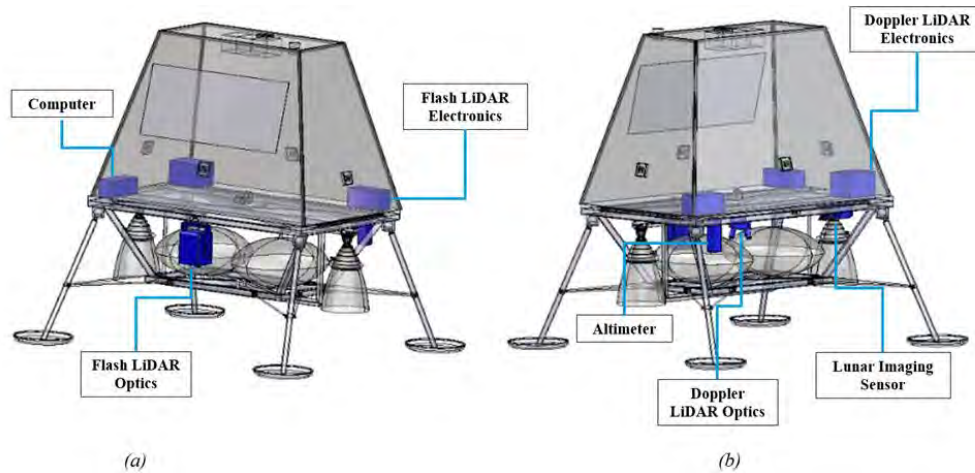


Figure 42: Lander Front and Back Isometric View with Avionics in Blue. The avionics called out in the diagram are the computer, Flash LiDAR, Altimeter, Doppler LiDAR, and Lunar Imaging Sensor.

The EDL trajectory needs to be followed closely to allow for the safe landing and deployment of the rover systems in the craters, whose components are called out in Figure 42. To accomplish this, the avionics of the lander need to provide and analyze information to the on-board computer rapidly to ensure the correct descent trajectory. The avionics required for this fall into three different operating scenarios which were described in the trajectory and power sections.

Throughout the entire descent, the lander's IMU will be giving approximate position data but there can be significant drift, sometimes over a kilometer, when venturing to the Moon [54]. Therefore, to provide more accurate altitude data, the lander will have a radar altimeter, Flash LiDAR, and Doppler LiDAR. These three instruments will ensure that even in the dark polar craters the lander will be able to accurately land. For the initial part of the burn, the lander will have to rely on the IMU for the approximate altitude data because the burn commences at 34 km above the surface. At 30 km, the altimeter will begin operating and providing altitude data. Once the lander has descended further, to about the 15 - 20 km altitude range, the Flash LiDAR will turn on and begin to operate. This will give redundant altitude readings to the computer to aid in the guidance.

Once the lander has continued the descent burn and lowered to 2.5 km, the Doppler LiDAR will begin to operate. The Doppler LiDAR will provide the velocity of the lander to the computer as well as more accurate altitude data, 10 cm accuracy instead of 20 cm [54]. This additional redundant altitude data will ensure that the computer is constantly

getting accurate data, which is critical for the timing of the burns. The combination of the IMU, altimeter, Flash, and Doppler LiDARs will provide the lander with accurate altitude and velocity data to allow for the safe descent to the Moon’s surface.

In order for the lander to use the altitude and velocity data from the sensors above to safely land at the target site, an on-board lunar imaging sensor will also be used. The lunar imaging sensor will provide additional data for hazard avoidance during landing. This will be critical as the landing site needs to be relatively flat in order to safely deploy the rover. The imaging sensor will be used sporadically to take images for analysis by the computer. This will be used to make sure no emergency situations come up. A concept of operations of the avionics usage for the lander can be seen in Figure 43.

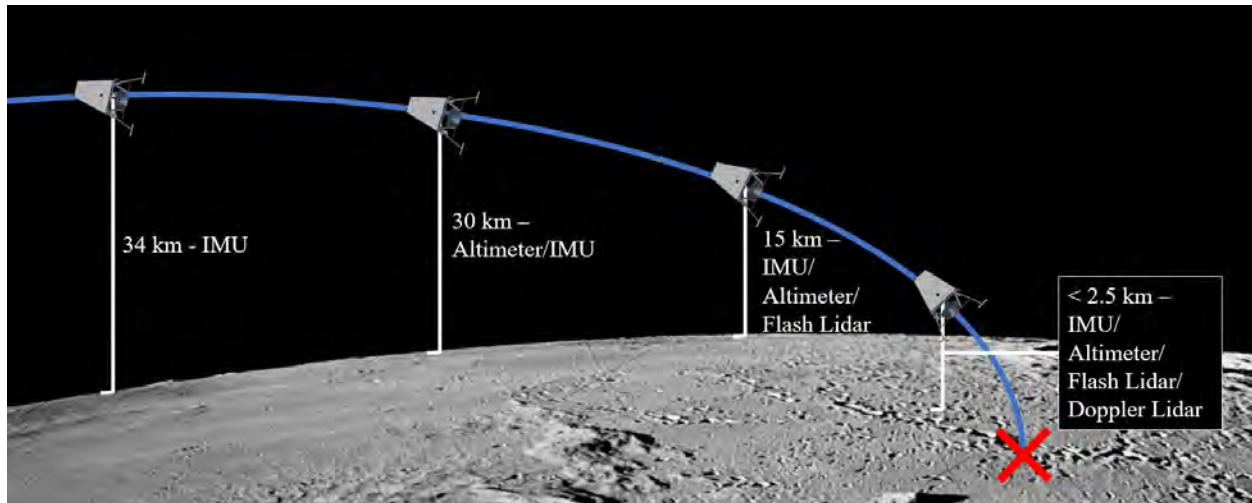


Figure 43: ConOps of Lander Avionics during EDL maneuver. The figure displays the different altitudes at which the avionics begin to operate. As the lander descends, additional items begin to operate to more accurately give the altitude and velocity of the lander to the on-board computer.

Overall, the lander avionics will be used to ensure a smooth and safe EDL trajectory which is achieved through redundant systems of altimeters, IMUs, and various types of LiDAR.

J. Mass Budget

The mass budget for each individual lander is found in Table 24. Each lander will have a dry mass of 345.3kg. With the 10% reserve fuel left onboard by the end of the EDL maneuver and the rover mass included, the landers will have a touchdown mass of 511.3kg. A basic stress analysis was performed to ensure the structure could withstand the loads

endured during landing. An analysis of the center of gravity was also performed in SolidWorks to ensure the vehicle would be stable upon landing.

Table 24: Mass Budget for Lander. This table indicates the mass allocation and limits for each of the lunar landers by subsystem at a component level.

Subsystem	Part	Basic Mass (kg)	MGA (%)	Predicted Mass (kg)	Mass Limit (kg)
Attitude Control	Control Mounted Gyroscope	2.5	5%	2.6	4
	Attitude Control Thrusters	2.1	5%	2.2	4
	Course Sun Sensor	1.3	5%	1.3	3
Navigation	Altimeter	1.4	5%	1.4	3
	Computer	6.5	5%	6.8	8
	IMU	0.2	5%	0.2	1
	Flash LIDAR FLSH	10	5%	10.5	15
	Flash LIDAR LED	5	5%	5.3	10
	Doppler LIDAR Optics	5	5%	5.3	10
	Doppler LIDAR Electronics	10	5%	10.5	15
	Lunar Imaging Sensor	8	10%	8.8	12
Power/Thermal	Batteries	10.3	15%	11.8	20
	Radiator	5	15%	5.8	10
Propulsion	Tanks and Feedlines	54.6	15%	62.8	75
	Engines	13.6	15%	15.6	20
Structure	Housing	54.4	30%	70.8	70
	Lander Base	27.8	30%	36.1	35
	Thrust Structure	27.6	30%	35.9	50
	Landing Legs	50.8	30%	66.1	100
	Secondary Struts	2	30%	2.6	6
	Ramp	44.2	30%	57.4	70
Miscellaneous	LIDAR Gimbal	2.3	5%	2.4	6
	Brackets	0.8	5%	0.8	3
Total		345.3		423	550

VII. Earth to Lunar Transfer

The final phase designed for Project Penguin was the initial phase, or the Earth to Lunar Transfer. In this phase, a spacecraft is launched into GTO and then propelled into a lunar polar orbit. This phase also outlines the operations of the Orbiter once the landers are deployed.

A. Requirements

The main requirements for the Orbiter include transportation from GTO to lunar polar orbit, communication relay for the duration of the mission, and deployment of the landers to the lunar surface. This includes maintaining environmental conditions while propelling from an Earth to a lunar orbit. Additionally, the Orbiter configuration needs to fit within the mass and volume envelope of the Falcon 9 payload fairing (PLF) and withstand the acceleration and vibrations of launch.

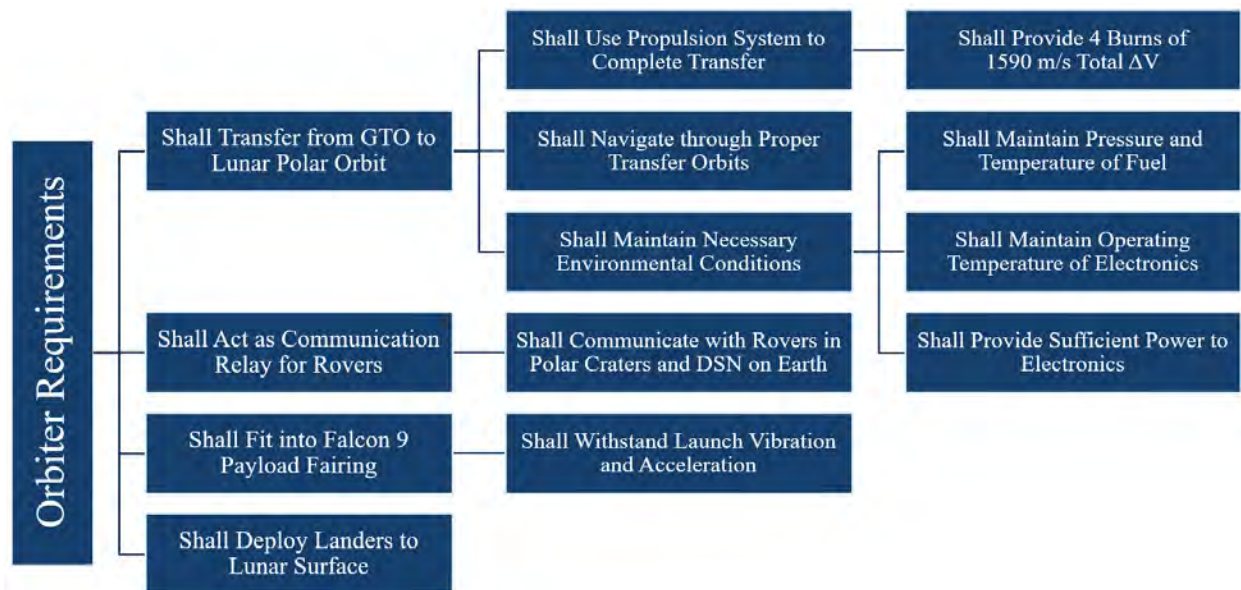


Figure 44: Orbiter Requirements Flowdown. The figure outlined the primary requirements set for the Orbiter and some derived requirements.

B. Launch Vehicle Selection

To allocate technical budgets and gauge the flexibility of the mission architecture under the mission constraints, the mass and cost envelopes for potential Earth launch vehicles were determined in the first steps of the decision-making process. Initial launch vehicle research included heavy-lift rockets such as the Space Launch Vehicle (SLS) and the Delta IV Heavy. However, as the proposed mission is unmanned, the larger payload mass gained from a heavy lift

rocket would not be necessary. Thus, focus was placed on medium-lift rockets, such as the Falcon 9, Delta IV, and Atlas V.

As Table 25 indicates, the comparison metrics for the launch vehicles were cost, maximum payload mass to GTO, and maximum PLF volume. Maximum weighting was placed on the cost to launch given the maximum allowance of \$500 million for the mission.

The payload masses were compared for launch to GTO after this was determined to be the trajectory with the optimal ΔV . The medium-lift rockets often had PLF diameters ranging from 4-5 m. As the mission was predicted to be more mass constrained rather than volume constrained, the smaller PLF diameters of approximately 4 m were deemed sufficient. As Table 25 indicates, the Falcon 9 Full Thrust (FT) presented itself as the obvious choice for the mission as this launch vehicle excelled in all metric categories. This launch vehicle had significantly higher allowable payload masses and PLF volumes while costing 50% less than the other options to launch. Thus, the Falcon 9 FT was chosen as the mission launch vehicle.

Table 25: Trade study to determine mission launch vehicle. Using the AHP a trade study was completed to determine the mission launch vehicle. The cost to launch metric was weighted the highest due to the mission budget constraint of \$500 million.

Parameters	Cost to Launch (\$ million)	PLF Volume (m ³)	Maximum Payload Mass GTO (kg)	Reliability (%)
Weight	0.46	0.04	0.17	0.33
Falcon 9 FT	62	145	8300	100
Delta IV	164	85	6160	100
Atlas V	121	89	5909	100



Total	
Falcon 9 FT	9.72
Delta IV	8.21
Atlas V	8.67

Figure 45 shows the overall PLF configuration and assembly. The bottom of the Orbiter WEB is connected to the in-space propulsion fuel tank and nozzle for GTO to Lunar Polar Orbit (LPO) transit. A pyrotechnic ring is used as the mechanism to deploy the landers. One pyrotechnic ring connects the top of the Orbiter WEB to Lander 2 (bottom), while a second ring connects Lander 1 (top) to Lander 2. Pyrotechnic bolts attached to the lander will explode upon deployment. The potential energy buildup in the ring's compressed spring will then apply the deployment force to the lander that will send it along the desired trajectory. Not pictured in this configuration is the secondary payload adapters for the Falcon 9 fairing that will be used to support the landers and orbiters during launch. The adapter is equipped with six vibration isolators surrounding the adapter ring, which will provide stability against vibrational loads during

launch. Figure 45 does not indicate the orbiter in correct PLF configuration, as the solar panels will be folded in against the side of the orbiter WEB and IPS fuel tank. The orbiter solar panels will only be deployed when the PLF separates from the secondary payload adapter.

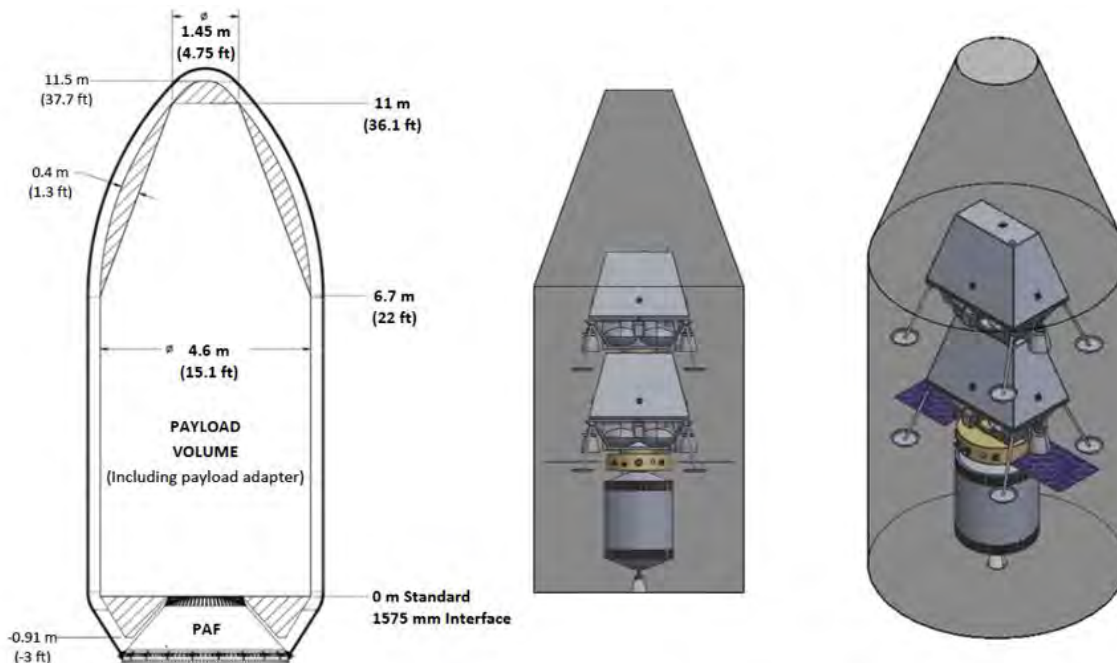


Figure 45: Falcon 9 FT PLF assembly containing the lunar orbiter and two landers. The Orbiter is connected to the in-space propulsion tank on the bottom. The two landers are stacked on top of each other via a pyrotechnic ring which will serve as the deployment mechanism. The bottom of the two landers is also attached to the Orbiter via a second pyrotechnic ring. Not pictured are the secondary payload adapters which will be used to support the payload inside the fairing during launch.

C. Transfer Trajectory

Since the objective of the mission is to have systems collect data from within lunar craters, the systems first need to be transported to the Moon. In determining the path to the Moon, the first consideration made was the final parking orbit around the Moon. The Orbiter needs to be able to receive data from the system on the Moon and therefore needs to orbit over the craters in question. Since the craters of interest are located on the South Pole of the Moon, a polar orbit will be used for the final parking orbit. This will allow for the Orbiter to communicate with the systems in the craters. While the communication will not be constant, the Orbiter will provide multiple passes per day.

After determining the parking orbit around the Moon, the transfer from the Earth to lunar orbit was investigated. The transfer trajectories considered were chosen to originate from either LEO or GTO as the chosen launch vehicle

could deliver its payload to either starting point. Trajectories from LEO and GTO will be compared to decide which the final transfer trajectory will be.

The first set of trajectories considered originated from LEO. The transfers considered were a Hohmann transfer, bi-elliptic transfer, and elliptic bi-parabolic. Due to research of previous lunar missions the Hohmann and bi-elliptic transfers were considered. This was discussed in a bulletin titled “Ways to the Moon?” posted by the European Space Agency (ESA) [55]. The bulletin discussed different methods to transfer to the Moon and cited both the Hohmann and bi-elliptic as common, fast transfers to the Moon [56]. The elliptic-bi-parabolic orbit was chosen to be considered as it’s designed to lower the amount of ΔV required through the use of a swing-by past the targeted natural satellite [55].

Theoretically, a Hohmann transfer is a low-energy transfer between two circular, coplanar orbits [57]. The transfer will usually use the least amount of ΔV out of all possible trajectories between these two circular orbits. The Hohmann transfer is performed using a tangent burn from the initial parking orbit to place the spacecraft on an elliptic transfer orbit. Once the desired final radius is reached for the final circular orbit, a second tangent burn is performed to circularize the orbit at this radius. These two tangent burns will require the lowest amount of ΔV possible but overall, longer TOFs are expected from this transfer [57]. A diagram of an example Hohmann transfer is shown in Figure 46-a. The two ΔV s are shown in Figure 41-a and are both tangent to the circular orbits. While Figure 46-a displays the theoretical Hohmann transfer, for the scenario of this mission, the Hohmann transfer will not be used in exactly the same manner. This is due to the final parking orbit not being centered about the Earth. Therefore, the transfer is not between two circular orbits about the same body but instead between an Earth-centered orbit and a Moon-centered orbit. While this means that an exact Hohmann transfer can’t be explored for the mission, a variation of the transfer can be used. This variation will consist of two tangential burns and an elliptical transfer orbit like the theoretical Hohmann transfer, however, the final ΔV will place the spacecraft into a polar parking orbit around the Moon.

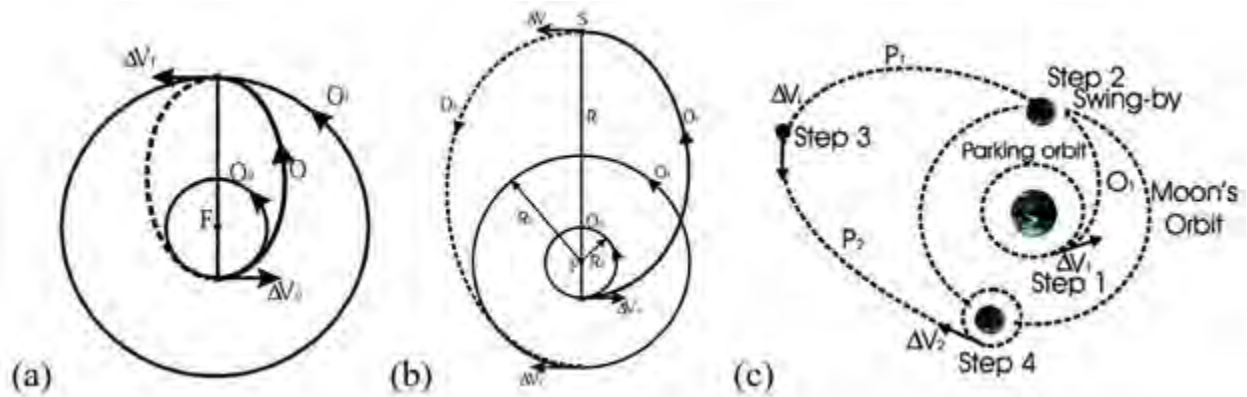


Figure 46: Diagram Theoretical Earth-to-Moon Transfers. (a) Hohmann transfer going from an initial orbit, O_0 , to the final orbit, O_f , using the transfer orbit, O and two tangent burns. (b) Bi-elliptic transfer displayed going from an initial orbit, O_0 , to the final orbit, O_f , using the two transfer orbits, O_1 and O_2 using three tangent burns. (c) Elliptic-bi-parabolic transfer going from an initial orbit about the Earth, to the final orbit around the Moon using the three transfer orbits, O_1 , P_1 , and P_2 using three tangent burns [55].

The next transfer considered was the bi-elliptic transfer. In certain cases, the bi-elliptic transfer can require less ΔV than the Hohmann transfer. This occurs when the final circular orbit radius is at least 11.94 times greater than the initial circular orbit radius [55]. When considering the Moon, this is the case and therefore, theoretically, the ΔV needed should be lower than the Hohmann transfer. The bi-elliptic transfer is performed by using three tangent burns and two transfer orbits. An example bi-elliptic transfer can be seen in Figure 46-b. In this figure, ΔV_i places the spacecraft onto the first elliptic transfer orbit before ΔV_j places the spacecraft onto the larger, second elliptic transfer orbit. The final ΔV_f places the spacecraft into the final circular orbit. Once again, the exact theoretical model can't be used for this mission. Instead of being placed onto a final circular orbit around the Earth, the final orbit will be around the Moon making an exact bi-elliptic orbit impossible. A scenario using three tangent burns in a similar manner will be used, however; the final burn will place the Orbiter into a circular orbit around the Moon.

The last transfer method considered was the elliptic-bi-parabolic transfer. This transfer is much different than the two discussed above as a gravity assist from the Moon is used. Theoretically, the orbiter will leave the Earth with the same ΔV_i as needed for both the Hohmann and bi-elliptic transfers but will require less to enter the final parking orbit. This will be achieved by accelerating the orbiter to a velocity similar to the Moon's to allow for less ΔV to be necessary to circularize the orbit. To accelerate the orbiter without using additional ΔV from the propulsion system, a swing-by of the Moon will be performed [55]. This can be seen in Figure 46-c as the first transfer orbit, O_1 , takes the orbiter to the Moon to provide an acceleration. This places the orbiter on the initial parabolic orbit away from the system. This

allows for the gravity effects from the Moon and Earth to be minimized during the second burn. Therefore, the burn ΔV_i will have a lower magnitude due to the lack of gravitational effects. This ΔV_i places the orbiter on the parabolic orbit back to the Moon at a velocity much closer to the Moon's. When the final burn, ΔV_f , occurs, less ΔV will theoretically be required to circularize the orbit. The orbit is designed for equatorial parking orbits around the Moon so the exact trajectory will not match the one shown in Figure 46-c. While the orbit will theoretically use less ΔV , to travel to an area far enough away to minimize gravity effects takes a much longer time than when compared to the other two transfers considered. This means that the overall TOF will be considerably larger.

For all the mentioned transfers, another reason their full theoretical algorithms cannot be used is because the lunar parking orbit is a polar orbit. Therefore, the transfer will not be coplanar, a requirement of the theoretical transfer discussed, unless an unusual initial parking orbit is used around the Earth. The unusual parking orbits would not be conducive to the normal launch sites used and would cost additional ΔV to be injected into. Therefore, slight alterations will be made to the transfers when targeting the final lunar orbit.

To decide the final LEO transfer trajectory to compare to the GTO transfer, the three transfers were modeled in STK to acquire exact values for the selected set of criteria. The criteria considered were number of burns, total ΔV , and TOF. The goal was to minimize the ΔV and the TOF while considering the added risk of additional burns. In order to obtain the values for ΔV and TOF, each of the scenarios were modeled in STK. The model of the Hohmann transfer can be seen in Figure 47. As described above, the transfer uses only two burns with one of them to escape Earth's gravity and the other to burn into the parking orbit around the Moon. Similarly, the bi-elliptic transfer model can be seen in Figure 48. The transfer requires three burns, one occurring to leave Earth, one occurring where the green and yellow lines merge on Figure 48 and the last to go into the final parking orbit. The last transfer, the elliptic-bi-parabolic, can be seen in Figure 49-a. This is the most complex of the transfers. While there are only three burns, the Orbiter initially performs a swing-by of the Moon. This swing-by can be seen in Figure 49-b shown by the yellow line. During this swing-by, the Orbiter gains ΔV and therefore allows the Orbiter to have a closer relative speed to the Moon at rendezvous.



Figure 47: Model of the Hohmann transfer in STK. The STK model of the Hohmann transfer displays the trajectory of the Orbiter on its way to the Moon. Once reaching the Moon, the Orbiter goes into a polar orbit to go over the desired craters.



Figure 48: Model of the bi-elliptic transfer in STK. The STK model of the bi-elliptic transfer displays the trajectory of the Orbiter on its way to the Moon. The middle burn is located where the yellow and green portions of the trajectory intersect.

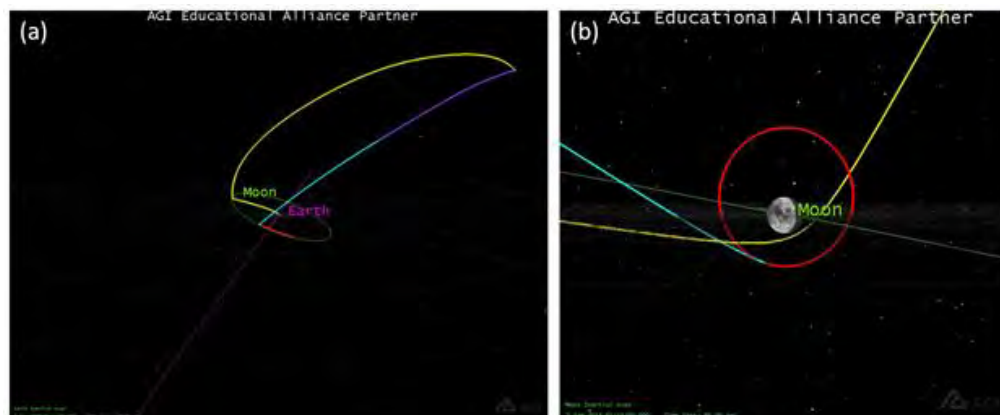


Figure 49: Model of the elliptic-bi-parabolic transfer in STK. (a) The STK model of the elliptic-bi-parabolic transfer displays the overall trajectory of the Orbiter on its path to the Moon. The middle burn occurs at the furthest point from Earth, where the yellow and purple portions of the trajectory intersect. (b) The swing-by at the Moon to reach the final polar orbit.

To model these three trajectories, the Astrogator feature of STK was utilized. This feature allows for STK to perform iterative methods to find acceptable trajectories for the desired final states. By modeling the orbits in STK, the total needed ΔV and TOF could be found. The calculated values can be found in Table 26. By looking at the table, the Hohmann transfer can be seen to perform the best of the three LEO trajectories. The Hohmann transfer uses the least amount of ΔV , has the lowest TOF, and the lowest number of burns. The total ΔV is approximately 4 km/s which is similar to previous missions [56]. The TOF is around 2.5 days and there are two total burns.

Table 26: Summary of STK model results for LEO Transfers. The total ΔV , TOF, and number of burns for the three considered transfers are summarized here. The Hohmann transfer has the minimum values for all three categories.

Transfer Type	Number of Burns	dV (m/s)	TOF (hrs)
Hohmann	2	4059	56
Elliptic-Bi-Parabolic	3	4701	2808
Bi-Elliptic	3	4092	360

Being launched into GTO would allow for the Orbiter to have a different trajectory to the Moon which would require less ΔV . The GTO transfer considered was discovered in the ESA bulletin discussed earlier. The one suggested in the bulletin can be seen in Figure 49.

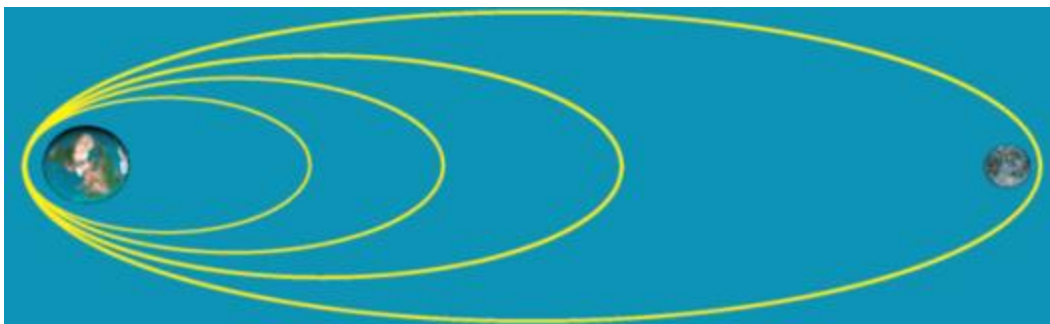


Figure 50: Theoretical GTO transfer to the Moon. The theoretical model of the GTO transfer trajectory to the Moon shown in the ESA bulletin [56]. The trajectory raises the apogee of the elliptic orbit until reaching the Moon.

The trajectory is achieved by using three separate burns at perigee to raise the apogee of the elliptic orbit. The burns happen each time the orbiter goes through perigee. Once arriving at the Moon, the orbiter will use one more burn to go into the required polar orbit. In order to calculate the needed ΔV , STK was once again to model the orbits. It was found that the first three burns to raise apogee each had a magnitude of 240 m/s while the final burn to go into

the lunar polar orbit was 871 m/s. This gives a total ΔV needed of 1591 m/s which is approximately 2400 m/s less than that of the Hohmann transfer discussed earlier. The STK model of the trajectory can be seen in Figure 51.

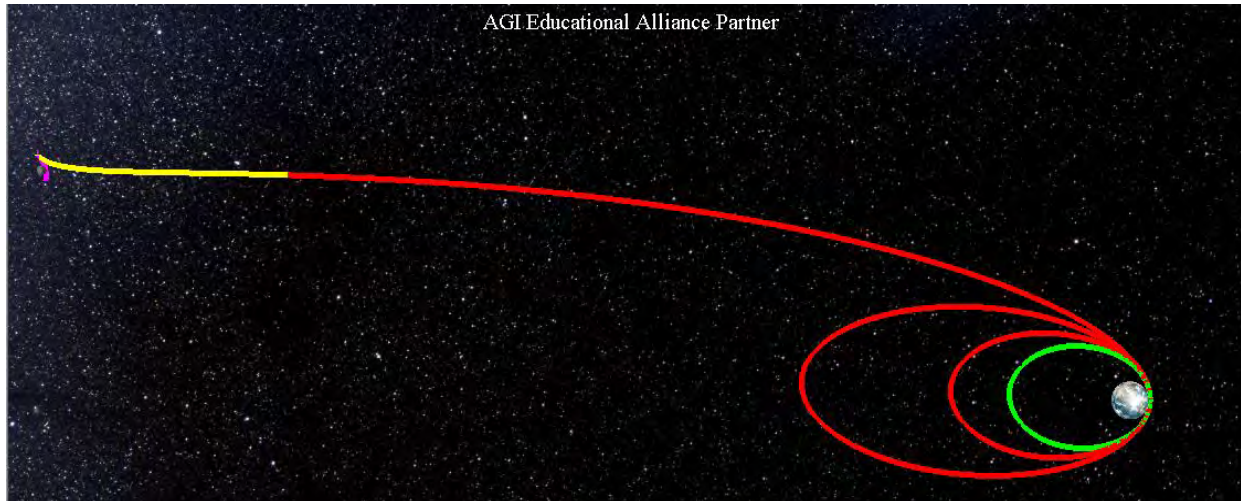


Figure 51: GTO transfer to the Moon. The figure shows the transfer orbit from GTO towards the Moon. The raising of the apogee of the elliptical orbit can be seen as well as the beginning of the path towards the Moon.

This trajectory has a total TOF of approximately 6 days. The amount of ΔV needed has dropped considerably from the LEO trajectories which will also lower fuel requirements. To decide between the possible transfers, an analysis on the impact on the overall mission was done.

To compare the two transfer trajectories, the Hohmann transfer-like trajectory from LEO, and the apogee raising GTO transfer, the impacts on the overall mission were considered. Due to the length of the overall mission, the TOF would be insignificant. Therefore, the main impact of the mission the transfer trajectory would be the amount of dry mass that could be carried by the Falcon 9. To calculate the fuel needed for the transfer portion of the mission, the maximum mass allowance for both types of launches was used. This means that the combined fuel and dry mass of the hypothetical launch payload inputted into STK were the values in Table 27. The results of these STK models can be seen in Table 28.

Table 27: Maximum fuel that can be carried by the Falcon 9. The maximum fuel that can be carried to LEO and GTO by the Falcon 9. The final destination of the payload greatly changes the final mass allowed due to the additional requirement on the Falcon 9.

Launch Destination	Maximum Mass Allowed (kg)
Falcon 9 to GTO	8,300
Falcon 9 to LEO	22,000

Table 28: STK model results for the LEO and GTO trajectories. The table displays the fuel requirements for both the LEO and GTO transfers as well as showing the overall dry mass allowed by both transfers.

Transfer Origin	Fuel Mass Needed (kg)	Maximum Dry Mass Allowed (kg)
GTO	3,337	4,963
LEO	17,244	4,756

As can be seen in Table 28, the GTO transfer allows for a more massive spacecraft to be taken to the Moon for the same price as going to LEO. Therefore, GTO was selected as the final transfer trajectory moving forward.

After deciding upon the final trajectory, the final mass values for the Orbiter system were put into the STK model to find the fuel values. Using the final mass of the Orbiter as 2254 kg, it was found that the Orbiter would require 1940 kg, which was then given an approximate 20% margin to give a final fuel value of 2400 kg.

D. System Overview

The Orbiter serves as both a vehicle to deploy the landers to the lunar craters as well as the intermediary for communication between mission control on Earth and the autonomous rovers on the surface, as outlined in Figure 44. Figure 52 shows engineering perspectives of the mission’s orbiter configuration. The following sections of this report will further elaborate on each of the Orbiter components by subsystem.

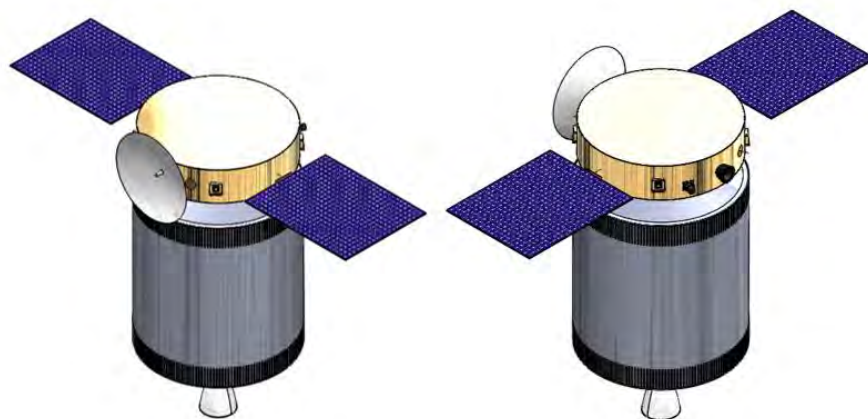


Figure 52: Engineering Views of Lunar Orbiter Exterior. Engineering perspectives of the exterior of the lunar orbiter are shown; a) front isometric view, b) back isometric view. The gold cylinder indicates the warm electronics box housing all of the instrumentation and the silver cylinder indicates the IPS fuel tank and HiPAT nozzle.

E. Orbiter Structure

As with the lunar rover, a majority of the Orbiter instrumentation is contained within the WEB, except for the instruments that are necessary for attitude control and communication which are required to be protruding to operate. The dimensions of the Orbiter WEB and overall structure are provided in Figure 53 and Table 29. A cylindrical design was chosen for the Orbiter WEB to minimize the number of possible stress concentrations. The interior of the Orbiter was configured so that the center of mass would remain along the center axis of the Orbiter WEB for ease of rotational axis attitude control. The Falcon 9 FT PLF diameter of 4.6 meters was sufficient to allow for the Orbiter solar panels to be readily extended during the launch phase. These solar panels would be structurally supported by a secondary payload adapter to minimize the applied vibrational loads during launch. The decision to have readily deployed solar

panels on launch was done to the probability of risk due to mechanical failure.

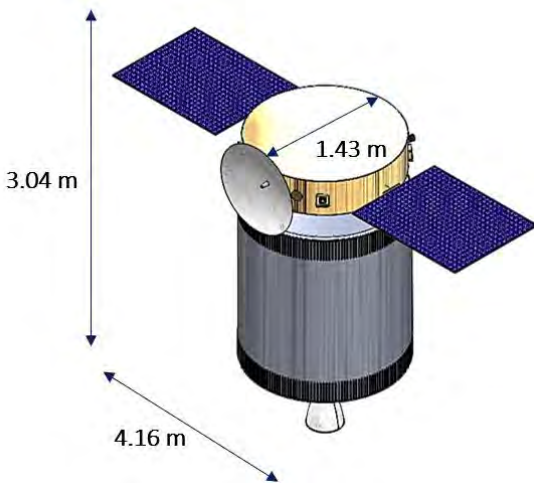


Table 29: Overall Orbiter Dimensions Table.

Orbiter	
WEB Dimensions	1.43 m diameter, 0.35 m height
Overall Height	3.04 m
Span Including Solar Panels	4.16 m

Figure 53: Orbiter Configuration Dimensions.

F. Orbiter Propulsion

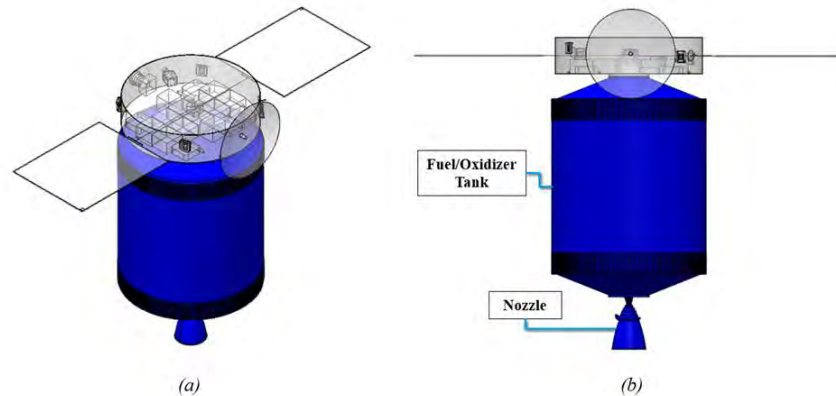


Figure 54: Overall Configuration of the Orbiter with the Propulsion System in Blue. The image points out the fuel and oxidizer housing as well as the Aerojet Rocketdyne HiPAT engine.

The requirement for the propulsion system for the Orbiter is that it must navigate the Orbiter, including both landers, from GTO to the lunar polar orbit, which requires providing a ΔV of 1.59 km/s. Additionally, the system must fit inside of the 4.6 m fairing inside the launch vehicle payload. The major features of this propulsion system are a hypergolic fuel and oxidizer combination as bipropellant and a single Aerojet Rocketdyne HiPAT engine. The propulsion system is mounted behind the warm electronics box on the posterior of the Orbiter. A turbopump drives the fuel and oxidizer through the pipe system from the tank to the engine. In addition, multilayer insulation covering the system ensures that the fuel and oxidizer are kept within the acceptable temperature ranges for maintaining a liquid state. In this case, NTO must be kept between -9.3 and 21.2°C and MMH must be kept between -52.4 and 87.5°C .

Similar to the selection of a propellant for the lander, electric and solid propellants were eliminated because electric propulsion systems could not perform the required burns quickly enough and solid propulsion systems did not have the ability to restart to complete the multiple burn maneuvers. Monopropellant options were disqualified as well because bipropellants exhibit the highest Isp of liquid propellants, meaning they have the lowest propellant mass. While the stage in the mission is earlier than the landing stage, the choice to avoid cryogenic propellants in favor of hypergolic propellants was also based on the requirement for active cooling systems and the abundance of industry engines that better suit the criteria.

In a similar manner to the lander propulsion decision making process, the selection of an engine drove the selection of a propellant pair because the design constraints were linked [57]. Five Aerojet bipropellant engines were

compared in a trade study shown in Table 30 to decide which engine would perform the best under the constraints of this stage of the mission [58, 59]. The parameters for comparison are the cost of the propellant in United States Dollar (USD) per kg, the temperature difference of the propellants in Kelvin, the density impulse of the engine using the preferred propellants, and the storage volume of the propellants given the required ΔV . The HiPAT engine has the lowest cost and temperature difference for its propellants and the highest density impulse, leading to its selection as the most appropriate engine choice [60]. Consequently, the fuel used in the HiPAT engine is Hydrazine and the oxidizer is NTO (MON-3).

Table 30: Trade Study of Different Orbiter Engines. Five options were analyzed in four categories. The temperature difference category depicts the difference between the fuel and oxidizer freezing points. The table on the right shows the results with HiPAT being the preferred engine.

Parameters	Cost (\$/kg)	Temperature Difference (K)	Density Impulse (kg*s/L)	Storage Volume (m ³)
Weight	0.52	0.06	0.15	0.28
HiPAT	79.95	10.7	342	4.75
R-42	86.87	43.1	325	5.35
R-42DM	86.87	10.7	342	4.67
AMR	91.48	10.7	342	4.58
R-40B	86.87	43.1	325	5.45



Engine	Total
HiPAT	8.282
R-42	6.457
R-42DM	7.485
AMR	6.454
R-40B	6.176

Using the Tsiolkovsky rocket equation as the underlying theory, the mass of propellant needed can be determined given the ΔV requirement for the maneuver. Given a combined mass for both landers and the orbiter of 2254 kg, an engine Isp of 326 s, and a ΔV of 1.59 km/s, the propellant mass needed is 1784 kg. This value was confirmed using the STK model of the trajectory. Assuming an oxidizer to fuel ratio of 0.85 for the HiPAT engine, the mass of fuel needed is 964.3 kg and the mass of oxidizer is 819.7 kg, which is reported in Table 31. The fuel and oxidizer tanks were sized using ellipsoid tanks and then encapsulated in a cylindrical structure for buckling support. This structure also allows for the propulsion system to interface with the WEB using struts. A 20% margin for both fuel and oxidizer was used as emergency propellant in case additional burns need to be performed and because the pumps are less effective at lower tank volumes. Therefore, the total mass of propellant is 2400 kg.

Table 31: Masses and Volumes of Propellant for the Landing Maneuver. The masses of propellant are found using theory in addition to STK simulations. The tolerance was added to leave emergency fuel in the tanks. The volume of propellant in each tank was used to determine the tank size.

Propellant	Mass Required (kg)	Mass with Tolerance (kg)	Tank Volume (m ³)
NTO	819.7	983.6	0.678
MMH	964.3	1157.2	1.336

G. Orbiter Power

Given the heritage of lunar Orbiter missions, solar power was selected as the Orbiter’s power source. The Azurspace Triple Junction Advanced 80 μm thick cell was selected due to being light weight and having a nominal efficiency of close to 29% [62]. Power draws above idle were designed to be accommodated by Li-Ion batteries.

Table 32 gives a breakdown of the Orbiter power budget. With all instruments/components operating simultaneously, the Orbiter requires close to 500 W of power, with a majority of that coming from the two on-board active heaters. Although this case is not likely, the power system is designed around this draw to mitigate the risk of not having enough power supplied to the Orbiter.

Table 32: Orbiter Power Draw Summary. This table outlines the power draw at idle and active modes for the instruments on-board the spacecraft. All components run at 28 V. During active, the spacecraft draws 18 A, which is within safe operating range for the Li-Ion batteries used.

Instrument/Component	Idle Draw (W)	Active Draw (W)
Computer (x2)	18	32
Star Tracker (x3)	15	36
IMU (x3)	36	36
IR Camera	4	40
Reaction Wheels (x4)	16	32
Transponder	10	80
Transponder (Moon) (x2)	2	20
Temperature Sensors (x4)	5	5
Control Mounted Gyros	1	4
HiPAT (Propulsion)	1	10
Heaters (x2)	2	200
Heat Pump	1	8
Total	129	507

The solar flux was assumed to be 1353 W/m², based off an average given in the Space Technology Library [36]. Using this and Equation 2, each Azurspace solar cell should produce 1.29 W of power in ideal conditions. Typically, a 28 V spacecraft bus should have solar cells strung to create between 32.9-42.3 V [36]. Taking 35 V to be the solar cell output 2.7 V to be the individual cell output, thirteen cells are required per string. The solar array was then designed to meet the given string dimension, extending in the second direction according to the desired output wattage. Given

a peak power requirement of about 500 W, the solar array was designed with a factor of safety of two. This accounts for times when the array may be partially or completely blocked by the spacecraft's shadow or when the array is not receiving direct sunlight.

$$P_{max} = \eta_{max}EA_c \quad (2)$$

Therefore, with a desired power output of 1000 W, the required number of solar cells is 780: 60 total strings of 13 cells. This is split between two arrays for a total array surface area of about 1.25 m² for each solar panel. From quotas given by Azurspace, the solar cells for this configuration costs a total of \$34,000 [62].

One primary concern with using solar energy to source power on the Orbiter is eclipse time, when the Orbiter is in the shadow of the Moon. STK analysis provided evidence that the Spacecraft will be in direct sunlight 88% during a year. This is broken up into long periods of continuous sunlight followed by long periods of 2.6 hour access to the sun with 2.3 hour gaps in eclipse. To allow for the spacecraft to operate at power requirements above idle during these periods, 10 Li-Ion batteries were added to the spacecraft bus. This provides confidence that utilization of high power devices for an extended amount of time will be possible, without constant sunlight [36]. This section shows that the Orbiter will successfully satisfy the requirement to maintain a consistent power supply to perform its operation throughout its entire mission.

H. Orbiter Thermal

The Orbiter is designed with an independent thermal control system, unlike how the landers uses RTG heat to maintain its thermal equilibrium. In lunar orbit, the Orbiter is subjected to a large temperature gradient: 50K-375K [63]. Analysis was performed for both extremes, to determine how many heaters would be necessary, assuming each would provide 100 W, based off existing Aerospace Corporation and Jet Propulsion Lab heater technology [64]. Since the Orbiter needs to maintain a 10°C temperature, the Stefan-Boltzmann Law was used to find that at -223°C the Orbiter loses 203 W; at 375°C the Orbiter intakes 496 W. This was computed assuming the Orbiter's thermal coating is Beryllium Lap finish, just like in the case of the lander.

This analysis shows that the heaters and pump system must provide 203 W and be able to reject 496 W. To accomplish the first task, two 100 W heaters were added to the design to bring the system to equilibrium during colder temperatures. A radiator is also included in the spacecraft to radiate the excess heat during hot cases. The heaters are

connected to an 8 W heat pump to distribute the heat throughout the spacecraft. This shows that the Orbiter satisfies the requirement to maintain thermal equilibrium during its mission.

I. Orbiter Communication

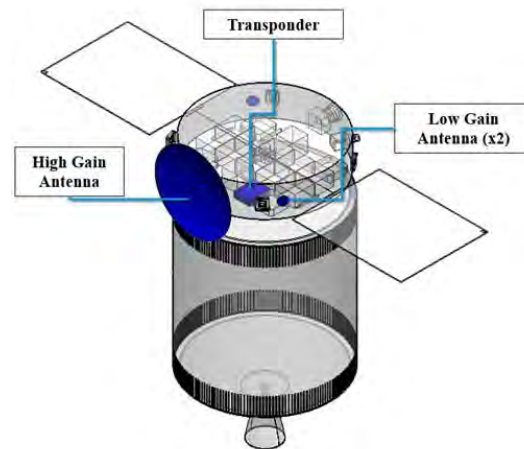


Figure 55: Isometric View of the Orbiter with the Communication System in Blue. All antennas and transponders are called out.

The requirement of the Orbiter communication system is to be able to relay commands from Earth to each rover and to relay data from each rover back to Earth. Additionally, the communication system shall have the capability to store data in case of communication link failures.

The Orbiter communication system, as seen in Figure 55, will consist of two small quadrifilar helix antennas which will be used for uplink and downlink with the rovers. These will not be actuated. A 0.87 m S-band dish antenna will be used for communications with the DSN. This antenna will be actuated on a gimbal, so that it can be pointed at the correct DSN station. Three transponders are also on the Orbiter, one for each antenna to be able to receive and transmit data. Connected to the transponders is an S-band power amplifier. In the Orbiter power budget this amplifier power requirement is factored in with the transponders for simplicity. All communication links will use BPSK modulation due to its history of use, efficient use of spectrum, and low susceptibility to disturbances. Communications for the Orbiter is a triple redundant system. Any of the three antennas can be used to communicate with the rovers. If the large dish antennas fail, the two smaller antennas should be able to transmit data to another spacecraft near the Moon which can send data back to Earth. These redundancy considerations were made to reduce the probability of catastrophic mission failure, if data could not be transmitted back to Earth.

Stations for the DSN are in California, Madrid, and Canberra. Each station is roughly 120° of longitude apart to ensure that objects can see at least one station at any point above Earth [65]. With this configuration the DSN has constant communication with objects at altitudes above 30,000 km [66]. Work in STK confirmed that the Orbiter will have nearly constant access to one of the DSN stations. Figure 56 shows a chart of the access times between each station and the orbiter over a one-week period. After this time, the access intervals will repeat in the same pattern. Figure 57 shows a picture of the full communication architecture done in STK.

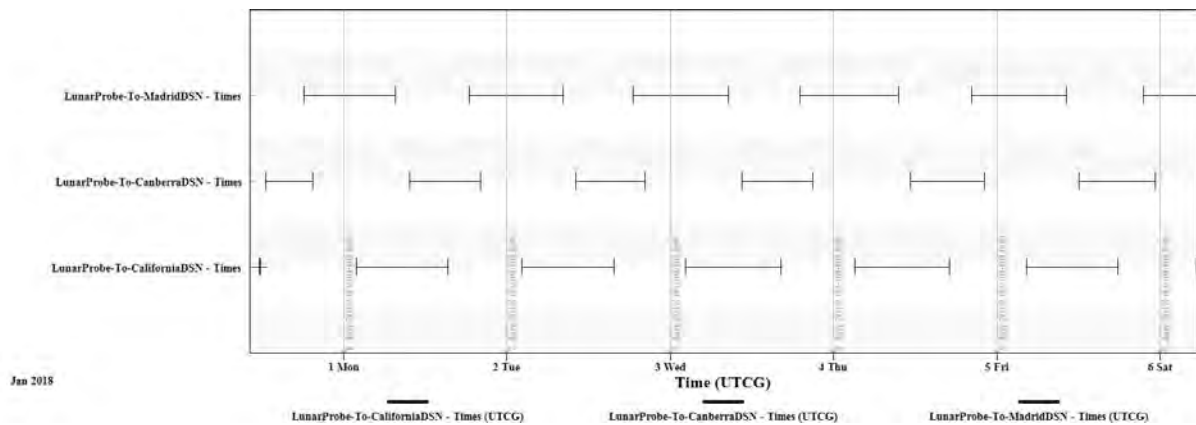


Figure 56: Graph of access times between Orbiter and rover. This is a graph of the access times between the Orbiter and the three DSN stations for a one-week time period. The graph shows that there is almost always an overlap between the end of access for one station to the beginning of access with another station. This means that the Orbiter will have near constant communication with Earth if necessary.

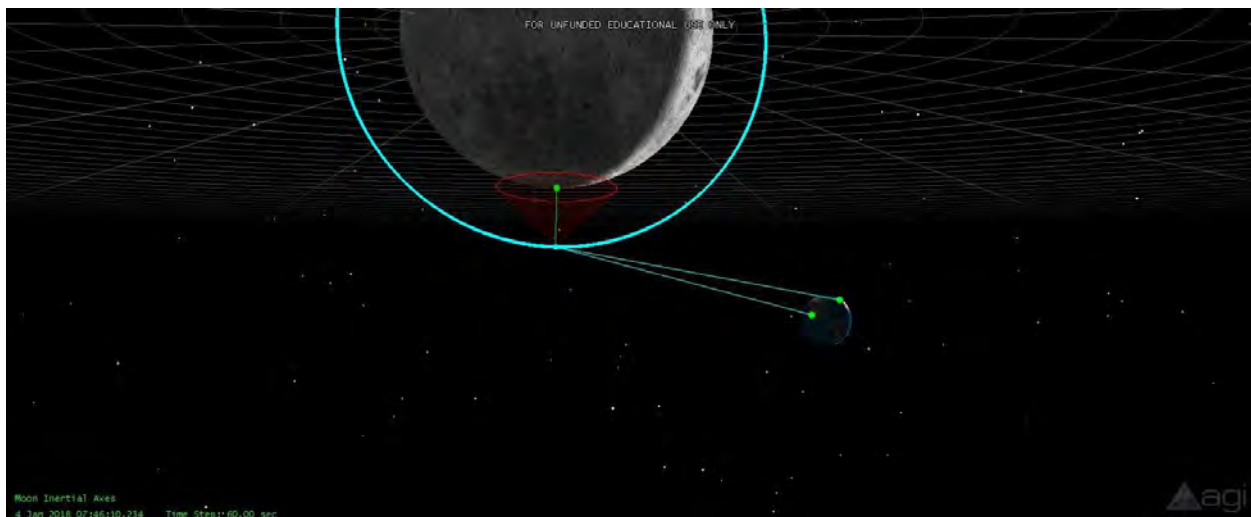


Figure 57: Picture of the full communication link shown in STK. Similar to the full communication link architecture picture, the communication between the DSN and a relay station is shown. Also shown is the communication between the Orbiter and the rover. The STK scenario is an extension of the scenario shown in Figure 19.

Since the cost of this mission is highly sensitive to changes in mass, it is preferred to operate on bands with higher frequencies, since the necessary antennae are smaller. The relationship between carrier frequency and diameter can be seen in Figure 58. The problem with high frequencies is that they have small wavelengths. As frequency increases the wavelength decreases. The wavelength of the signal drives the free space spreading loss of the antenna. This is the largest source of loss in a communication system [67]. A larger loss means that less power is received by the receiver thus requiring more power to be transmitted. For the link from Earth to the Orbiter, power requirements are not a problem, but power requirements for the transmission from the Orbiter to Earth are significant. This is because the power must be generated and stored on-board the Orbiter which is expensive. Due to this fact, carrier signals with a larger wavelength are desired for this mission. That is why S-band was selected over X-band for communication between the DSN and the Orbiter. Also, the required data rate factored into this decision.

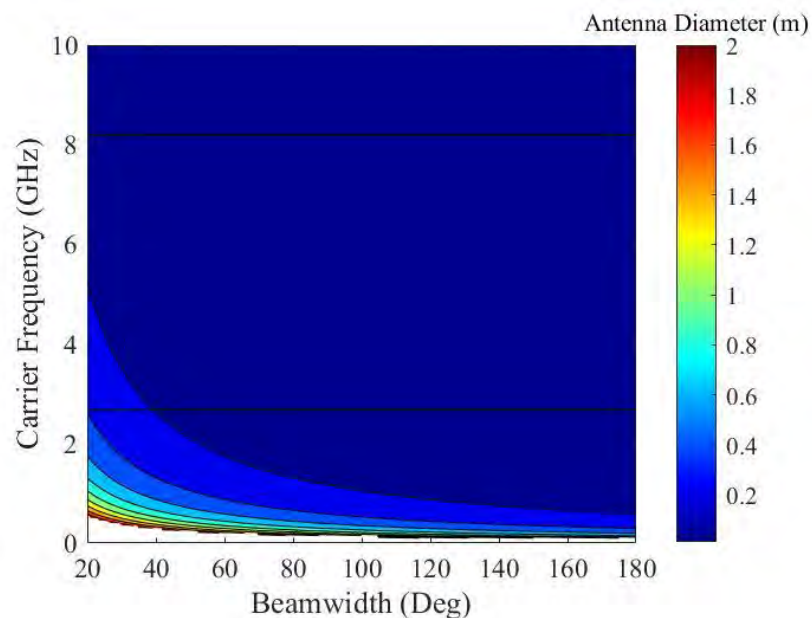


Figure 58: Contour plot of beamwidth, carrier frequency, and antenna diameter. The horizontal lines are the carrier frequencies for S-band(lower) and X-band(higher). As beamwidth increases the antenna diameter can be seen to increase. A similar relationship for carrier frequency and antenna diameter can be seen as well.

A contour plot of beamwidth, power required, and carrier to noise ratio is shown in Figure 59. The plot shows that a high beamwidth requires more power to have a high carrier to noise density ratio when compared to a low beamwidth antenna. For the short distance between the Orbiter and rover, a high beamwidth is acceptable because the losses from other factors like free space spreading loss are much smaller. On the other hand, for the link between the Orbiter and the DSN, a high beamwidth would require a significant amount of power to have a high enough carrier to

noise density ratio to offset the losses from other factors. The problem with a small beamwidth is that it requires a larger antenna.

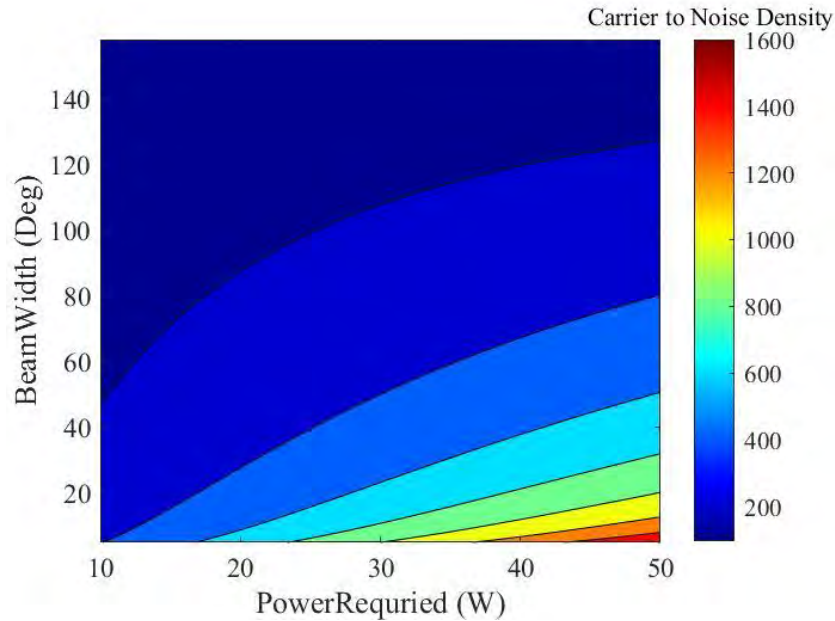


Figure 59: Contour plot of power required, beamwidth and carrier to noise density ratio. The graph shows that a higher power required results in a higher carrier to noise density ratio. Also, as beamwidth increases the carrier to noise density decreases. This means that a high beamwidth antenna requires a high power to achieve the desired carrier to noise density ratio.

Taking into consideration the theory outlined above, a link budget for a 0.87 S-band dish antenna was created and can be seen in full in Table 33. This link will also transmit at a data rate of 1 Mbps to allow for the energy per point over the noise energy to be above the required value, and for a lower power transmitted. By doing this the amplifier does not need to be as large or consume as much power. This communication system on the Orbiter with allows for uplink and downlink from Earth and from both rovers which satisfies the requirements of the communication system.

Table 33: Link budget between the Orbiter and the DSN. This table shows all the link budget parameters for the link between the antenna on the Orbiter and on of the antennas of the DSN.

Frequency	<i>GHz</i>	2.67	Propagation and Polarization Loss	<i>dB</i>	-20
Transmitter Power	<i>Watts</i>	1.1	Receive Antenna Diameter	<i>m</i>	26
Transmitter Power	<i>dBW</i>	0.41	Peak Receive Antenna Gain	<i>dB</i>	55.68
Transmitter Line Loss	<i>dB</i>	-1	Receive Antenna Beamwidth	<i>deg</i>	0.14
Transmit Antenna Beamwidth	<i>deg</i>	9	Receive Antenna Pointing Error	<i>deg</i>	0.2
Peak Transmit Antenna Gain	<i>dB</i>	25.22	Receive Antenna Pointing Loss	<i>dB</i>	-24.06
Transmit Antenna Diameter	<i>m</i>	0.87	Receive Antenna Gain	<i>dB</i>	31.62
Transmit Antenna Pointing Offset	<i>deg</i>	0.05	System Noise Temperature	<i>K</i>	135
Transmit Antenna Pointing Loss	<i>dB</i>	0	Data Rate	<i>Mps</i>	5.00
Transmit Antenna Gain	<i>dB</i>	25.21	Eb/No	<i>dB</i>	13.40
Equiv. Isotropic Radiated Power	<i>dBW</i>	24.63	Carrier-to-Noise Density Ratio	<i>dB-Hz</i>	87.37
Propagation Path Length	<i>km</i>	3.84E+05	Bit Error Rate		1.00E-06
Space Loss	<i>dB</i>	-152.67	Required Eb/No	<i>dB</i>	11

J. Orbiter ADCS

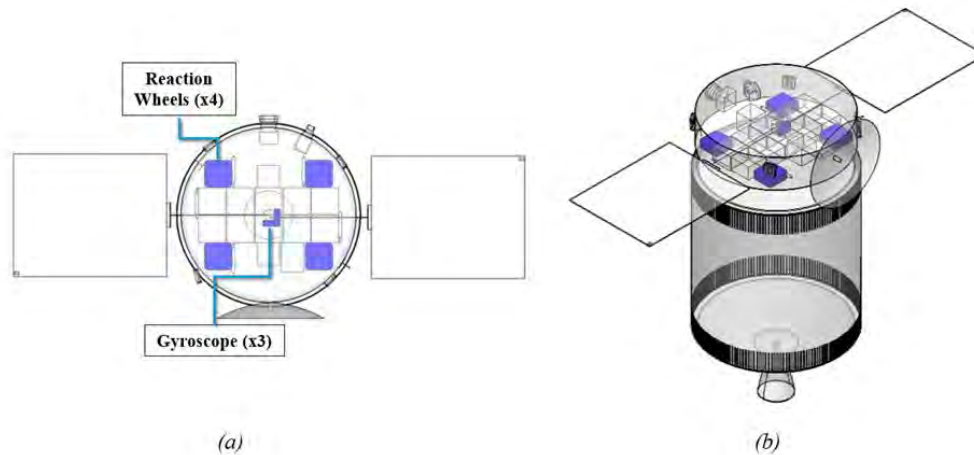


Figure 60: Top and Isometric View of Orbiter with ADCS in Blue. Both the CMG and reaction wheels are called out in the figure.

The requirements of the ADCS are ensuring that the Orbiter is pointed towards Earth and is spinning at a maximum rate of 0.2 degrees per second. To meet these requirements the Orbiter first needs to know its absolute attitude. This is accomplished through two redundant systems. Primary attitude determination is done using a star tracker with an accuracy of 1.5 arcseconds. It can operate with full performance at a slew rate of one degree per second and remains operation up to three degrees per second. The star tracker will ensure a low slew rate and low attitude error. The secondary system will be four sun sensors. These will slow down the slew rate of the spacecraft into operation levels for the star tracker. Also aiding in the reduction of the rotational velocity will be an IMU. This will help to determine the slew rate of the spacecraft. These systems are standard for most spacecraft attitude determination outside of GPS range. Whenever possible the star tracker will be used for attitude determination, but if for any reason the slew rate of the spacecraft increases above three degrees per second the Orbiter will switch into safe mode which will use the sun sensors and IMU.

Once the attitude is determined, the Orbiter must be able to point the antennas in the desired directions. This requires a control system. A trade study was conducted to determine the best system for attitude control. The options included a Reaction Wheel Assembly (RWA), Control Mounted Gyroscopes (CMG), and thrusters. Each option was compared in the parameters of mass, effectiveness, cost, complexity, and lifetime. Table 34 shows the results of the trade study. The RWA won mainly due to its low mass and long lifetime. Reaction wheels tend to be used for less

agile spacecraft compared to CMG. Also, there are more commercial options for reaction wheels with more flight heritage [68].

Table 34: Results of a trade study for the Orbiter ADCS. The trade study compared RWA, CMG, and thrusters. RWA received the highest score and was selected. This was mainly due to its low mass and complexity.

Parameters	Mass (kg)	Effectiveness	Cost (\$)	Complexity	Lifetime (yrs)
Weight	0.387	0.119	0.061	0.311	0.121
RWA	12	9	20000	7	10
Control Mounted Gyros	1	8	5000	3	5
Thrusters	28	8	15000	9	≤1



Total	
RWA	7.06
Control Mounted Gyros	6.59
Thrusters	6.75

The RWA consists of four reaction wheels canted around different axes. Based on research, the optimal cant angle is about 35° [69]. This is based on an equal torque and momentum requirement system. The fourth wheel is redundant and not necessary for attitude control. Another potential issue with reaction wheels is that momentum has to be unloaded from them after a certain amount of time because they can only spin so fast. Due to the relatively short duration of this mission a secondary attitude control system to unload momentum from the reaction wheels does not need to be large. Due to this, a small CMG system was also added to the Orbiter to unload momentum from the wheels if necessary. The CMG system can produce up to 177 Nm of torque. The four reaction wheels will take about a day to saturate due to environmental torques from the Sun of around 9e-5 Nm [70]. Figure 61 shows a graph of the momentum over time for the Orbiter. It can be seen that the momentum builds up until 10 Nm at which point the CMG system is turned on and run for 20 seconds. This unloads the momentum from the RWA. The graph shows that the CMG system will have to be turned on for about 20 seconds once a day. Each wheel is capable of producing 0.3 Nm of torque which is sufficient to overcome the torque caused from solar pressure. Also, each wheel can store up to 4 Nms of momentum. Through the use of the star trackers and the RWA, the Orbiter will be able to maintain a slew rate of less than 0.2 degrees per second and satisfy the requirement to point the antennas in the desired directions.

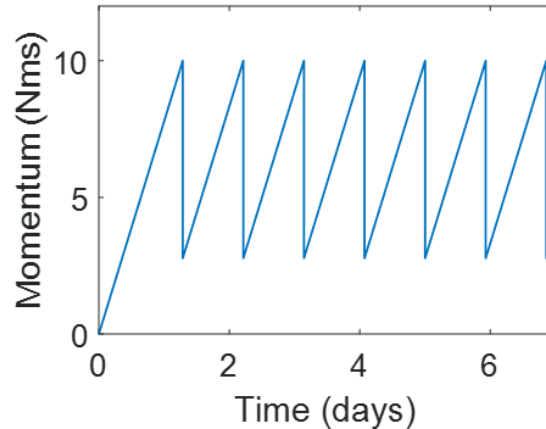


Figure 61: Graph of momentum versus time of the Orbiter. The momentum builds up in the reaction wheels until it reaches a total of 10 Nm over all four wheels. Then the CMG system is turned on for 20 seconds to unload the momentum. With only solar torques this occurs roughly once a day.

K. Mass Budget

Table 35 below indicates the breakdown of the mass budget for each of the Orbiter within the PLF assembly by subsystem. The total mass shown in the table includes the mass of the payload (i.e. Landers, Rovers, and Lander propulsion). The dry mass of the Orbiter is 294 kg, where most of the weight is in the propulsion system. The propellant and propulsion system alone encompass the majority of the Orbiter mass, and therefore were the driving factors when determining the payload configuration and designing the orbiter to have a central center of mass. The overall spacecraft weight and center of mass will also greatly change when the spacecraft arrives at the Moon and after it deploys both landers. This necessitated the focus on having a robust attitude control system for the Orbiter. The overall mass of the Orbiter assembly was well within the maximum mass threshold of 4658 kg, allowing ample room for the system to grow as the design progresses without exceeding the Falcon 9 PLF mass constraints.

Table 35: Mass Budget for Lunar Orbiter. This table indicates the mass allocation and limits for the lunar orbiter within the PLF assembly. The total mass of the table includes the mass of the mission payload (i.e. Lander and Rover assemblies)

Subsystem	Part	Basic Mass (kg)	MGA (%)	Predicted Mass (kg)	Mass Limit (kg)
Attitude Control	Control Mounted Gyroscopes	2.5	10%	2.8	15
	Reaction Wheels	12	10%	13.2	50
Avionics	Computer	6.5	10%	7.2	35
	IMU	0.8	10%	0.8	10
Communication	DSN Antenna	9	10%	9.9	35
	Moon Antenna	0.5	10%	0.6	5
	Transponder	2.7	10%	3	10
	Transponder Moon	0.1	10%	0.1	5
Instrumentation	IR Camera	1.6	12%	1.8	13
Navigation	Coarse Sun Sensor	1	7%	1.1	13
	Star Tracker	2	7%	2.1	12
Power	Battery	34.3	7%	36.7	100
	Solar Panel Support	5	8%	5.4	20
	Solar Panels	1.3	8%	1.4	30
Propulsion	Fuel Tank	100	2000%	200	250
	HiPAT	5.2	20%	6.2	30
	ISP Fuel	2400	20%	2880	3700
Structures	Orbiter WEB Bottom	24.2	15%	27.8	60
	Orbiter WEB Cylinder	21.2	15%	24.4	60
	Orbiter WEB Top	17.4	15%	20	60
	Pyrotechnic Rings	43.5	15%	50	100
Thermal	Heaters	0.1	3%	0.1	5
	MLI	2	3%	2.1	30
	Temperature Sensors	1.1	3%	1.2	10
TOTALS:	-	2694	-	3297.9	4658

VIII. Systems Analysis

A. Mission Mass Budget

The total mass of the spacecraft was constrained by the launch vehicle; the Falcon 9 can bring up to 8300 kg to GTO. Table 36 outlines the overall mass budget of the Project Penguin Spacecraft, describing the basic mass, the allowable increase in mass as the project moves forward, and the mass limits. At 4654 kg, the spacecraft is well within the payload capacity of the Falcon 9 and has allowable room to grow as the mission progresses. The fuel required to maneuver the Orbiter to the Moon and perform the EDL for the landers encompasses the majority of the mass at 78.3%.

Table 36: The Overall Mission Mass Budget. The table shows the mass of each major subsystem as well as the predicted mass growth as the mission continues in development and the mass limit from the Falcon 9 Payload size.

Subsystem	Basic Mass (kg)	MGA (%)	Predicted Mass (kg)	Mass Limit (kg)	Percent of Overall Mass (%)
ISP Propellant	2400	15%	2760	4200	51.6%
Orbiter Dry Mass	294	8%	318	1000	6.3%
EDL 1 Propellant Mass	516	20%	619	850	11.1%
EDL 2 Propellant Mass	516	20%	619	850	11.1%
Lander 1 Dry Mass	345	8%	373	550	7.4%
Lander 2 Dry Mass	345	8%	373	550	7.4%
Rover 1 Mass	119	5%	125	150	2.6%
Rover 2 Mass	119	5%	125	150	2.6%
TOTALS:	4654	-	5311	8300	-

B. Mission Cost Budget

As previously mentioned, this mission has a NASA budget of \$500 million and a requirement to maximize scientific data return. To maximize the scientific data return, this mission utilized the entire budget provided by NASA to maximize the instrumentations and ensure overall mission success. Table 37 outlined the cost budget for Project Penguin, depicting the upper and lower bounds of the estimated monetary cost per subsystem. The largest portion of the mission was the EDL system, which included the infrastructure and propulsion systems on both landers. While this is the most expensive portion of the trip, EDL is also the highest risk of mission failure due to the complication and difficulty of the maneuver. The EDL system includes expensive, gimbale, throttleable rockets, high resolution

lunar surface imaging equipment, and a sophisticated computer to complete real time calculations. Estimates for cost in this mission came from looking at similar lunar and Martian missions and from the Space Mission Analysis and Design reference text.

Table 37: Overall Mission Cost Budget. Each subsystem has an upper and lower cost with a margin. This is to ensure no cost overrun as the mission develops.

Sub-System	Lower Cost (\$ millions)	Upper Cost (\$ millions)	Margin (%)	Overall % of Budget
Communications	\$0.48	\$0.50	2%	0.10%
Thermal System	\$0.47	\$0.50	3%	0.10%
Orbiter Structure	\$0.90	\$1.00	5%	0.20%
Orbiter Power Systems	\$4.70	\$5.00	3%	1.00%
Rover Structure	\$4.50	\$5.00	5%	1.00%
Navigation	\$33.60	\$35	2%	7.00%
Rover Power Systems	\$40.30	\$42	2%	8.40%
In-Space Propulsion	\$56.40	\$60	3%	12.00%
Instrumentation	\$50.20	\$66	12%	13.20%
Operation/Engineering/Testing	\$67.50	\$75	5%	15.00%
Launch Vehicle	\$72.00	\$90	10%	18.00%
EDL System	\$106	\$120	6%	24.00%
TOTAL	\$437	\$500	-	-

C. Mission Risk Analysis

Risks for the mission were identified and given a probability of occurrence and a consequence. Table 38 describes the definitions of each consequence category. The lowest rating means that the impact on the mission is insignificant while the highest rating means that the mission was a complete failure.

Table 38: Risk Consequence Definition. This table describes each consequence in detail.

Consequence	Definition
Negligible	Little to no impact on the mission
Minor	Small changes to mission design needed
Moderate	Large changes to mission design needed
Critical	Partial mission failure. Data is only received from one crater
Catastrophic	Total mission failure. No data is sent back to Earth

Table 39 shows the different risk events, their probability of occurrence, and the impacts they would have on the mission. Green boxes indicate that with current mitigation the risk is acceptable. Yellow boxes mean that with current mitigation the risk is potentially too high for the mission, and red boxes mean that the risk is unacceptable for the mission. Each event is given a number in Table 39 that corresponds to the ranking of importance of the risk. A high probability and a high consequence lead to a high ranking. From Table 38 all the events can be seen to reside in the green or yellow boxes. This means that currently there are no unacceptable risks for the mission.

Table 39: Risk Assessment Matrix. This table shows the probability of occurrence and the consequence of different risk events. Green boxes mean risk is acceptable. Yellow boxes mean that the risk needs to be improved, and red boxes mean that the risk is unacceptable for the mission.

		System Level Risks				
		0-5%	5-20%	20-40%	40-65%	65-100%
Consequence of Event	Catastrophic	3,4,8,11	1			
	Critical	5,6	2,9			
	Moderate					
	Minor			10		
	Negligible			7		
		0-5%	5-20%	20-40%	40-65%	65-100%
		Probability of Event				

Event No.	Event Name
1	Thermal Environment Disrupts Instrumentation
2	Impact Strut Failure
3	Instrumentation Breaks during EDL
4	Antenna Failure
5	EDL Rocket Failure
6	Power System Failure
7	Failure to meet launch window
8	Pyrotechnic Bolt Deployment Failure
9	Rover Stuck on Lunar Surface
10	Dust Disrupts Rover Operations
11	Cost Overrun

Table 40: Risk Events, Status, and Mitigation Strategies. This table defines each risk and number described in Table 38.

Risk	Status	Strategy
1 If the Thermal Environment Disrupts Instrumentation then instruments break	Mitigate	Test system on ground to ensure operations in lunar crater temperatures. Redundant instrumentation systems.
2 If the Impact Struts Fail upon landing then rover can not be deployed	Mitigate	Complete ground testing to ensure struts will not buckle or break on impact to lunar surface.
3 If the Instrumentation Breaks during EDL then data can not be sent back to the Orbiter from the Rover	Transfer	Conduct structural load tests for the instrumentation to withstand launch and EDL.
4 If Antenna Failure occurs then data will not be relayed to Earth	Mitigate	Set up redundant communication paths to ensure no failure in communication. Maximize communication time with rover, orbiter, and Earth.
5 If EDL Rocket Failure occurs then the Rover will not be deployed	Mitigate	Propulsion system has proven to work through flight heritage of the contracting propulsion company.
6 If Power System Failure occurs then instruments on the Rover will not operate	Mitigate	Complete ground testing. Carry redundant power sources.
7 If there is a Failure to meet launch window then the mission might not be accomplished on time	Accept	Multiple launch opportunities are available. Enough time is already budgeted into the mission, the spacecraft would be launched again.
8 If there is a Pyrotechnic Bolt Deployment Failure then the landers will not release from the Orbiter	Accept	The pyrotechnic bolts selected have better than a 99% success rate. With such a low probability of failure, the risk will be accepted.
9 If the Rover Stuck on Lunar Surface then the Rover will be unable to continue to collect data	Mitigate	Provide redundant navigation systems to ensure a rover is never lost on the surface. In addition, use the Rocker-bogie system to avoid being stuck on obstacles.
10 If Dust Disrupts Rover Operations then the Rover will not be able to accomplish data collection	Mitigate	Use an active electrodynamic system to move the dust off of the surface of the rover.
11 If there is a Cost Overrun the team may lose the contract	Mitigate	Have anticipated costs be lower than the \$500 million budget to allow for overruns to occur without overall failure.

Table 40 has three different statuses for each risk event. The statuses were defined: “accept,” “transfer,” and “mitigate.” The “accept” status means that no action needs to be taken to lower the risk while “transfer” means that the risk will be given as a responsibility to another entity. “Mitigate” means that steps will be taken to lower the probability or consequence of the risk. This mitigation will be accomplished through redundancy or testing.

The highest risks for the mission are instrumentation failure and landing strut failure. Without instrumentation the mission requirement cannot be met. The strategies to mitigate the risk included carrying multiple instruments on-

board that can make the desired regolith to water ratio measurement and performing ground tests in simulated crater environments to ensure that the instruments function under the expected conditions. This mitigation was accomplished by having three instruments capable of calculating the water-to-regolith ratio. To reduce the risk of landing strut failure, ground testing will be completed. The last two risks in Table 38 focus more on the overall mission. While they don't focus on individual components of the mission, these risks cause failure on various projects. To mitigate the cost overrun risk, the project has used less than the \$500 million budget to allow for overruns to occur on individual components without causing a total cost overrun. The launch vehicle failure risk is just accepted because there is nothing that can be done to mitigate this risk. The other risk events described have been mitigated through testing, adding deterrent systems like the active electrodynamic system for the dust, and adding redundant systems to ensure individual failures of components won't compromise the entire mission.

IX. Conclusion

A. Summary

As NASA prepares to send manned missions beyond LEO, payload becomes an increasingly vital resource that affects initial launch cost. If future missions were to forfeit some water payload and mine it in water-rich locations, humanity could incrementally step further towards Mars at drastically lower launch cost and extended mission lifetime. Previous lunar missions such as Chandrayaan-I and Lunar Reconnaissance Orbiter (LRO) have identified high water concentrations in the lunar South pole. AIAA recently released an RFP for a mission to the Moon to identify two concrete water-to-regolith concentrations from two separate lunar craters. The mission was given a \$500 million NASA budget and a deadline of mission completion by EOY 2024. The mission must also maximize the scientific output.

Project Penguin proposes to send a rover to both the Haworth and Shoemaker crater on the lunar South pole to investigate the presence of ice in the PSR. The spacecraft will be launched on a Falcon 9 on January 7th, 2023 into GTO and then transfer to a lunar polar orbit. The spacecraft will deploy two landers to perform the EDL maneuver and safely land the rovers on the lunar surface. Each rover will be equipped with redundant instruments to map the entire crater surface and determine concrete water deposits. This prospecting mission will additionally investigate some of NASA's STG and national scientific priorities regarding the geological properties of the lunar South pole and

the formation of the Moon. Both rovers will operate autonomously, unless abnormal issues occur, and are estimated to complete mapping the craters in 345 days. Once the original mission is complete, the rovers will still have the capability to operate due to the extended lifetime of the STEM-RTGs. If the rovers are still operational, Project Penguin can apply for NASA to extend the mission lifetime beyond EOY 2024 and the rovers will attempt to traverse outside of Haworth and Shoemaker craters.

The Project Penguin spacecraft is a low risk mission, using many aspects of heritage Martian and lunar spacecraft designs while maximizing data sent back to Earth. The mission is well within the \$500 million NASA budget, having margins to allow for possible cost overrun and accounting for two years of mission operations back on Earth. Overall, the spacecraft fits into the PLF of the Falcon 9 FT mass and volume constraints. The overall spacecraft mass is 4654 kg, with 78% of the overall mass allocated to propellant. The mission was designed so that even as the mission progressed through design and construction the spacecraft will still fit into the Falcon 9 FT payload constraints.

B. Conclusion

As evident throughout this paper, the proposed mission, Project Penguin, meets all mission requirements while allowing room to maximize the scientific instrumentation and mitigating most critical mission risks. The system design robustly tackles the challenges of operating inside PSRs, mitigating destruction from lunar dust, and obtaining water concentrations below the lunar crater crust. Sending these rovers to the lunar South pole allows for abundant new information of regions difficult to observe from orbit.

The mission technically meets the requirements outlined in the AIAA RFP when each rover takes a single sample from each crater, fulfilling the requirement to obtain a water to regolith ratio from two lunar craters. To maximize the performance for the allocated budget and maximize scientific data returned from the mission, Project Penguin will complete the mission and requirements set when each rover fully maps out the respective lunar crater and determines specific locations within the crater of larger water deposits while confirming the data found in previous lunar orbital missions. Overall, Project Penguin will obtain over 150 samples from each crater and determine four additional science objectives which fill in knowledge gaps from both NASA and the NASEM.

X. References

1. National Research Council. 2007. The Scientific Context for Exploration of the Moon. Washington, DC: The National Academies Press. <https://doi.org/10.17226/11954>.
2. National Academy of Sciences, Engineering, & Medicine. (n.d.). New Report: NASA Should Develop U.S. Strategy for International Space Station Beyond 2024. Retrieved from <http://www8.nationalacademies.org/onpinews/newsitem.aspx?RecordID=24966>
3. NASA. (2016, September 1). Strategic Knowledge Gaps Theme 1. Retrieved from <https://www.nasa.gov/sites/default/files/atoms/files/skg-sat-theme-1-sept-2016.pdf>
4. Vikram Sarabhai Space Centre. (2012). Moon Impact Probe (MIP). Retrieved from Vikram Sarabhai Space Centre: http://www.vssc.gov.in/VSSC_V4/index.php/payload/82-chandrayaan-1/966-Moon-impact-probe
5. Indian Space Research Organization. (2008, October 22). Chandrayaan-I. Retrieved from Department of Space Indian Space Research Organization: <https://www.isro.gov.in/Spacecraft/chandrayaan-1>
6. Pieters, C. M., Boardman, J., Buratti, B., Chatterjee, A., Clark, R., Glavich, T., . . . Sunshine, J. (2009, February 25). The Moon Mineralogy Mapper (M3) on Chandrayaan-I. *Current Science*, pp. 500-505.
7. Vikram Sarabhai Space Centre. (2012). Moon Impact Probe (MIP). Retrieved from Vikram Sarabhai Space Centre: http://www.vssc.gov.in/VSSC_V4/index.php/payload/82-chandrayaan-1/966-Moon-impact-probe
8. Retherford, K., “The Lyman-Alpha Mapping Project: Seeing in the Dark,” Southwest Research Institute, Available: <http://www.boulder.swri.edu/lamp/>.
9. National Research Council. 2007. The Scientific Context for Exploration of the Moon. Washington, DC: The National Academies Press. <https://doi.org/10.17226/11954>.
10. Garner, R. (2016, June 02). LRO Spacecraft Instruments. Retrieved from https://www.nasa.gov/mission_pages/LRO/spacecraft/index.html
11. Lunar Reconnaissance Orbiter Camera. (n.d.). Retrieved from <http://quickmap.lroc.asu.edu/>
12. Meyer, C. (2003). *Lunar Regolith*. Retrieved from National Aeronautics and Space Administration: <https://curator.jsc.nasa.gov/lunar/letss/regolith.pdf>
13. The Economist. (2016, November 10). *How to solve the lunar dust problem*. Retrieved from The Economist: <https://www.economist.com/news/science-and-technology/21709943-sharp-jagged-dust-grains-get-everywhere-and-break-things-how-solve-lunar>
14. NASA. (n.d.). Sample Analysis at Mars (SAM) Instrument Suite - Mars Science Laboratory. Retrieved from <https://mars.nasa.gov/msl/mission/instruments/spectrometers/sam/>
15. NASA. (n.d.). Chemistry & Camera (ChemCam) - Mars Science Laboratory. Retrieved from <https://mars.nasa.gov/msl/mission/instruments/spectrometers/chemcam/>
16. NASA. (n.d.). Dynamic Albedo of Neutrons (DAN) - Mars Science Laboratory. Retrieved from <https://mars.nasa.gov/msl/mission/instruments/radiationdetectors/dan/>
17. Litvak, Mitrofanov, Barmakov, Behar, Bitulev, Bobrovniksky, . . . Vostrukhin. (2008, August 12). The Dynamic Albedo of Neutrons (DAN) Experiment for NASA’s 2009 Mars Science Laboratory.

18. Woodard, S. (2011, October 1). SansEC Sensing Technology - A New Tool for Designing Space Systems and Components. Retrieved from <https://ntrs.nasa.gov/archive/nasa/casi.ntrs.nasa.gov/20110008236.pdf>
19. Xu, R., Li, C., Wang, B., Shu, R., Wang, J., Gang Lv, & Liyin Yuan. (2015, October 12). Visible and near-infrared imaging spectrometer (VNIS) for in-situ lunar surface measurements. Retrieved from <https://www.spiedigitallibrary.org/conference-proceedings-of-spice/9639/1/Visible-and-near-infrared-imaging-spectrometer-VNIS-for-in-situ/10.1117/12.2194526.full?SSO=1>
20. Zacny, Fong, Wilson, Lee, Kobayashi, Deans, . . . Santoro. (2008). PERCUSSIVE DYNAMIC CONE PENETROMETER FOR GEOTECHNICAL SURFACE ASSESSMENT WITH A PLANETARY ROVER. Retrieved from <https://www.lpi.usra.edu/meetings/nlsc2008/pdf/2138.pdf>
21. Grant, J., & Leuschen, C. (2011, July 22). The STRATA ground penetrating radar as a means for constraining the near surface properties of the Moon and Mars. Retrieved from <https://ieeexplore.ieee.org/document/5960711/?reload=true>
22. NASA Jet Propulsion Laboratory. (n.d.). Spacecraft: Surface Operations: Rover. Retrieved from Mars Exploration Rovers: https://mars.nasa.gov/mer/mission/spacecraft_rover_wheels.html
23. National Aeronautics and Space Administration. (n.d.). Wheels and Legs. Retrieved from Mars 2020 Rover: <https://mars.nasa.gov/mars2020/mission/rover/wheels/>
24. Dunbar, B. (2017, June 29). An Algorithm Helps Protect Mars Curiosity's Wheels. Retrieved from National Aeronautics and Space Administration: <https://www.nasa.gov/feature/jpl/an-algorithm-helps-protect-mars-curiositys-wheels>
25. Kilkenny, N. S. (2017, October 26). Reinventing the Wheel. Retrieved from NASA Glenn Research Center: <https://www.nasa.gov/specials/wheels/>
26. Ilyas, M., Hong, B., Cho, K., Baeg, S., and Park, S., “Integrated Navigation System Design fo Micro Planetary Rovers: Comparison of Absolute Heading Estimation Algorithms and Nonlinear Filtering”, MDPI, Sensors (Basel), May 2016, Available: <https://www.ncbi.nlm.nih.gov/pmc/articles/PMC4883439/>
27. Beckman, M., “Mission Design for the Lunar Reconnaissance Orbiter”, Goddard Space Flight Center, February 2006, Available: https://lunar.gsfc.nasa.gov/library/LRO_AAS_Paper_07-057.pdf
28. Wahlquist, E.J. and Furlong, R.R., “U.S. Space Missions using Radioisotope Power Systems” Office of Nuclear <http://staff.diviner.ucla.edu/science.shtml>
29. “Lunar Reconnaissance Orbiter: Permanently Shadowed Regions on the Moon” NASA. Available: <https://lunar.gsfc.nasa.gov/images/lithos/LRO%20litho5-shadowedFinal.pdf>
30. Colozza, A.J. and Cataldo, R.L., “Applicability of STEM-RTG and High-Power SRG Power Systems to the Discovery and Scout Mission Capabilities Expansion (DSMCE) Study of ASRG-Based Missions” Vantage Partners, LLC and NASA Glenn Research Center. 2015. Available: <https://ntrs.nasa.gov/archive/nasa/casi.ntrs.nasa.gov/20150023042.pdf>.
31. Xiao, X. and Whittaker, W.L., “Energy Considerations for Wheeled Mobile Robots Operating on a Single Battery Discharge” Carnegie Mellon University. 2014. Available: https://www.ri.cmu.edu/pub_files/2014/8/TR-14-16.pdf.

32. “28V Space Grade Battery System - Rechargeable Li-Ion battery system” Saft Space and Defense Division. 2015.
33. Kramer, H.J., “LRO (Lunar Reconnaissance Orbiter) + LCROSS” Earth Observation Portal Available: <https://directory.eoportal.org/web/eoportal/satellite-missions/l/lro>.
34. Bhandari, P., et al , “Mars Science Laboratory Thermal Control Architecture” Jet Propulsion Laboratory, California Institute of Technology. Available: https://www.researchgate.net/publication/228764337_Mars_Science_Laboratory_thermal_control_architecture.
35. Bhandari, P., et al , “Performance Of The Mechanically Pumped Fluid Loop Rover Heat Rejection System Used For Thermal Control Of The Mars Science Laboratory Curiosity Rover On The Surface Of Mars”. Available: https://trs.jpl.nasa.gov/bitstream/handle/2014/44145/13-2330_A1b.pdf?sequence=1.
36. G. Sebestyen et al., Low Earth Orbit Satellite Design, Space Technology Library 36, Chapter 4, Available: https://link.springer.com/content/pdf/10.1007%2F978-3-319-68315-7_4.pdf
37. William, D. R., “The Apollo Program (1963-1972),” NSSDC Available: <https://nssdc.gsfc.nasa.gov/planetary/lunar/apollo.html>.
38. “About the DSN,” Deep Space Network Available: <https://deepspace.jpl.nasa.gov/about/#>.
39. Calle, C. I., and Buhler, C. R., “Active dust control and mitigation technology for lunar and Martian exploration,” *Acta Astronautica* Available: <https://www.sciencedirect.com/science/article/pii/S0094576511001883>.
40. Calle, C. I., and Buhler, C. R., “Particle removal by electrostatic and dielectrophoretic forces for dust control during lunar exploration missions,” *Journal of Electrostatics* Available: <https://www.sciencedirect.com/science/article/pii/S030438860900103X>.
41. Dunbar, B., “Mars Pathfinder Air Bag Landing Tests,” *NASA* Available: <https://www.nasa.gov/centers/glenn/about/history/marspbag.html>.
42. “Mars Exploration Rover,” *NASA Facts* Available: <https://mars.nasa.gov/mer/newsroom/factsheets/pdfs/Mars03Rover041020.pdf>.
43. “Spacecraft - Mars Science Laboratory,” *NASA* Available: <https://mars.nasa.gov/msl/mission/spacecraft/>.
44. “Apollo 11 Landing Site,” *Apollo 11 Landing Site | National Air and Space Museum* Available: <https://airandspace.si.edu/explore-and-learn/topics/apollo/apollo-program/landing-missions/apollo11-landing-site.cfm>.
45. “Entry, Descent, and Landing - Mars Science Laboratory,” *NASA* Available: <https://mars.nasa.gov/msl/mission/timeline/edl/>.
46. Stooke, P., “Lunar Farside Landing Plans,” The Planetary Society Blog Available: <http://www.planetary.org/blogs/guest-blogs/2016/0527-lunar-farside-landing-plans.html>.
47. Hayhurst, M., Eftekharzadeh, S., and Wood, B., “Mission Operations Cost Estimation Tool (MOCET)” Available:

- https://www.nasa.gov/sites/default/files/files/20_MOCET_NASA_Cost_Symposium_Briefing_2015-08-21.pdf.
48. Braeunig, R. A., "Rocket Propellants," *Basics of Space Flight: Rocket Propellants* Available: <http://www.braeunig.us/space/propel.htm>.
 49. Zandbergen, B. T. C., "Modern Liquid Propellant Rocket Engines" Available: https://www.researchgate.net/profile/Btc_Zandbergen/publication/267047129_Modern_Liquid_Propellant_Rocket_Engines_2000_Outlook/links/5444b3dc0cf2a76a3ccd7b48/Modern-Liquid-Propellant-Rocket-Engines-2000-Outlook.pdf.
 50. Wade, M., "R-40B," R-40B Available: <http://www.astronautix.com/r/r-40b.html>.
 51. Pasandm, M., Hassani, A., and Ghorbani, M., "A Study of Spacecraft Reaction Thruster Configurations for Attitude Control System," IEEE Aerospace and Electronic System Available: https://www.researchgate.net/publication/320559313_A_Study_of_Spacecraft_Reaction_Thruster_Configurations_for_Attitude_Control_System
 52. Bakalski, I., Foster, M., Bellis, S., and Fisackerly, R., "Imaging LiDARs for Space Applications," *Proceedings of SPIE- The International Society for Optical Engineering*, published online 02 Jan. 2014.
 53. Kauder, L., "Spacecraft Thermal Control Coatings References" NASA. 2005. Available: <http://www.aztechnology.com/pdfs/nasa-tp-2005-212792-lauder.pdf>.
 54. Amzajerjian, F., Pierrottet, D., Petway, L., Hines, G., and Roback, V., "Lidar systems for precision navigation and safe landing on planetary bodies," International Symposium on Photoelectronic Detection and Imaging 2011: Laser Sensing and Imaging; and Biological and Medical Applications of Photonics Sensing and Imaging, Sep. 2011., Available: <https://ntrs.nasa.gov/archive/nasa/casi.ntrs.nasa.gov/20110012163.pdf>
 55. Biesbroek, R., and Janin, G., "Ways to the Moon?", European Space Agency, bulletin 103, August 2000, Available: <http://www.esa.int/esapub/bulletin/bullet103/biesbroek103.pdf>.
 56. Prado, A.F.B.A., "The elliptic-bi-parabolic planar transfer for artificial satellites", Journal of the Brazilian Society of Mechanical Sciences and Engineering, Vol. 25, No. 2, 2003, pp. 122-128, Available: http://www.scielo.br/scielo.php?script=sci_arttext&pid=S1678-58782003000200003.
 57. Prado, A.F.B.A., "The elliptic-bi-parabolic planar transfer for artificial satellites", Journal of the Brazilian Society of Mechanical Sciences and Engineering, Vol. 25, No. 2, 2003, pp. 122-128, Available: http://www.scielo.br/scielo.php?script=sci_arttext&pid=S1678-58782003000200003.
 58. Wade, M., *Reduced Apollo Block II service propulsion system for Saturn IB missions* Available: <https://web.archive.org/web/20100201055835/http://astronautix.com/details/red17167.htm>.
 59. Harper, S., "Bipropellant Rocket Engines," *Bipropellant Rocket Engines | Aerojet Rocketdyne* Available: <http://www.rocket.com/propulsion-systems/bipropellant-rockets>.
 60. "Aerospace Energy Standard Prices for DoD Customers" Available: http://www.dla.mil/Portals/104/Documents/Energy/StandardPrices/AerospacePrices/E_2016Oct1AerospaceStandardPrices_160921.pdf.

61. Wade, M., “HiPAT,” *HiPAT* Available: <http://www.astronautix.com/h/hipat.html>.
62. Horst, T., “Space Grade Solar Cells” AzurSpace: Solar Power GMBH Available:
<http://www.azurspace.com/index.php/en/products/products-space/space-solar-cells>.
63. Paige, D., “DIVINER Lunar Radiometer Experiment” UCLA Lab. Available:
<http://staff.diviner.ucla.edu/science.shtml>
64. Gilmore, D.G. and Lyra, J.C. and Stulz, J.W., “Heaters” The Aerospace Corporation and Jet Propulsion Lab. Available:
http://matthewturner.com/uah/IPT2008_summer/baselines/LOW%20Files/Thermal/Spacecraft%20Thermal%20Control%20Handbook/07.pdf
65. “About the DSN,” Deep Space Network Available: <https://deepspace.jpl.nasa.gov/about/#>.
66. Mai, T., “Deep Space Network (DSN),” NASA Available:
<https://www.nasa.gov/directorates/heo/scan/services/networks/dsn>.
67. Scales, W., “GPS Communication Link Concepts: Theory and Applications,” ECE 4164 Lecture Set 11 Virginia Polytechnic Institute and State University.
68. Votel, R., and Sinclair, D., “Comparison of Control Moment Gyros and Reaction Wheels for Small Earth-Observing Satellites”, Skybox Imaging Inc. and Sinclair Interplanetary August 2014, Available:
<https://digitalcommons.usu.edu/cgi/viewcontent.cgi?referer=&httpsredir=1&filename=0&article=1080&context=smallsat&type>
69. Hablani, H., “Sun-Tracking Commands and Reaction Wheel Sizing with Configuration Optimization”, Rockwell International, Space Systems Division, August 1994, Available:
<https://arc.aiaa.org/doi/pdf/10.2514/3.21270>
70. Brown, C., “Elements of Spacecraft Design”, *Attitude Control*, AIAA Education Series 1994, pp 273-274